Report No. KTRAN: KSU-02-3
FINAL REPORT

EVALUATING FIBER REINFORCED POLYMER REPAIR METHOD FOR CRACKED PRESTRESSED CONCRETE BRIDGE MEMBERS SUBJECTED TO REPEATED LOADINGS PHASE 2

Kyle H. Larson, Ph.D.
Hayder A. Rasheed
Robert J. Peterman, Ph.D., P.E.

Kansas State University

May 2007

A COOPERATIVE TRANSPORTATION RESEARCH PROGRAM
BETWEEN:

KANSAS DEPARTMENT OF TRANSPORTATION
KANSAS STATE UNIVERSITY
UNIVERSITY OF KANSAS

1 Report No. KTRAN: KSU-02-3	**2 Government Accession No.**	**3 Recipient Catalog No.**
4 Title and Subtitle **EVALUATING FIBER REINFORCED POLYMER REPAIR METHOD FOR CRACKED PRESTRESSED CONCRETE BRIDGE MEMBERS SUBJECTED TO REPEATED LOADINGS PHASE 2**		**5 Report Date** May 2007 **6 Performing Organization Code**
7 Author(s) Kyle H. Larson, Ph.D., Hayder A. Rasheed, Robert J. Peterman, Ph.D., P.E.		**8 Performing Organization Report No.**
9 Performing Organization Name and Address Kansas State University 215 Durland Manhattan, KS 66506		**10 Work Unit No. (TRAIS)** **11 Contract or Grant No.** C1331
12 Sponsoring Agency Name and Address Kansas Department of Transportation Bureau of Materials and Research 700 SW Harrison Street Topeka, Kansas 66603-3754		**13 Type of Report and Period Covered** Final Report September 2001 - May 2007 **14 Sponsoring Agency Code** RE-0278-01

15 Supplementary Notes
For more information write to address in block 9.

16 Abstract

This research is intended to investigate the fatigue performance of pre-cracked prestressed concrete T-beams for a specific strand stress range and its relationship to the level of strengthening gained. Controlling the strand stress range is accomplished by iterative cycles of nonlinear analysis to determine the amount of external carbon Fiber Reinforced Polymers (FRP) reinforcement needed for that purpose. Five pre-tensioned prestressed concrete T-beams were cast at a prestressed concrete plant in Newton, Kansas. Beam 1 was tested under static loading up to failure as a control specimen. Beams 2 and 3 were strengthened with Carbon Fiber Reinforced Polymers (CFRP) to have a design stress range of 18 ksi under service load condition. Beams 4 and 5 were also strengthened to have a higher stress range of 36 ksi. Beams 2 and 4 were loaded monotonically to failure while Beams 3 and 5 were cycled over a million times before they were brought to failure. The design yielded one layer of flexural CFRP wrapped around the web sides up to 2.25” from the bottom for the 18 ksi stress range design. It also resulted in two layers of longitudinal CFRP for the 36 ksi stress range design, the inner layer wrapped around the web sides up to 0.5” and the outer layer went up 3” on the web sides. External CFRP stirrups were used to prevent the longitudinal CFRP from premature separation. Beams 2 and 4 successfully reached their target strengthening design levels and Beams 3 and 5 performed very well in fatigue.

17 Key Words prestressed concrete, T-beams, FRP, CFRP, Carbon Fiber Reinforced Polymer		**18 Distribution Statement** No restrictions. This document is available to the public through the National Technical Information Service, Springfield, Virginia 22161	
19 Security Classification (of this report) Unclassified	**20 Security Classification (of this page)** Unclassified	**21 No. of pages** 120	**22 Price**

Form DOT F 1700.7 (8-72)

PREFACE

The Kansas Department of Transportation's (KDOT) Kansas Transportation Research and New-Developments (K-TRAN) Research Program funded this research project. It is an ongoing, cooperative and comprehensive research program addressing transportation needs of the state of Kansas utilizing academic and research resources from KDOT, Kansas State University and the University of Kansas. Transportation professionals in KDOT and the universities jointly develop the projects included in the research program.

NOTICE

The authors and the state of Kansas do not endorse products or manufacturers. Trade and manufacturers names appear herein solely because they are considered essential to the object of this report.

This information is available in alternative accessible formats. To obtain an alternative format, contact the Office of Transportation Information, Kansas Department of Transportation, 700 SW Harrison Street, Topeka, Kansas 66603-3754 or phone (785) 296-3585 (Voice) (TDD).

DISCLAIMER

The contents of this report reflect the views of the authors who are responsible for the facts and accuracy of the data presented herein. The contents do not necessarily reflect the views or the policies of the state of Kansas. This report does not constitute a standard, specification or regulation.

EVALUATING FIBER REINFORCED POLYMER REPAIR METHOD FOR CRACKED PRESTRESSED CONCRETE BRIDGE MEMBERS SUBJECTED TO REPEATED LOADINGS

PHASE 2

Final Report

Prepared by

Kyle H. Larson, Ph.D.
Kansas State University

Hayder A. Rasheed
Kansas State University

Robert J. Peterman, Ph.D., P.E.
Kansas State University

Project Monitor
Stephen G. Burnett
Kansas Department of Transportation
Bureau of Design

A Report on Research Sponsored By

THE KANSAS DEPARTMENT OF TRANSPORTATION
TOPEKA, KANSAS

KANSAS STATE UNIVERSITY
MANHATTAN, KANSAS

May 2007

ABSTRACT

This research is intended to investigate the fatigue performance of pre-cracked prestressed concrete T-beams for a specific strand stress range and its relationship to the level of strengthening gained. Controlling the strand stress range is accomplished by iterative cycles of nonlinear analysis to determine the amount of external carbon Fiber Reinforced Polymer (FRP) reinforcement needed for that purpose. Five pre-tensioned prestressed concrete T-beams were cast at a prestressed concrete plant in Newton, Kansas. Beam 1 was tested under static loading up to failure as a control specimen. Beams 2 and 3 were strengthened with Carbon Fiber Reinforced Polymer (CFRP) to have a design stress range of 18 ksi under service load condition. Beams 4 and 5 were also strengthened to have a higher stress range of 36 ksi. Beams 2 and 4 were loaded monotonically to failure while Beams 3 and 5 were cycled over a million times before they were brought to failure. The design yielded one layer of flexural CFRP wrapped around the web sides up to 2.25” from the bottom for the 18 ksi stress range design. It also resulted in two layers of longitudinal CFRP for the 36 ksi stress range design, the inner layer wrapped around the web sides up to 0.5” and the outer layer went up 3” on the web sides. External CFRP stirrups were used to prevent the longitudinal CFRP from premature separation. Beams 2 and 4 successfully reached their target strengthening design levels and Beams 3 and 5 performed very well in fatigue.

ACKNOWLEDGEMENT

This research was made possible by funding from KDOT and the University Transportation Center located at the University of Missouri, Rolla. **Prestressed Concrete Inc**, of Newton, Kansas provided the pre-tensioned prestressed concrete T-girders tested under this study. Master Builders Technologies, Cleveland, Ohio provided the FRP materials for strengthening. Special thanks are extended to Dave Meggers and Steve Burnett of KDOT, Bob Snider of Master Builders Technology, and Calvin Reed of Wilson and Company for their assistance with this research.

Thanks are further extended to Ken Hurst, Loren Risch and Steve Burnet for their interest in the project and their continuous support and feedback that made it possible to arrive at important findings advancing the state of the art.

TABLE OF CONTENTS

APPENDICES

LIST OF TABLES

LIST OF FIGURES

CHAPTER 1

INTRODUCTION

1.1 OVERVIEW

Many of the bridges in the United States are labeled as structurally deficient. A large number of these bridges were built in the 1960's and 1970's. Over the years, the bridges have aged due to the deterioration of their structural materials or have been overloaded. The overloading of the bridges is due to the fact they were designed to carry a lighter volume of traffic compared to today's massive standard truck loading. The time has now come to either repair the existing bridges or build new ones. Building new bridges is very costly. Accordingly, there have been many attempts to invent less expensive ways to repair and strengthen bridges. Repairing or replacing the bridge deck is a relatively inexpensive and easy process. The expensive part arises when bridge girders need to be replaced. For the past fifteen to twenty years researchers have been trying to develop cost effective ways to repair and upgrade the bridge girders. One of the most popular ways is to strengthen such girders with externally bonded Fiber Reinforced Polymers (FRP).

FRP is a composite material that is composed of fibers that are generally made out of Carbon, Glass, or Aramid. The aerospace industry was the first to introduce this material in modern times. Then, the automotive industry started using composites in manufacturing automobile parts. In recent years, composites found yet a new application in Civil Engineering in strengthening damaged structural girders, columns, and slabs. FRP can be used to help increase both the flexure and shear capacity of the beam as well as its flexural stiffness. FRP is typically applied to the tension face of the

beam by using a high strength polymer matrix. FRP is a very brittle material having a linear-elastic behavior to failure along the fiber direction. Other advantages of this material are its high Young's Modulus (E), high ultimate strength, ease of application, and lightweight compared to other materials.

1.2 OBJECTIVES

The objective was to set up an experimental program that would test a number of pre-cracked Prestressed Pretensioned Concrete (PC) T-girders. The first of these girders (Beam 1) was tested as a control beam, while the remaining (Beam 2, 3, 4, and 5) were strengthened with Carbon Fiber Reinforced Polymer (CFRP) then tested. The goal was to design the CFRP to control the stress range under service load conditions in the prestressing strand of the strengthened beams to 18 ksi in Beams 2 and 3 and 36 ksi in Beams 4 and 5. Static tests were run on specimens 2 and 4 to determine the monotonic strength and stiffness degradation of these beams. Fatigue tests were also run on specimens 3 and 5 to examine their long term serviceability performance.

1.3 SCOPE

Chapter Two reviews the studies addressing strengthening of pre-cracked and prestressed concrete beams as well as fatigue behavior of strengthened concrete members.

Chapter Three addresses the experimental test setup and the strengthening process of PC girders. Specimen geometric and material properties, experimental setup and procedure, and the pre-cracking process will be described here. Beam strengthening details will also be presented in a thorough way that is ready to implement into KDOT specification documents.

Chapter Four shows the design steps for strengthening the PC girders with CFRP to satisfy certain serviceability limit states. This design covers both flexure and shear. An incremental deformation analysis approach combined with iterative serviceability-strength design checks will be used for calculating the needed CFRP for strengthening.

Chapter Five presents the experimental, analysis and comparative results of the tested beams. It further discusses the findings and their implication on FRP design, state of practice, construction procedures and KDOT implementation.

Chapter Six presents the conclusions reached and provides suggestions or recommendations for future research in the area.

CHAPTER 2

LITERTURE REVIEW

This chapter covers the review of all the papers that were published on the topic of interest. Articles on FRP flexural strengthening of PC girders and fatigue performance are highlighted.

2.1 PC STRENGTHENING REVIEW

Currently, there are that many articles that deal with strengthening of PC bridge girders with FRP that have been fatigued. For that reason the literature that will be looked into will deal with pre-cracked RC beams, fatigued RC beams and prestressed systems strengthened with FRP.

Arduini and Nanni (1997) performed an analytical study that investigated pre-cracked RC beams with different geometric and material properties. The thickness and mechanical properties of the FRP was also varied to give designers a guideline for design. The study looked into two categories, stiffening and strengthening. They showed that stiffening can also be reached. For any FRP, a stiffer FRP will give better results as well as more layers of FRP will provide more stiffness. The strengthening of the pre-cracked beam is less reliable. Three main factors can limit the strengthening process. They are the shear strength of the existing member, failure mode of the system to be repaired and finally the deflection of the new service load.

Shahawy and Beitelman (1999) did experimental work on RC T-beams that were tested under static and fatigue loading conditions. The cross-sectional properties of all the tested beams were identical and the beams were tested under 4-point bending. The fatigue loading was sinusoidal and the loads varied from 25% to 50% of the ultimate

capacity. The three FRP methods use dfor this study were 1) Not plated, 2) Plated on the bottom of the web only and 3) Plated by wrapping the entire web. Different numbers of FRP layers were used on the beams. For the beams that were tested statically, the ones that had plates all the way up the web performed better. Delamination occurred in the beams that just had the bottom web plated with FRP. Under fatigue the beams were able to handle over 2 million cycles.

El-Tawil et al. (2001) performed an analytical study of RC T-beams. They tried to use strain compatibility to develop a model that correlated with previous work on static and fatigued RC beams strengthened with FRP. Two factors that were considered in the model were strain hardening of the steel reinforcement and tension stiffening of the concrete. The study concluded that the strain compatibility model could predict the behavior of the static and fatigue response of the RC beams.

Hassan and Rizkalla (2001) tried different approaches for flexural strengthening of prestressed bridge slabs. FRP rods and sheets were both used in the strengthening process. The bridge slabs that were used consisted of one simply-support slab and two overhanging cantilevers. A nonlinear finite element program was also introduced for this work.

Reed (2002) took 30 year old prestressed T-Girders and repaired them with FRP. The girders were existing bridge girders that may have been over loaded at one time in their life span. The girders were repaired and then strengthened with FRP in order to maintain the stress in the strand to 37 ksi. All the girders that were tested failed prematurely. This current research is an extension of the work that was done in this project and this research was phase I of this current research.

CHAPTER 3

EXPERIMENTAL TEST SETUP OF PC GIRDERS

This chapter describes the prestressed concrete specimens used in the experimental program, their geometric and material properties, the experimental test setup, their precracking process, and the CFRP strengthening procedure for the different full scale tests performed.

3.1 SPECIMEN GEOMETRY PROPERTIES

The pre-tensioned prestressed concrete T-beams were cast at the prestressed concrete plant, Prestressed Concrete Inc, in Newton, Kansas. Each specimen was 16.5 ft long and had an 18-inch flange width, 4-inch flange depth, a tapering web ending at 4-inch width at the bottom, and 14-inch total depth, Figure 3.1. Two 3/8-inch straight prestressing stands were placed in the web at 2 and 4 inches from the bottom respectively. Four layers of mild D4 welded wire reinforcement (WWR) were used longitudinally at depths of 1.25, 3, 4, and 7 inches from the top, to hold the shear stirrups in place. Shear reinforcement confined the Tee section with D4 WWR in the

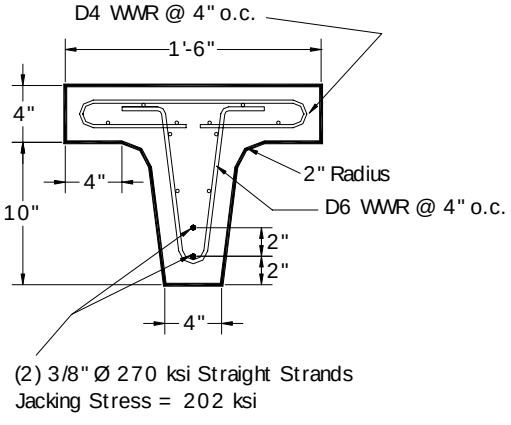

FIGURE 3.1. Cross-section geometry of specimen.

flange and D6 WWR in the web, both at 4 inch spacing, Figure 3.1, shows a cross-sectional view of the T-beam along with the internal steel layout. A crack former was embedded at the bottom of the cross section in three locations to guarantee that a crack would initiate there, Figure 3.2. These locations are at mid-span and 3.5 feet to both sides of mid-span, outside of the constant moment region. The specimen properties and geometry of the beams were chosen so that they would relate to the beams that were used in phase I of this project.

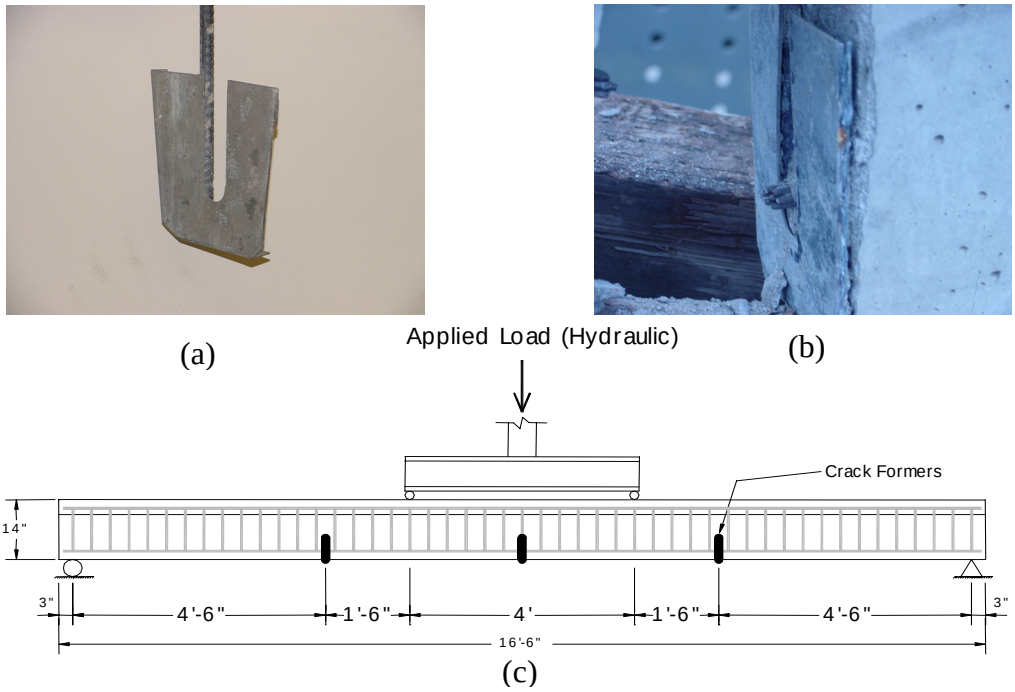

FIGURE 3.2. a) Crack former b) Crack former in beam c) Location of three crack

3.2 MATERIAL PROPERTIES

The plant that manufactured the T-beams provided the concrete strength of the specimens through standard cylinder testing. The average 28-day strength was found to be 7,043 psi, while the specimens were designed to have a nominal concrete strength of 5000 psi. The actual 28 day value of f'_c was used for all the analysis and

strengthening design calculations. The concrete, at the critical section, was assumed to carry no tensile stresses after the strengthening design process because all the beams were pre-cracked prior to applying the CFRP sheets. Refer to section 3.4 for the precracking process. The prestressing strands were assumed to have an elastic modulus of 28,300 ksi and an ultimate strength of 270 ksi. Prestressing plant reports of materials used can be seen in Appendix C. After calculating all losses (See Appendix A for Loss Calculations), the average prestressing stress of both strands was estimated to be 165 ksi. The reinforceing steel used for stirrups and longitudinal top and side reinforcement was assumed to have yield strength of 80 ksi and modulus of 29,000 ksi. Master Builder's Technologies of Cleveland, Ohio provided the CFRP sheets. The Master Builder's CF130 carbon fiber system was chosen for this project. The CFRP, along the fiber direction, behaves linearly elastic to failure and a reported modulus of 33,000 ksi based on the fiber area (0.0065 inch thickness for each layer) and ultimate strain of 0.017 in/in (M-Brace 1998). Experimental coupon testing showed that the modulus is accurate and yielded a lower average ultimate strain of 0.014 in/in (Reed 2002).

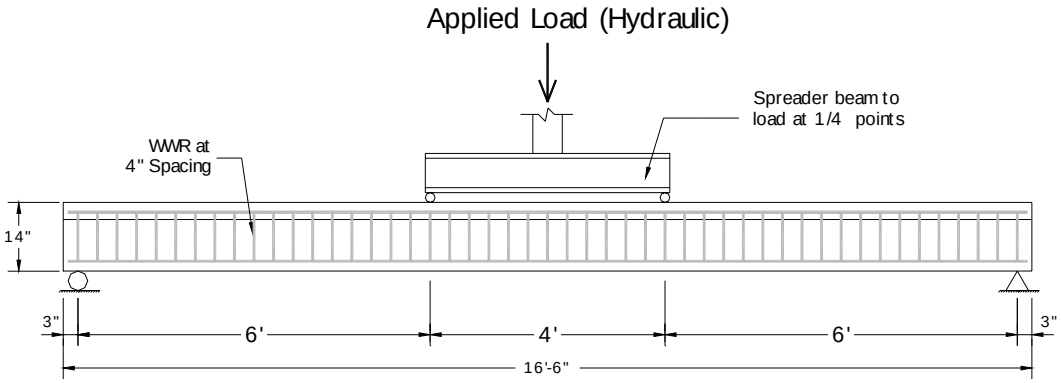

FIGURE 3.3. Flexural test setup.

3.3 EXPERIMENTAL TEST SETUP

The beams were tested in four-point bending to allow critical stresses to develop along a sizeable region instead of a single section, as shown in Figure 3.3. The clear span was 16 ft with a shear span of 6 ft and leaving 4 ft for the constant moment region. The tests were run in load-control, which is known to yield accurate failure predictions in concrete members at a reasonable loading rate. The specimens were tested either monotonically or cyclically. When the specimens were loaded monotonically, a loading

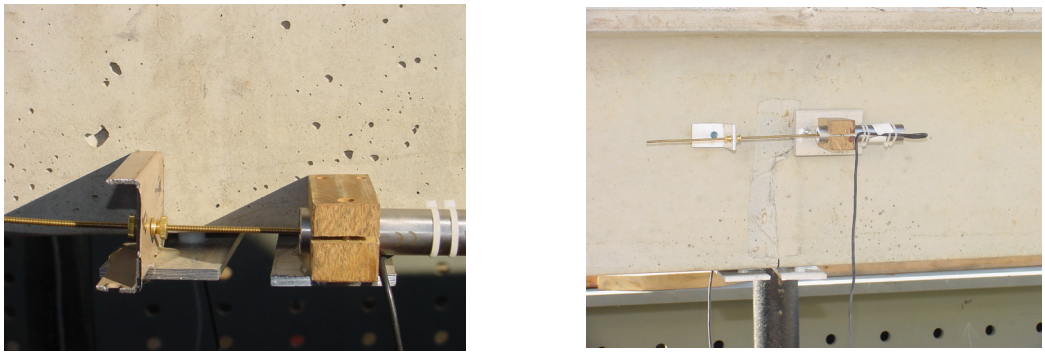

(a) (b)

FIGURE 3.4. a) LVDT to measure crack opening at bottom of beam b) LVDT to measure crack opening 5.75” from bottom.

rate of 500 lb/min was used. When the specimens were loaded cyclically, a frequency of 3 Hz was used to vary the load between the upper and lower load limits. Mid-span deflection was measured using two Linear Variable Displacement Transducers (LVDTs) mounted on either side of the flange. The average reading was typically reported to exclude rigid body twisting, if any. During the precracking stage, the crack width opening at the bottom of the web and 5.75 inches up the web side was also measured with LVDT's, see Figure 3.4. Electrical resistance strain gages were placed on top of the flange in the constant moment region, on the bottom side of the web (applied directly to the CFRP, when applicable), at the level of the strand (applied to the CFRP), on the transverse CFRP, and directly on the prestressing strand for one specimen to record strain values during loading. The specific locations of strain gages are shown for all specimens on the strain gage map, Figure 3.5.

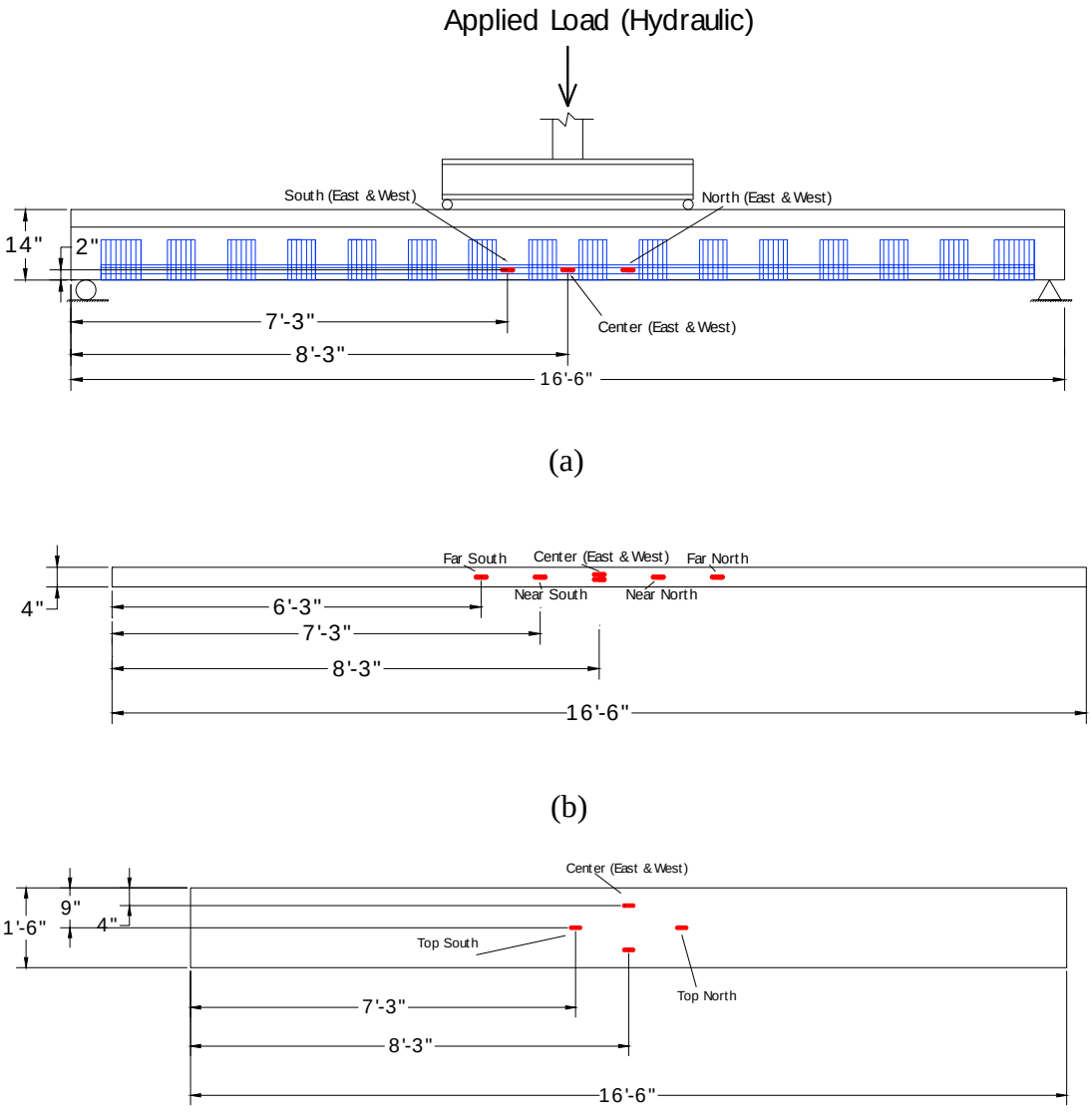

FIGURE 3.5. (a) Gage location for web side (b) Gage location for top flange (c) Gage location for web bottom, Note: Beam 2 had gages on stirrups while it did not have any gages on web side FRP (2" up) in longitudinal direction.

3.4 PRE-CRACKING PROCESS

Before the beams were strengthened, they were all loaded past their mid-span cracking moments. The first loading cycle was performed to initiate the mid-span crack. The beams were loaded to 9 kips. This load level was chosen because it enabled the

mid-span crack to be clearly visible. Twenty-five additional loading cycles were then applied to identify the crack opening load and to back calculate the existing prestressing force. Beam 1 was loaded to failure at this point and was used as a control specimen for all the strengthened beams. The beams were loaded using the 500-kip capacity Havens Steel test frame and all remaining testing was done there, Figure 3.6.

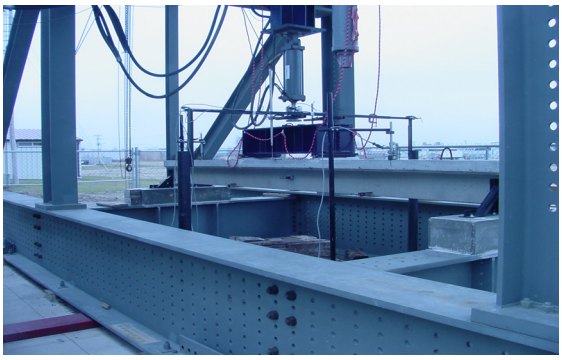

FIGURE 3.6. Beam in test frame.

3.5 STRENGHTENING PROCEDURE

The T-beams were flipped over onto their flanges and strengthened while in the upside down position for ease of applying the CFRP. To accomplish this smoothly without inducing any additional stresses, the center of gravity of the cross-sectional area was identified as a rotation axis point. At this point, a 7/8” diameter hole was drilled 3” deep. Next a 3/4” diameter bolt, 6 inches long (the head of the bolt was cut off) was inserted and epoxy-grouted into the hole, Figure 3.7. After letting the epoxy dry, the beam was then supported on side blocks right at the inserted rotation bolts and the beam was then rolled over onto its flange. The beam was then supported by at least three points along its spans to reduce tensile stresses the flange of the inverted T under its self-weight.

FIGURE 3.7. Inserted side bar used for flipping beams over.

FIGURE 3.8. Concrete surface preparation by sandblasting.

The next step was to sandblast the beam over the regions that the CFRP was to be applied. For this, the entire web was sandblasted using a fine graded silica sand. This was done to remove any dirt or other foreign substance that was attracted to the concrete and to leave a clean etched surface to which the CFRP could easily bond to, Figure 3.8.

Once the beam was sandblasted, the CFRP was cut to the dimensions specified by the design, see Chapter 4. The flexural CFRP fibers run in the longitudinal direction and the shear CFRP fibers run transversely, so it was important to cut the CFRP in the correct direction. Another helpful step was to apply duct tape to the beam that outlined the limits of the areas to be covered by CFRP. The duct tape should be placed so that the outer limits of the CFRP should be adjacent to the duct tape edges, Figure 3.9.

FIGURE 3.9. Placement of duct tape.

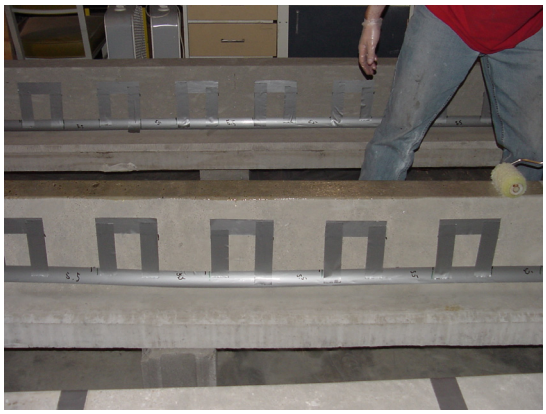

FIGURE 3.10. Applying the primer layer.

The final step was to apply the CFRP sheets. This was done using a three step wet lay-up process. A two-part primer is first applied to all the beam surfaces to be bonded to CFRP. The primer was applied by using a paint roller, see Figure 3.10.

(a) (b)

FIGURE 3.11. a) Applying the resin layer b) Straightening the CFRP fibers with a ribbed roller.

Immediately following the primer application, epoxy putty was used to fill any small holes that existed in the concrete. This was done to give the FRP a larger and more uniform bonding surface. The next step was to apply the FRP. The epoxy resin was first applied to the beam using the same paint roller, Figure 3.11(a). Next the FRP was placed over the resin. Another layer of resin was then added and the FRP was straightened with a ribbed roller, Figure 3.11(b). This was done to remove any air bubbles that were trapped under the first layer of CFRP sheet. If more than one layer of CFRP was required by design, then the second layer was immediately placed on the beam followed by another layer of resin over the CFRP then rolling it with the ribbed roller again to remove any air bubbles. This procedure was continued until the desired numbers of CFRP layers were installed in place. It must be noted that all layers must be applied before the resin is allowed to cure. This guarantees that a continuous bond is maintained between all layers.

3.6 EXPOSING PRESTRSSING STRAND

During experimental fatigue testing of Specimen 3 strain gages were also installed on the prestressing strands to verify the stress range that the strand was actually undergoing. This applies to specimen 3, the beam that was cycled under 18 ksi stress range fatigue. To do this, the concrete around the upper strand in the constant moment region, at 12 inches from mid-span, between two of the external stirrups was removed. First, holes were drilled that went completely through the web with a concrete drill along the outline of the desired concrete area to be removed, Figure 3.12. Then, an air-powered chipper was used to carefully remove the concrete. Extreme care was taken when removing the concrete bonded to the strand to avoid indenting or notching it, Figure 3.13.

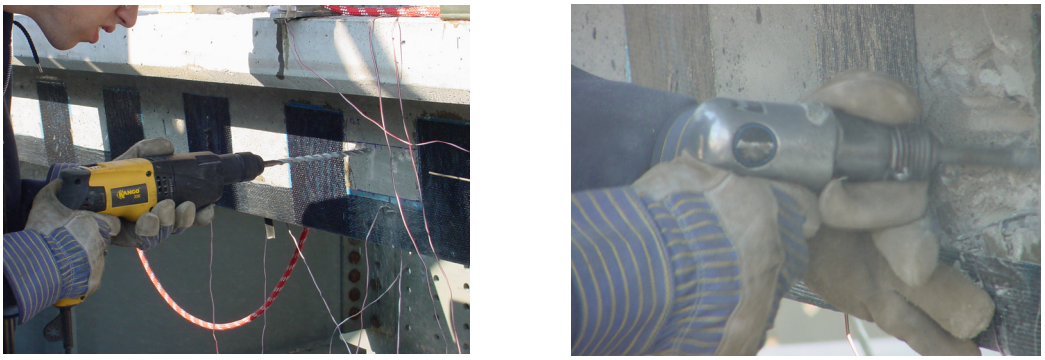

(a) (b)

FIGURE 3.12. a) Drilling the holes for strand exposure b) Chipping concrete away from strand

3.7 STRAIN GAGE APPLICATION

There were three types of electrical resistance strain gages used and they were all manufactured by Measurements Group, Inc. EA-06-250UN-350 gage were used for all the gages that were applied directly to the CFRP. This gage was chosen because its gage width was roughly the same as the width of one of the fiber rows. EA-06-20CBW-120 gage was used for all the gages that were bonded to the concrete. It is recommended that the minimum gage length be three times the largest aggregate size. In the case of exposed upper strands, gages were applied directly to the strand in the constant moment region and the gage used there was a EA-06-015DJ-120, Figures 3.13 and 3.14. For this gage, the width of one wire in the prestressing strand governed the gage selected. When applying the concrete gages, the objective is to create a smooth, even, nonporous surface for best possible bonding. For all gages that were placed on concrete, a grinder was used to remove any high surface points that existed on the surface. The surface was then lightly sanded by using 320-grit abrasive paper to level off the gaging area. Next, the surface was cleaned using M-Prep Conditioner A

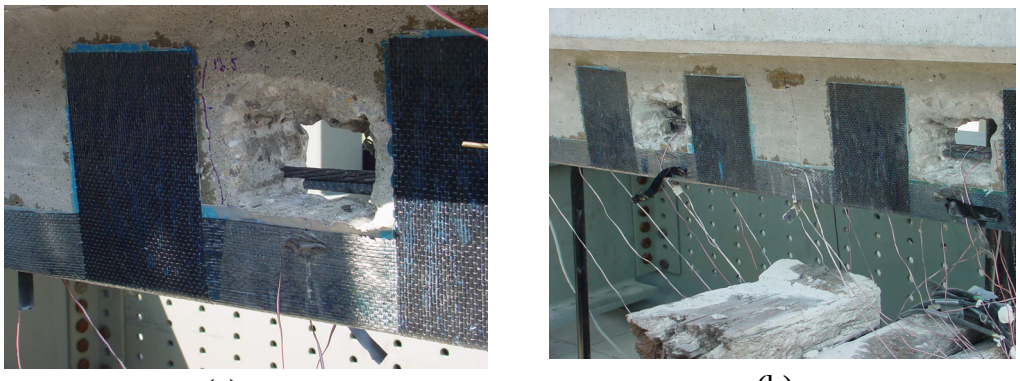

(a) (b)

FIGURE 3.13. a) Exposed strand b) Both exposed strand areas, on either side of mid-span.

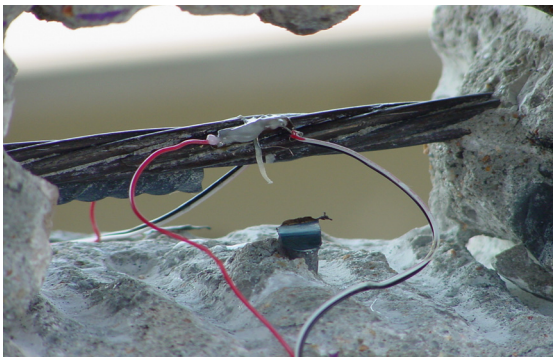

FIGURE 3.14. Placement of strain gage on exposed prestressing strand.

and M-Prep Neutralizer 5A. Applying the acidic Conditioner A solution to the surface on and around the gaging area, using a brush and gauze sponges removed all possible contaminates. The surface was then rinsed off with the Neutralizer agent to reduce the acidity. It was then allowed to dry off for a few minutes. The surface was then ready to apply the gages to. Normal procedures were followed for bonding the gage to the prepared gaging surface. This includes cleaning the strain gage box with the Neutralizer 5A solution, applying the tape to the strain gage, and then applying the gage to the surface of the concrete, CFRP, or strand by using the M-Bond AE-10 or the M-Bond 200. Maintaining accurate gage alignment and even application of pressure, as the adhesive is cured, are more difficult to sustain when bonding longer gages. Thus, it requires two individuals to be involved when applying the gages to the surface of the beam. A slower curing adhesive, like M-Bond AE-10 allows more time for realigning the gage, whenever it is necessary. Thus this was the adhesive used to bond the gages on the concrete and CFRP. It also enabled the use of a suitable pressure pad and clamping fixture as outlined in Vishay Measurements Group Tech-Tip TT-610, Strain Gage Clamping Techniques (Vishay 2001). The M-Bond 200 was used on the

prestressing strand wire due to the fact that the adhesive dries in less than five minutes and clamping the gage to the strand was less difficult.

Soldering the lead wires was the next step. Concrete and adhesive fillers are relatively poor heat conductors. Accordingly, care was taken when soldering leads onto the strain gages to avoid excessive heating of the tabs. Normal procedures were followed when soldering the lead wires onto the strain gage. After each lead wire was soldered to an individual strain gage, it was checked with a voltmeter to verify that it was working properly. When utilizing one active strain gage (quarter-bridge configuration), Micro Measurements suggests the use of a three-lead wire system.

The gages also required protection from the outdoor environment. To protect the gages, application of a polyurethane coating was done. After the polyurethane was allowed to dry, a layer of melted wax was brushed over the gage. The final step in protecting the gage was to apply a layer of M-Coat J. This prohibited any outside containment to harm the gage over a period of time. It also protected the gage from moisture during the fatigue process.

CHAPTER 4

FRP STRENGTHENING DESIGN FOR PC GIRDERS

This chapter will address the details of the design procedure that was used to satisfy the target strengthening requirements. Two main CFRP flexural strengthening designs were developed for this experimental program. The first was to design the amount of CFRP to limit the average stress range in the prestressing strand to 18 ksi under service live load and relate that to the ultimate level of strengthening. Two beams (2 and 3) were strengthened using this design. Beam 2 was loaded monotonically to failure. Beam 3 was cycled just over a million times before it was monotonically loaded to failure. The second design was based on the serviceability requirement of maintaining a 36 ksi average prestressing strand stress range under service live load conditions. It is also directly related to the ultimate strengthening index. This design was implemented for the remaining two beams (4 and 5). Beam 4 was monotonically loaded to failure while beam 5 was cycled over three million times before it was also monotonically tested to failure.

4.1 FLEXURAL DESIGN PROCEDURE

A non-linear analysis program solving for the moment-curvature and the load-deflection response of simple prestressed concrete tapered T-beams was used for strengthening design in this study. The program uses the incremental deformation approach to generate the sectional response. It was developed during phase I of this project by Calvin E. Reed (Reed 2002). An iterative design approach was devised here to determine the amount of CFRP that was needed to maintain the desired stress range under service load while producing the ultimate moment specified by AASHTO. From

the precracking process and corresponding calculations, the stress in the strand was found to be 165 ksi. (see section 5.1 for complete details). For the 18 ksi stress range design, the average stress estimate in the prestressing strands corresponding to the upper service live load level was 183 ksi. The final design was completed once the analytical ultimate nominal moment capacity (M_n), calculated by the program with the beam geometry, material properties, and added amount of CFRP, converged at the same factored ultimate moment capacity (M_u) that AASHTO 3.22.1 specifies, which relates to service live load as follows:

$$M_u = 1.3\left[M_D + 1.67\left(M_{LL}\right)\left(1+I\right)\right] \tag{4.1}$$

where M_D is the dead load moment of the beam (4.3 k-ft), M_{LL} is the live load moment, including the weight of the spreader beam, corresponding to the upper limit of the target stress range. I is the impact factor found using AASHTO equation 3.8.2.1

$$I = \frac{L}{L+50} \leq 0.3 \tag{4.2}$$

where L is the length of the loaded area in feet. The impact factor is conservatively taken as 0.3 in all of the design calculations.

The process starts by performing section analysis for the unstrengthened beam. The program plots the average prestressing stress at the centroid of strands against the applied moment, Figure 4.1. The desired stress range is mapped in place on the y-axis of the graph. Then, the service moment ($M_{service}$) corresponding to the upper level of stress range is determined, Figure 4.1. The corresponding live moment is simply:

$$M_L = M_{service} - M_D - M_{SB} \tag{4.3}$$

where M_{SB} is the maximum moment due to the weight of the spreader beam used to impose 4-point bending (1.4 k-ft), M_L is the live moment excluding the weight of the spreader beam.

The M_L moment is substituted into equation (4.1) to determine M_u, which in turn is not expected to equal to M_n from the analysis in the first few iterations. Accordingly, CFRP sheets are added to the section and a new section analysis is performed to generate the updated Prestressing Stress-Applied Moment graph, Figure 4.2. The steps in iteration 1 are then repeated up to convergence. Step by step procedures on calculating M_u is as follows:

1. Run the program with the desired amount of CFRP and obtain a curve like the one in Figure 4.1.
2. After specifying a lower limit for the applied moment (1.5 k-ft in this case), find the average prestressing stress for that moment. The lower limit of moment is specified to prevent the actuator separation from the beam during each fatigue unloading cycle and to prevent impact/shifting during each fatigue reloading cycle
3. For the value found in step 2, add the desired stress range to that value, this will be the upper limit of the prestressing stress.
4. $M_{service}$ is the moment which is found by taking the value which corresponds to the upper stress range
5. M_L is then found using equation (4.3).
6. Finally M_u is found by using equation (4.1) and compared to M_n.

7. If M_n is less than M_u, then more CFRP needs to be added for convergence to happen. In case M_n is greater then M_u, some CFRP needs to be removed for convergence to take place.

Detailed calculations, that are specific to the two design cases considered, are presented below:

Case 1: 18 ksi stress range:

1. For the first iteration, using the bare beam, M_n was 48.9 k-ft. With a stress range of 18 ksi and $M_{service}$ was 26.7 k-ft. Using equation (4.3), M_L became 21.0 k-ft and using equation (4.1), M_u became 68.8 k-ft. Since M_u is greater than M_n, CFRP needs to be used

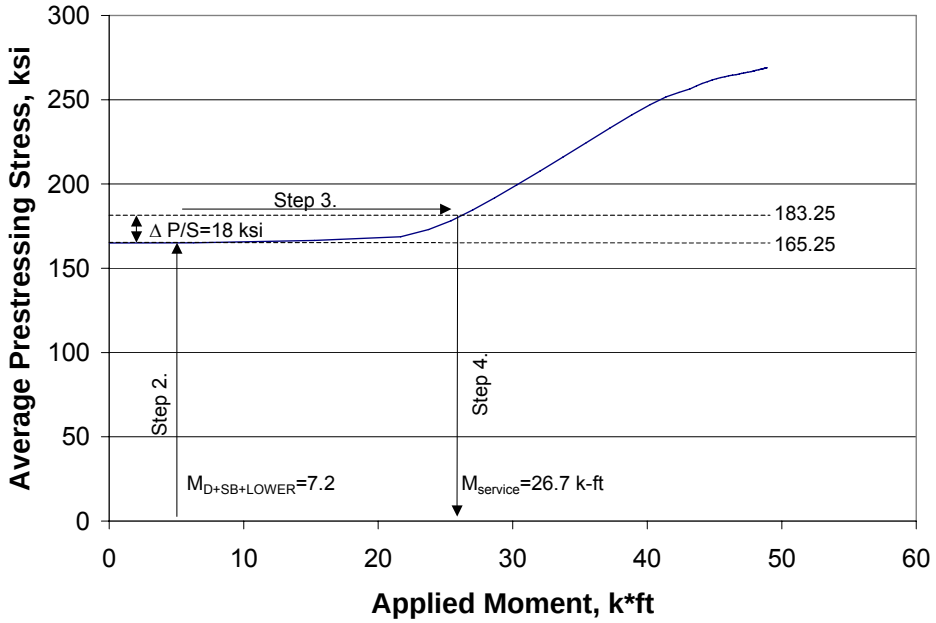

FIGURE 4.1. Strand stress variation with Applied Moment: Design iteration 1 (Unstrengthened Beam).

: CFRP

that was selected (A_f= 0.0455 in^2). With a stress range of 18 ksi,

$M_{service}$ was 27.6 k-ft. Using equation (4.3), M_L became 21.9 k-ft and using equation (4.1), M_u became 71.4 k-ft. Since M_u was greater than M_n, more CFRP needed to be applied.

3. The third iteration had M_n of 71.9 k-ft for A_f= 0.052 in^2, $M_{service}$ with an 18 ksi stress range was 27.7 k-ft, M_L became 22.0 k-ft and M_u was 71.6 k-ft. These values are close to convergence, however a small amount of CFRP needs to be added so that the longitudinal CFRP will have a final height higher than the bottom prestressing strand to enable mounting strain gages at that level.

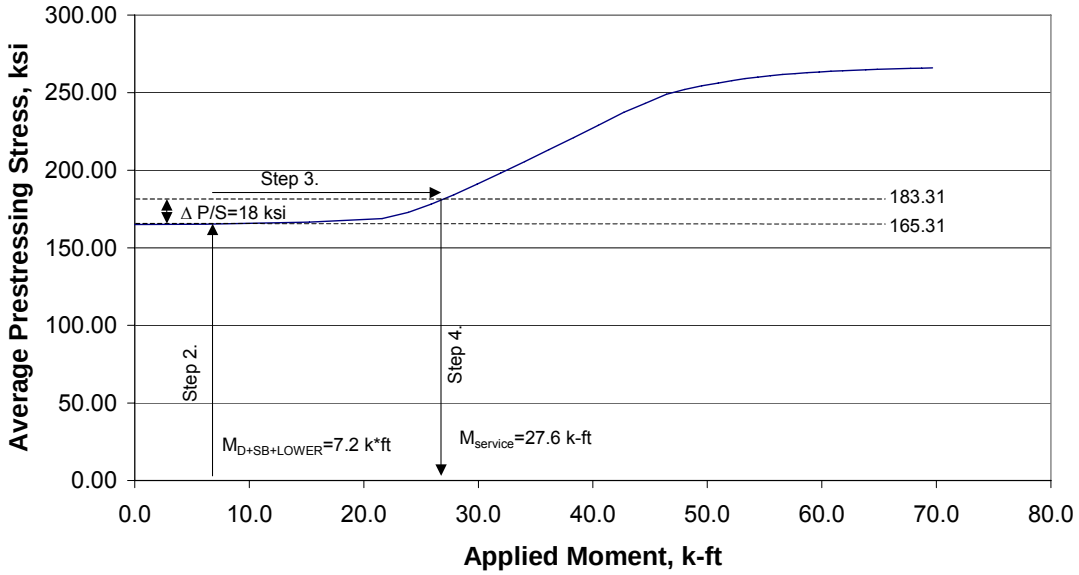

FIGURE 4.2. Design iteration 2 (CFRP sheets included).

with A_f= 0.05525 in^2. $M_{service}$ was 27.66 k-ft and, M_L was 21.96 k-ft. The M_u became 71.52 k-ft, which is acceptable, due to the explanation in step 3 above.

This final trial was the design that was used for the 18 ksi strengthening, Figure 4.3.

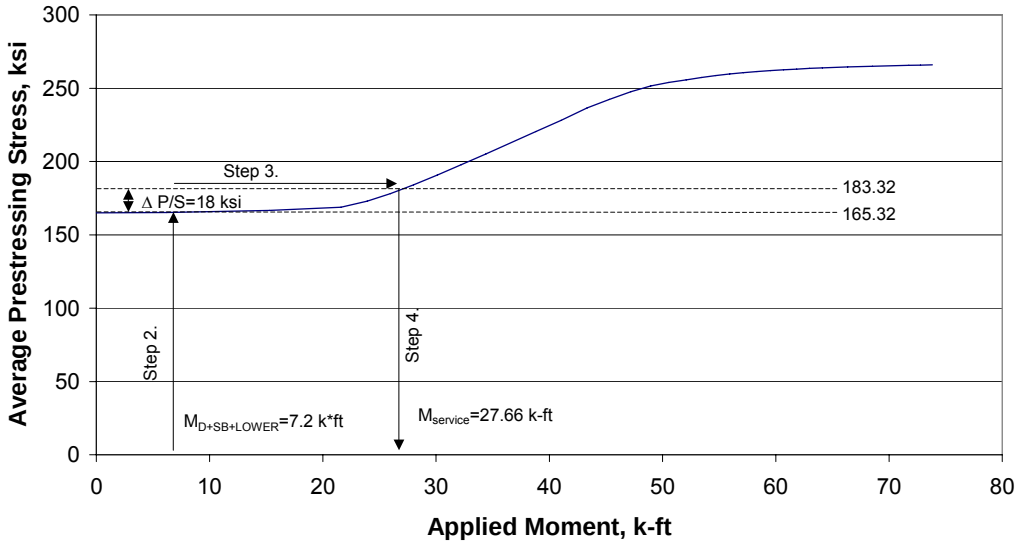

FIGURE 4.3. Final converged design curve for 18 ksi.

Figure 4.4 shows the final design of the longitudinal CFRP used to furnish the 18 ksi stress range. One layer of CFRP sheet covering the entire bottom of the web and wrapping 2.25 inches up the two sides is applied along the entire clear span of the beam.

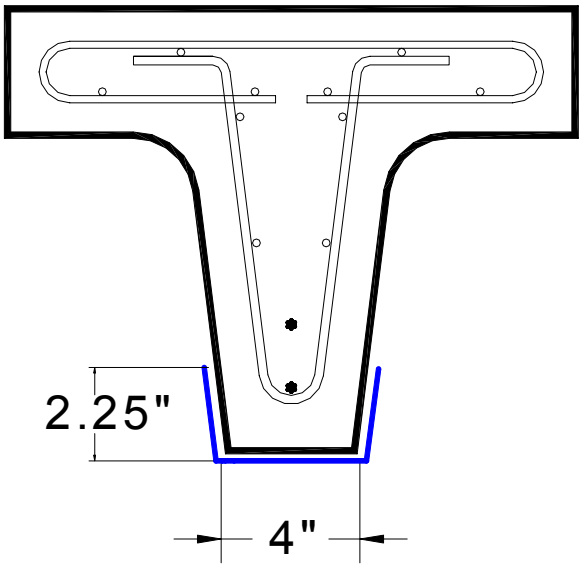

FIGURE 4.4. Strengthening design details for 18 ksi.

This design offers an ultimate nominal moment capacity of 73.8 k-ft. and a live moment level of 21.96 k-ft. This corresponds to a strengthening index of 51% and a service live load upgrade index of 64% where:

$$Strengthening\ index\,\% = \frac{\overline{M}_n - M_n}{M_n} * 100 \qquad (4.4)$$

$$LL\ upgrade\ index\,\% = \frac{\overline{M}_L - M_L}{M_L} * 100 \qquad (4.5)$$

where $\overline{M}_n$ is the nominal ultimate moment of the strengthened beam, M_n is the nominal ultimate moment of the unstrengthened beam, $\overline{M}_L$ is the live load moment of the strengthened beam, and M_L is the live load moment of the unstrengthened beam. Finding both the live load moments are done by taking their respective M_n and using equation (4.1) to back solve for them. For the use of equation (4.1) M_n is substituted for M_u.

Case 2: 36 ksi stress range:

1. For the first iteration, M_n was 80.7 k-ft for the amount of CFRP that was selected (A_f= 0.078 in^2). With a stress range of 36 ksi, $M_{service}$ was 33.90 k-ft. Using equation (4.3), M_L became 28.2 k-ft and using equation (4.1) M_u became 89.13 k-ft. Since M_u was greater than M_n, more CFRP needed to be applied.

2. The second iteration had M_n of 85.3 k-ft for A_f= 0.078 in^2, $M_{service}$ with a 36 ksi stress range was 34.47 k-ft, M_L became 28.77 k-ft and M_u was 90.74 k-ft. Once again M_u was greater than M_n, so more CFRP should be added.

3. The third iteration had M_n of 92.9 k-ft for A_f= 0.104 in^2, $M_{service}$ with a 36 ksi stress range was 35.24 k-ft, M_L became 29.54 k-ft and M_u was 92.91 k-ft. This design would have worked, however less CFRP on the web sides wanted to be used, per KDOT design.

4. The final iteration, which led to convergence, resulted in M_n being 93.0 k-ft for A_f= 0.0975 in^2. $M_{service}$ was 35.20 k-ft and after using equation (4.3), M_L was 29.50 k-ft. The M_u became 92.80 k-ft that is close enough to the value of M_n. This final trial was the design that was used for the 36 ksi strengthening. Other iterations could have been performed to get M_n and M_u even closer. However, this one was chosen since it was accurate enough from a design standpoint. Figure 4.5 shows the graph for this final design iteration.

Figure 4.6 illustrates the CFRP design converged to accomplish the 36 ksi

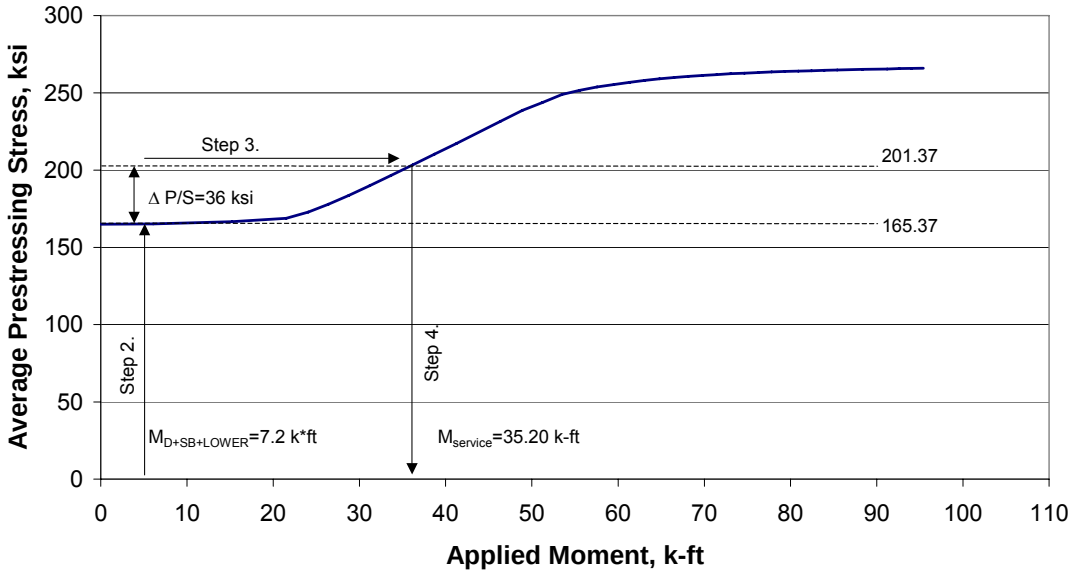

FIGURE 4.5. Final converged design curve for 36 ksi.

stress range. Two layers of CFRP sheets covers the bottom of the web extending up 0.5 inches up the sides of layer 1 and 3 inches on each side for the second layer. It is applied all the way along the clear span.

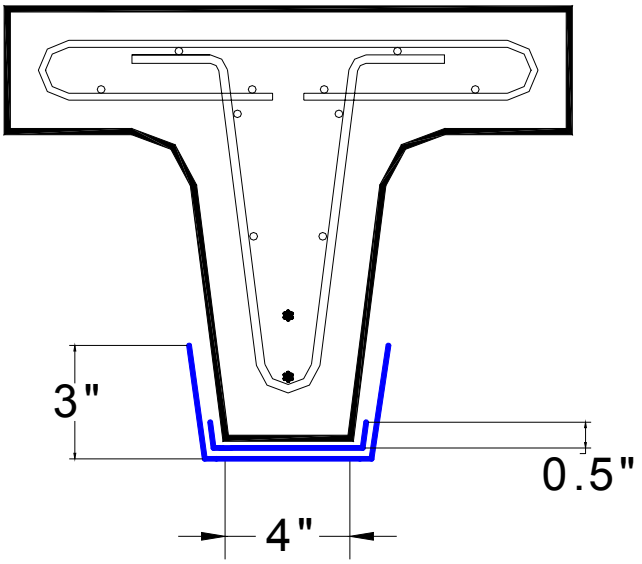

FIGURE 4.6. Strengthening design details for 36 ksi.

The 36 ksi stress range design yields an ultimate nominal moment capacity of 93.0 k-ft and a live moment value of 29.4 k-ft. This corresponds to a strengthening index of 90% and a service load upgrade of 113%. Figure 4.7 shows the curves for all three of the beams, un-strengthened, 18 ksi and 36 ksi strengthened beams.

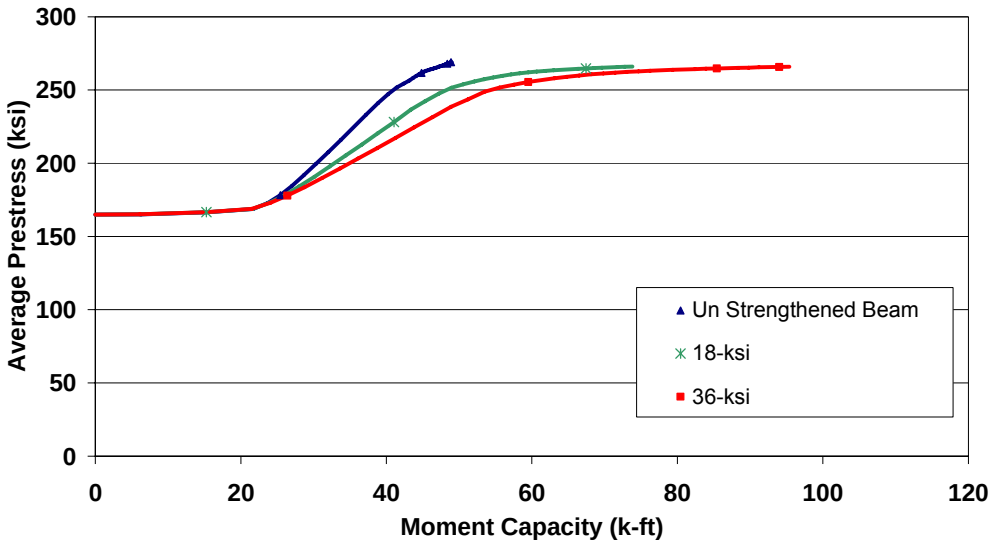

FIGURE 4.7. All three beams for prestressing strand stress range.

4.2 SHEAR DESIGN PROCEDURE

The beams were overly reinforced for shear with internal steel stirrups see Appendix B: Shear Calculations. However, external CFRP stirrups were still used to prevent the separation failure of flexural of CFRP due to horizontal shear cracking. The ACI 318-99 model on shear friction was used in the design. This model computes the tension force to be developed in transverse CFRP during horizontal shear cracking to maintain such cracking tightly closed. By limiting the level of tensile CFRP stresses, a stirrup distribution or spacing is obtained. To maintain consistent external stirrup layout for both flexural designs, the required stirrup dimensions and spacing in the case of 36 ksi stress range were implemented. The maximum axial tension in FRP is found first by taking the CFRP fiber area times the modulus of the CFRP fibers times the CFRP strain at ultimate flexural failure:

$$T = E_f A_f \varepsilon_{fu} \ \ in\, case\, of\ FRP\, rupture$$

$$= E_f A_f \left(\varepsilon_f = \frac{d_f - c}{c} .003 \right) \ \ in\, case\, of\ concrete\, crushing \tag{4.6}$$

Then the horizontal shear force per unit length of shear span is directly calculated:

$$V_{hu} = \frac{T}{L_a} \tag{4.7}$$

where V_{hu} is the horizontal shear force per unit length, L_a is the shear span. Thirdly, finding the tension force per unit length in the transverse CFRP from the shear friction model:

$$T_{sf} = \frac{V_{hu}}{\mu} \tag{4.8}$$

with μ=1.4. Finally, the area of transverse CFRP external stirrups per unit length is determined by specifying the allowable tensile strain of bonded FRP stirrups. ACI 440.2R-02 section 10.4.1.2 limits this strain (ε_{fe}) to 0.004. To be more conservative, this limit is reduced to 0.003 in the present study. This corresponds to FRP tensile stress f_{fe}=100 ksi

$$T_{sf} = \phi A_{vf} \varepsilon_{fe} E_f = .85 A_{vf} f_{fe} \tag{4.9}$$

where A_{vf} is the area of transverse CFRP used to prevent premature separation failure:

$$A_{vf} = 2nt_f w_f \tag{4.10}$$

with t_f is the thickness of one stirrup layer, w_f is the width of each stirrup, and n is the number of stirrup layers.

Based on the above equations, it was found that T=42.8 kips, V_{hu}=7.1 k/ft, and A_{vf}=0.06in^2/ft leading to the use of stirrups that are 5.5 inches wide and spaced 12 inches center to center. The two end stirrups were cut to be 8 inches wide to control any possible end shear cracks causing plate end shear stress concentration and premature separation. Also the stirrups were run 8 inches up the web, Figure 4.8. They were stopped at this height so that they did not get bonded to the rounded web-to-flange juncture to avoid inviting undesirable peeling off.

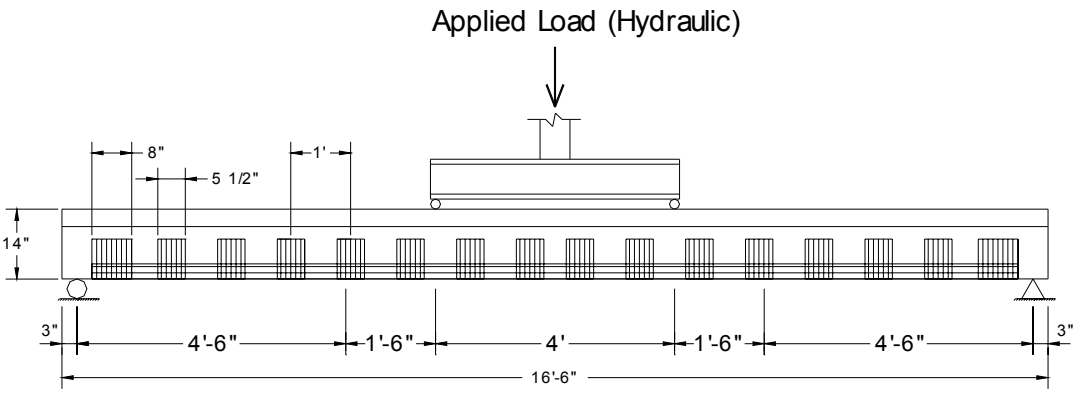

FIGURE 4.8. Stirrup layout.

CHAPTER 5

RESULTS AND DISCUSSIONS OF PC GIRDERS

This chapter will present and discuss the results that were obtained in the experimental program of the PC girders. This program consists of testing five PC T-girders. Specimen 1 was tested as a control beam with no additional strengthening applied. The analysis of the control beam resulted in the determination of the average prestressing strand stress history. Beams 2 and 3 were strengthened to limit the average stress range in the strand to 18 ksi under service load conditions. Beams 4 and 5 were strengthened to maintain a 36 ksi average stress range in the strand under service load conditions. Beams 2 and 4 were loaded monotonically to failure while beams 3 and 5 were cyclically loaded over a million times to examine their fatigue performance before they were monotonically loaded to failure.

5.1 PRESTRESSING STRAND STRESS CALCULATIONS

The average prestressing strand stress (f_{se}) induced in the girders, prior to any external loading, was first estimated by a series of calculations of prestress losses according to the PCI Handbook, see Appendix A for calculations. The calculations yielded an f_{se} value of 167 ksi. To verify the accuracy of this value, f_{se} was also back calculated from experimental results generated by pre-cracking all the beams. The first loading cycle involved initiating the crack at the crack former, which was embedded at mid-span, by overcoming the tensile strength (f_r) of concrete. The result of this first cycle will be used to estimate the effective tensile strength of the concrete due to debodning of metal crack former and concrete. To perform this calculation, the average prestressing strand stress, f_{se}, must be found first. This is done by loading and

unloading the beam (25 times for this project) to insure completely overcoming any residual concrete tensile strength at the extreme tension fiber. The results of the 2nd-10th cycles are used to determine the actual prestressing force, as that required to keep the crack just closed at zero concrete tension. The experimental crack opening load was, thus, needed to determine the prestressing force or stress. Having an LVDT bridging the cracked section and recording the crack opening displacement response at the bottom of the web was used to recover the external load needed to start opening the crack, see Figure 3.4a. Using an LVDT that is measuring vertical beam deflection will not give accurate crack opening load results since it provides global response data and not section-specific results. Bonded strain gages cannot be used for this purpose also since it gets damaged upon crack opening. By using the Applied Load-Crack Opening Displacement graph, Figure 5.1, the point of end of linearity identified to correspond to the load at which the crack begins to open.

The point at which the linearity ends is found to be 4.28 kips. This corresponds

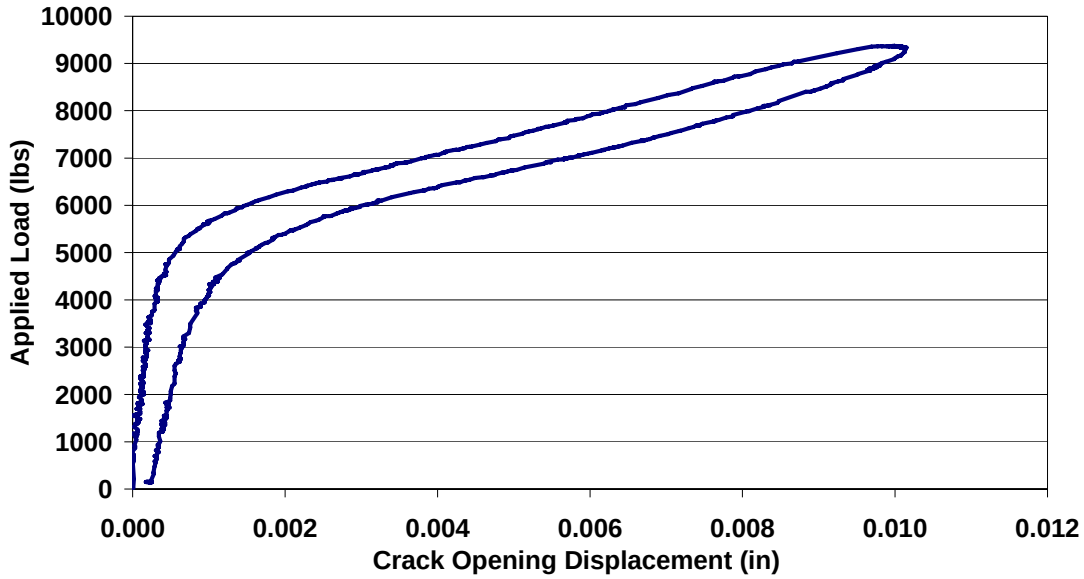

FIGURE 5.1. Crack opening response at web bottom mid-span for control beam.

to an applied moment (M_L) of 12.84 k-ft, excluding the contribution of the spreader beam. Knowing that the tensile strength (f_r) of concrete is equal to zero for crack re-opening, the following equation for f_r can be written for linear elastic analysis of transformed section:

$$f_r = -\frac{P_e}{A_{g_t}} - \frac{P_e e}{I_{g_t}} y_t + \frac{M_{co} y_t}{I_{g_t}} = 0 \qquad (5.1)$$

where $M_{co} = M_{DL} + M_{SB} + M_L$ = crack opening moment, A_{gt} is the uncracked transformed area, I_{gt} is the un-cracked transformed moment of inertia, e is the eccentricity of prestress force to the section centroid, y_t is the centroid height from the extreme tension fiber, P_e is the actual prestressing force found to be 28.26 kips. The average prestressing strand stress was directly determined to be 164.6 ksi:

$$f_{se} = \frac{P_e}{A_p = 2A_{strand}} \qquad (5.2)$$

This corresponds very well with the prestressing strand stress determined from losses calculation in Appendix A resulting in a value of 167 ksi. It can be seen in Table 5.1, that f_{se} calculated using the overall Load-Deflection curve for the LVDT recording beam vertical deflection at mid-span resulted in a higher estimate of f_{se}, 188.1 ksi. This is attributed to the fact that the end of linearity in the global Load-Deflection curve corresponds to a sufficiently widened crack beyond the initiation stage, Figure 5.2. Once f_{se} is determined, the initial tensile strength of the concrete can be evaluated using the results of the first cycle. This can still be found using equation 5.1 except that M_L will be higher than the one used for calculating f_{se} due to the contribution of concrete in tension. The external load corresponding to M_L is easily identified from end of linearity on Figure 5.3 to be 6.97 kips. M_L is, in this case, the moment that caused the first crack

to initiate at mid-span for the first loading cycle of the beam. This value is accordingly equal to 20.9 k-ft. The PCI equation for f_r is specified to be $7.5\sqrt{f_c'}$. Experiments show that the coefficient of f_r equation is seldom as high as 7.5 due to differential shrinkage tensile strains expected to pre-exist prior to loading. Solving equation (5.1) with the given numbers $f_r = 5.72\sqrt{f_c'}$.

	LVDT over crack at web bottom				LVDT for beam deflection at mid-span			
Cycle	**P_{co}-End***	**M_L**	**P_e**	**f_{se}**	**P_{co}-End***	**M_L**	**P_e**	**f_{se}**
1	6.98	20.93	40.60					
2	4.40	13.20	28.81	167.81	5.50	16.50	33.84	197.14
3	4.30	12.90	28.35	165.15	5.00	15.00	31.55	183.81
4	4.25	12.75	28.12	163.81	4.30	12.90	28.35	165.15
5	4.25	12.75	28.12	163.81	5.00	15.00	31.55	183.81
6	4.30	12.90	28.35	165.15	4.80	14.40	30.64	178.48
7	4.26	12.78	28.17	164.08	5.25	15.75	32.70	190.47
8	4.25	12.75	28.12	163.81	5.95	17.85	35.90	209.14
9	4.25	12.75	28.12	163.81	5.15	15.45	32.24	187.81
10	4.26	12.78	28.17	164.08	5.50	16.50	33.84	197.14
Averages for cycles 2-10	4.28	12.84	28.26	**164.61**	5.16	15.48	32.29	**188.10**

* P_{co}-End = External load at initation of crack opening from end of linearity

TABLE 5.1. Results for finding f_{se}.

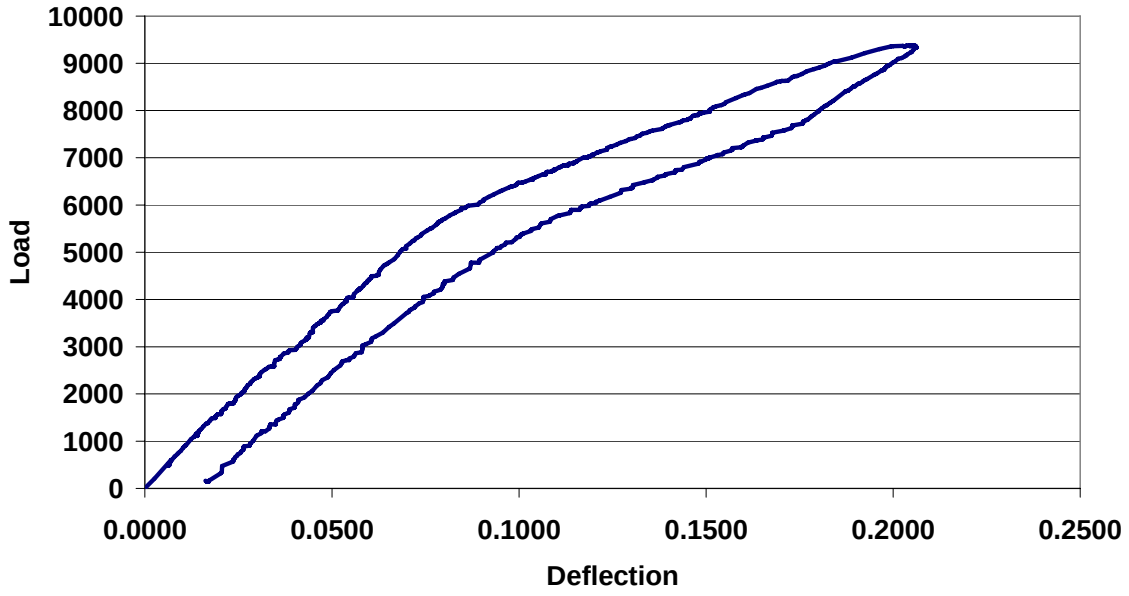

FIGURE 5.2. 2nd cycle of load-mid span deflection response for pre-cracking.

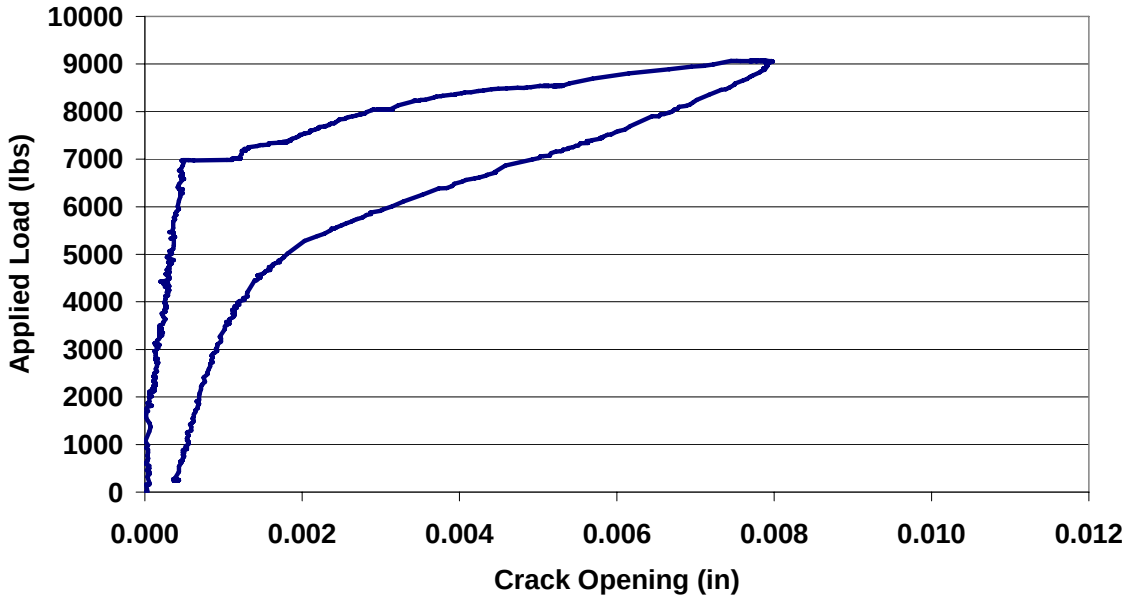

FIGURE 5.3. Load-crack opening for the 1st cycle used to determine f_r.

The graphs in Figure 5.4 show that as more cycles are applied to the beam, the loading and unloading paths draw closer to each other. This is due to overcoming the friction between the strand and the concrete resulting from the helical concrete interlock in between the surface wires along the strand. As more cycling occurs the friction and bond gradually degrades bringing the unloading path towards the loading

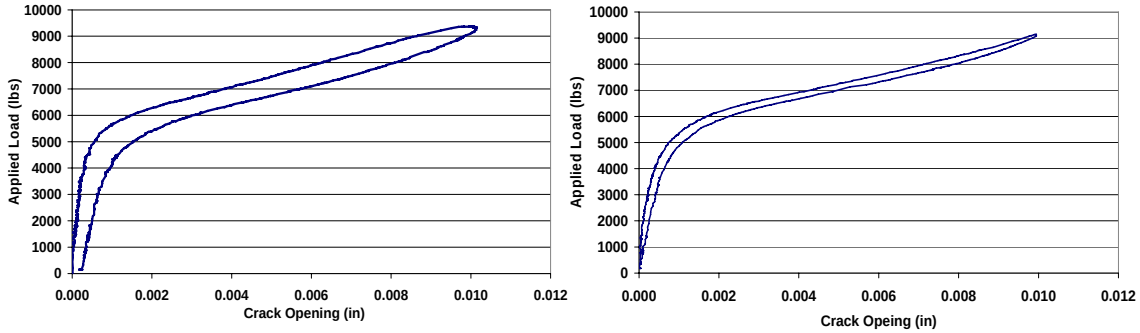

(a) (b)

FIGURE 5.4. Load-crack opening across crack former (a) 3rd cycles (b) 10th cycle.

5.2 EXPERIMENTAL BEHAVIOR OF PC GIRDERS

The experimental results of all the PC girders that were tested for this program are presented and discussed in this section. All load readings are recorded through a load cell connected to the loading actuator. All deflection readings are simultaneously taken by means of LVDT's at mid-span in the constant moment region, which are attached to the two sides of the flange and record vertical deflection. Strain gages were placed, see Figure 3.5, to record the strain values during loading. Load, deflections and strains are collected and synchronized by an Optum data acquisition system.

5.2.1 Control Beam (Beam 1)

This beam was loaded just past its cracking moment at the mid-span crack former so that the cracking load can be used to determine the actual prestressing force, as described above in, sections 3.4 and 5.1. This pre-cracking was also important to establish a similarity in the specimen condition with the decommissioned girders tested under phase I of this project. The control beam will serve as a baseline for all the strengthened beams. Figure 5.5 shows the load-deflection plot of the control beam. This deflection data was recorded at mid-span and the plotted curve reflects the average deflection of the two top flange LVDT measurements.

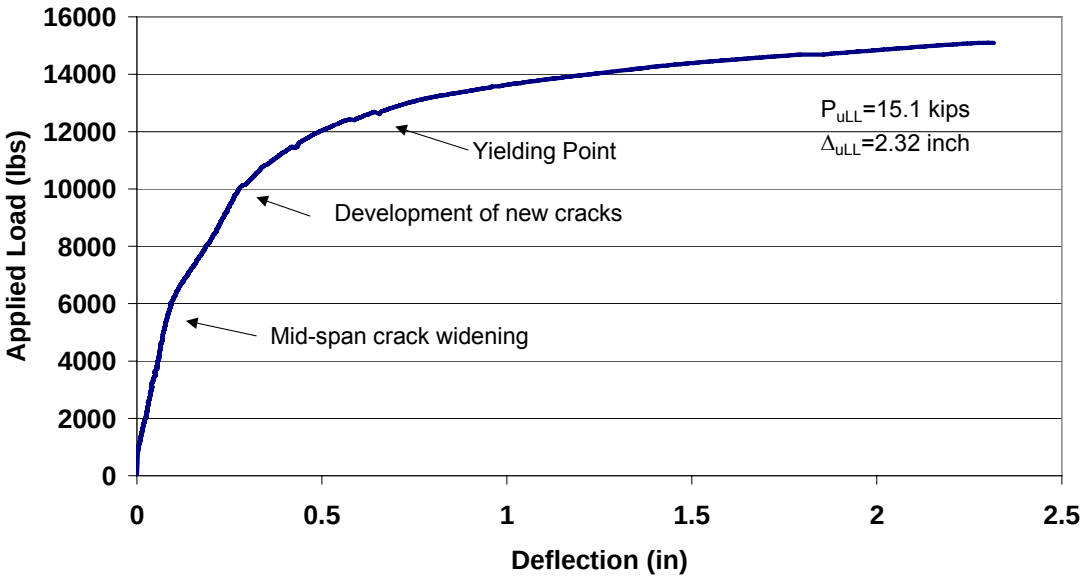

FIGURE 5.5. Load-deflection curve for control beam.

The ultimate failure load for the control beam was 15.1 kips with a maximum deflection of 2.32 inches including the effect of the spreader beam. The beam failed due to the rupture of the prestressing strand, Figure 5.6.

FIGURE 5.6. Failure configuration of control beam.

5.2.2 Beam 2

Beam 2 was strengthened with CFRP to satisfy the serviceability criterion of furnishing the 18 ksi average strand stress range under service live load conditions, as

detailed in section 4.1. This beam was loaded monotonically to failure while recording the load, deflection at mid-span and strain that the concrete top flange and CFRP was undergoing in the locations shown in Figure 3.5. Figure 5.7 shows the load-deflection response for this beam. From this figure, it can be seen that the load at the mid-span crack opening is 5.7 kips and the load at which other cracks in the constant moment region start developing is 11.0 kips.

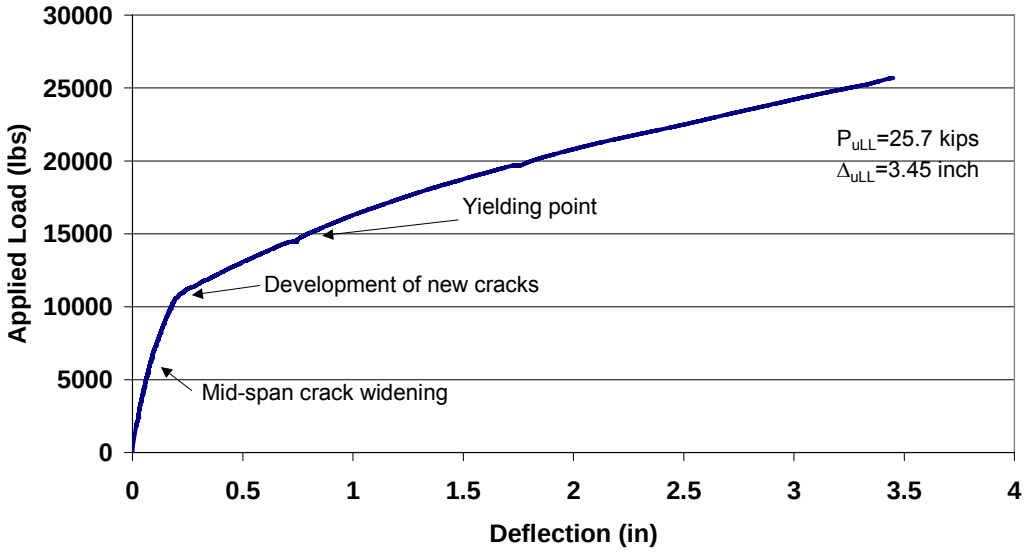

FIGURE 5.7. Load-deflection curve for Beam 2.

The beam failed by CFRP rupture at a load of 25.7 kips with a deflection of 3.45 inches including the weight of the spreader beam. The FRP ruptured at a maximum average strain of 14,730 microstrain at mid-span, Figures 5.8 and 5.9. This is in excellent agreement with the coupon testing value found to be 14,000 microstrain.

FIGURE 5.8. CFRP rupture of Beam 2.

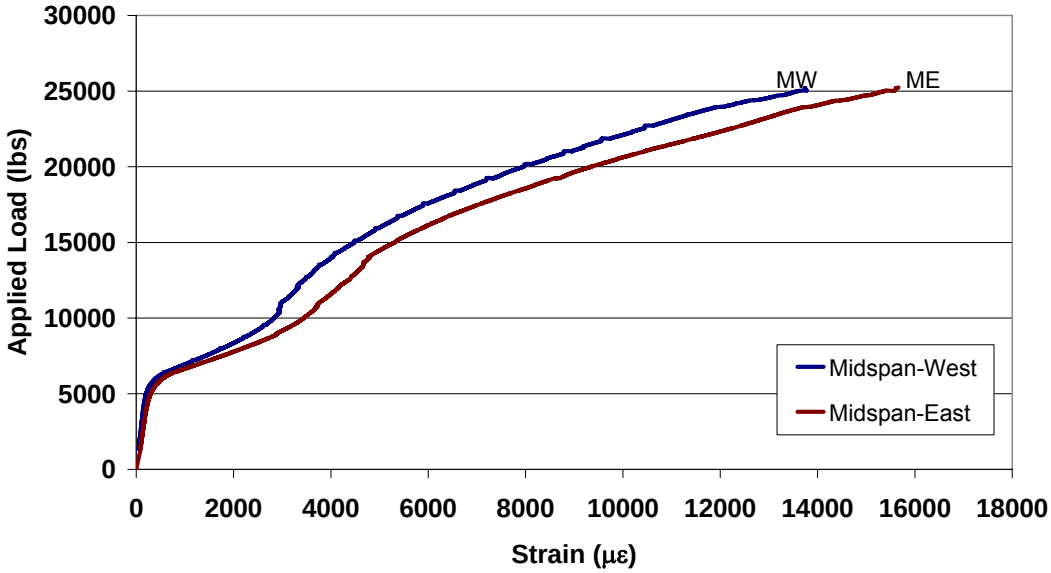

FIGURE 5.9. Load strain for CFRP at bottom mid-span.

The load-strain responses of the bottom CFRP sheet at mid-span are shown in Figure 5.9. It is evident that the CFRP picks up noticeable higher strain values (compared to those from strain compatibility) between the mid-span crack opening (around 5 kips) and the development of flexural cracks (around 14 kips) at the cracked

section. This should correspond to a similar reduction in the prestressing strand strains to maintain the same tensile force. This is attributed to the better bond the CFRP has with the concrete compared to that of the strand causing points adjacent to crack faces to develop faster. This effect erodes under higher loads as CFPR slips on both sides of the crack. CFRP strains at 1' (Near) and 2' (Far) on the bottom of the web on both sides of the mid-span crack were also recorded. These strains were slightly lower than those recorded at mid-span due to later development of flexural cracks (P=10 kips), Figure 5.10. The phenomenon described above is further supported here in Figure 5.10. It is evident that the new cracks in the constant moment region do not develop until P=10 kips. A sudden increase in FRP strain takes place at this level and continues up to P=17.5 kips when the CFRP bond across the crack sides starts degrading and the strand begins to pickup comparable strain values.

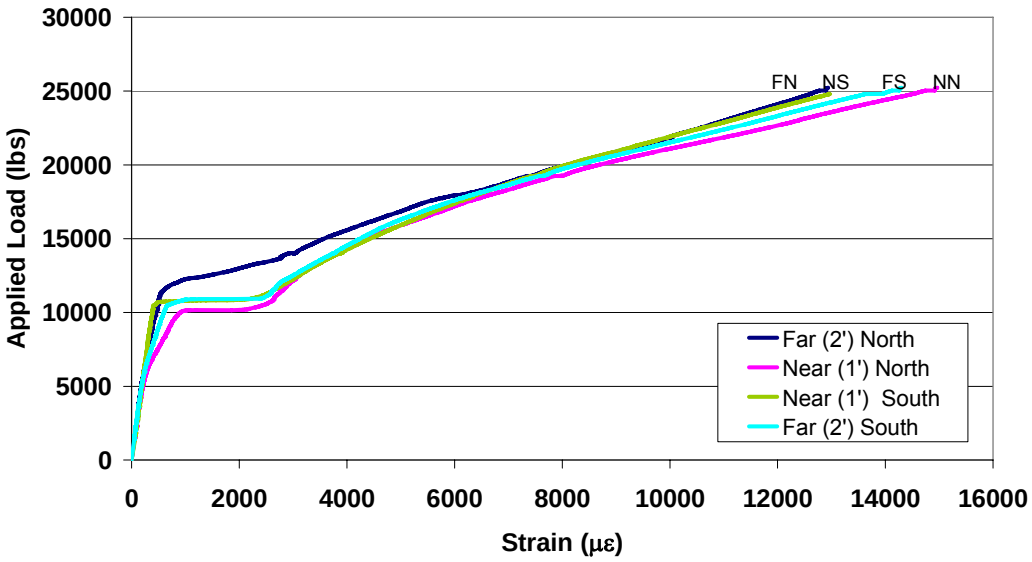

FIGURE 5.10. Load-strain data for Beam 2, on bottom CFRP web.

Strain readings were also taken on the stirrups that were just outside the constant moment region, Figure 5.11. The reason for installing these gages was to

verify that the CFRP allowable design strain for the stirrups (3000 μ_ε) is conservative. The largest change in strain for any of the four stirrups was around 100 microstrain. Accordingly, the remaining beams did not have any gages placed on their stirrups.

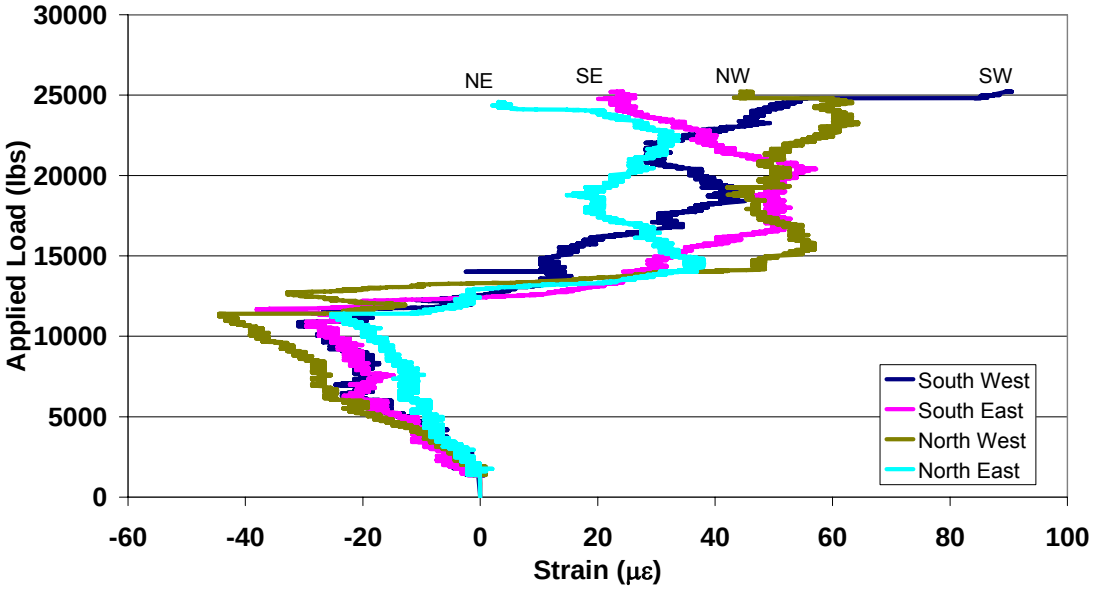

FIGURE 5.11. Load-transverse strain readings for stirrups of Beam 2.

Finally, gages were also put down on the top flange in the constant moment region to record the strains of the extreme compression concrete fiber during the loading process, Figure 5.12. The largest measured strain values for the concrete in compression were around 1600 microstrain upon CFPR rupture, which are noticeable lower than that corresponding to f'_c (0.002). It must be noted for both beams strengthened for the 18 ksi stress range (Beam 2 and 3) that a 2" wide piece of duct tape was placed over the crack at mid-span. This was done to create an unbonded region between the CFRP and the concrete at the strain gage location to avoid recording highly localized unsmeared measurements. Accordingly, it is further evident that the prestressing strand slips beyond this region and it requires more than 1 inch on either side of the crack face to develop its' tensile force of the constant moment region.

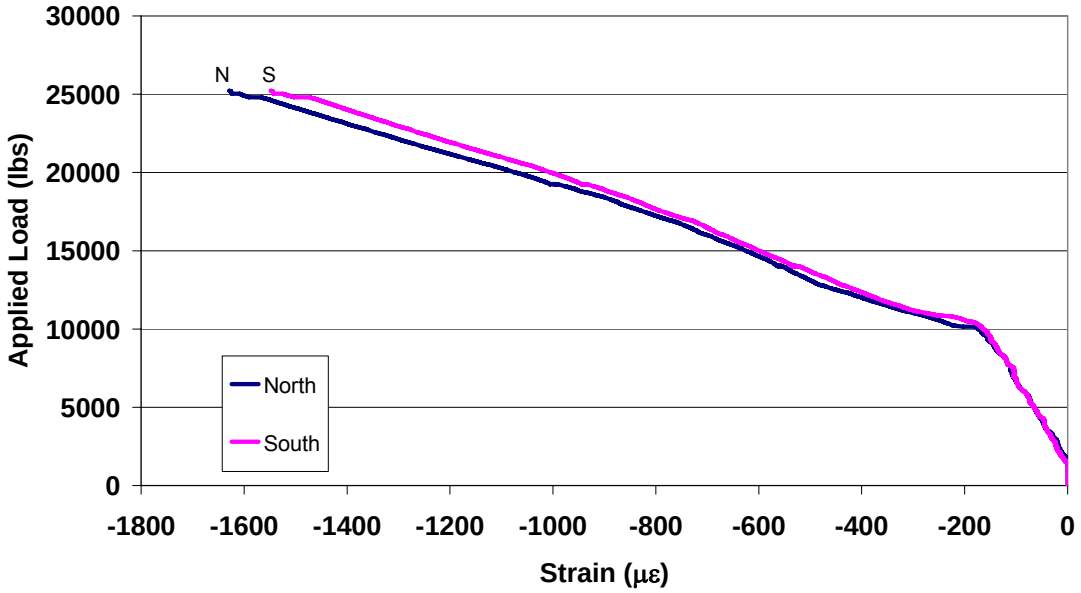

FIGURE 5.12. Load-strain response for top concrete in compression at mid-span.

5.2.3 Beam 3

Beam 3 was also strengthened with the 18 ksi stress range design. This beam was cyclically loaded over 1 million times (1,065,540 cycles) before it was brought to failure. This beam showed a noticeable stiffness loss at full service load after this number of cycles, Figure 5.13. It was, accordingly, thought that a wire in the prestressing strand might have broken. Therefore, the beam was loaded monotonically to failure at that point. However, after testing the strand alone, extracted from the end of the same beam, in fatigue, section 5.5, and observing the behavior of Beam 5, it was concluded that a wire should not have actually broken and the loss of stiffness might have been due to developing more secondary flexural cracks that opened up in the constant moment region and further degrading the strand and the CFRP. Figure 5.13 shows the load-deflection curves for the static readings taken in between the continuous fatigue cycling. The static readings were taken from zero load to 7.5 kips. During the cycling process, however, the lower load limit was 0.5 kips and the upper load was 5.5

kips, to avoid having a complete unloading that may cause impact effects or mis-alignment upon immediate reloading. The presence of creep effect is evident due to the rigid body progressive shifting of the load deflection curves to the right with the increasing number of cycles. Not all the static readings taken are shown, Figure 5.13, to make the graph presentable.

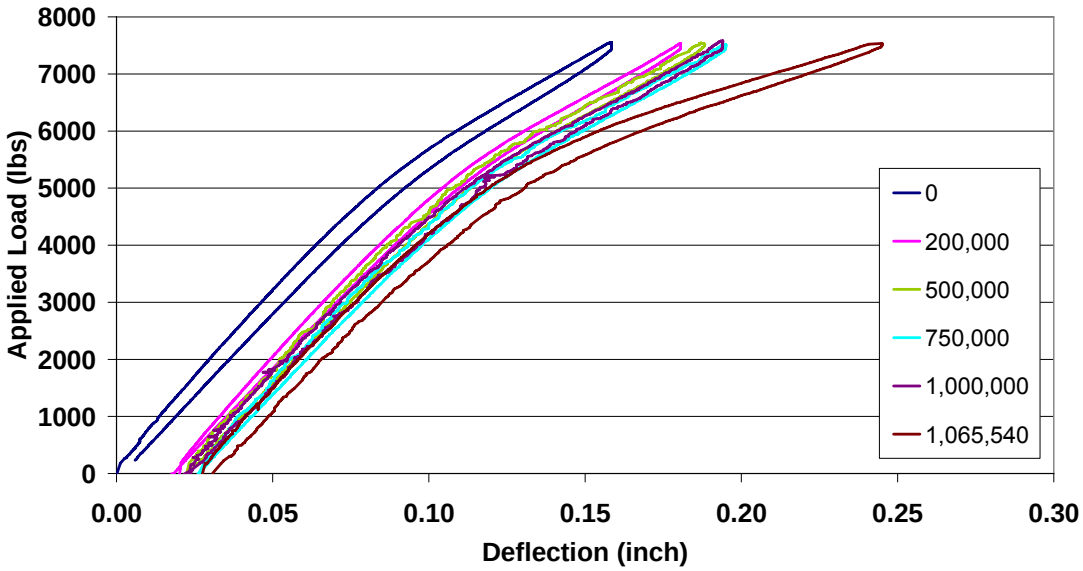

FIGURE 5.13. Fatigue response of Beam 3 under service load condition.

The CFRP strains at the bottom of the web at mid-span is also measured here. As more and more cycles were applied to the beam, the maximum strain values of the CFRP are seen to gradually decrease. The values for the CFRP strain taken at the bottom of the web for the first static reading are shown in Figure 5.14a. Figure 5.14b has the same strain readings recorded after 700,000 load cycles. It can be noted that not only does the strain values decrease with the same applied load, but the loops in between the loading and unloading paths have closed. The strain readings that were taken at positions other than mid-span did not change that much with cycling. However it is important to mention that these CFRP strains are significantly lower than these

recorded at mid-span since they were not in the same proximity to flexural cracks, Figure 5.14a-b.

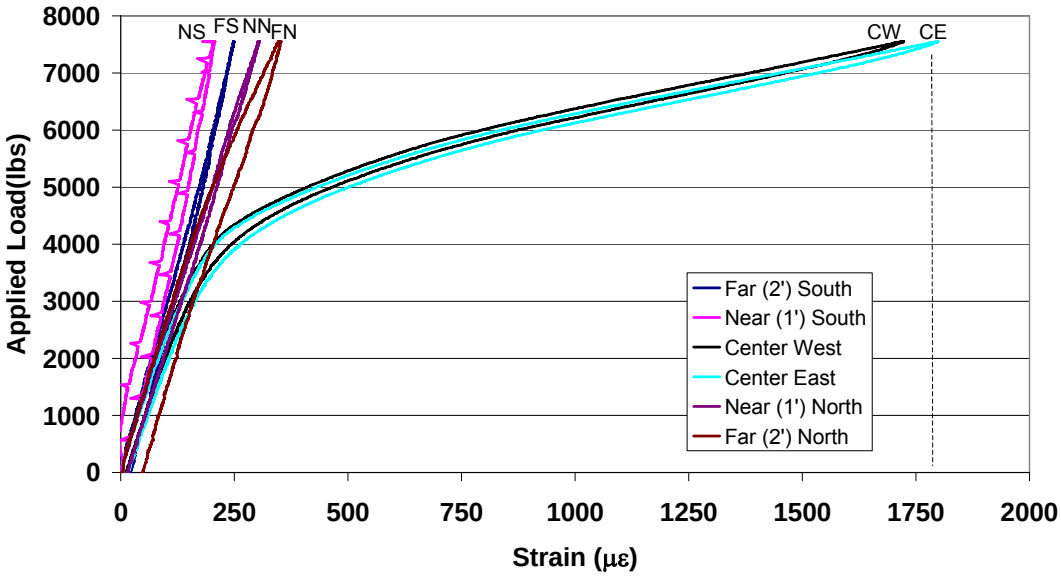

(a)

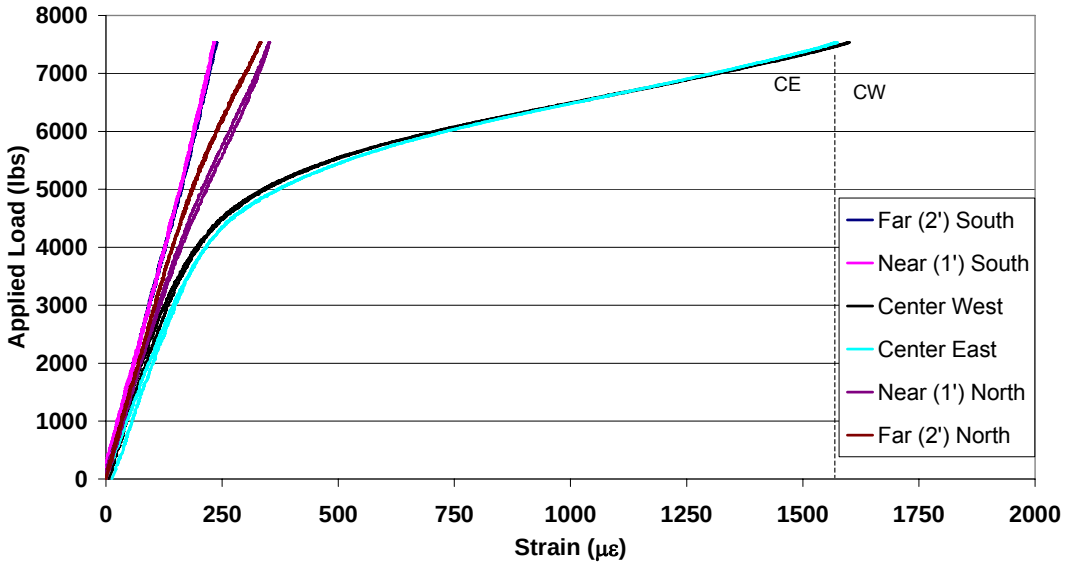

(b)

FIGURE 5.14. Load-CFRP strain response at bottom of web (a) At 0 cycles. (b) At 700,000 cycles.

Strain gages were also placed on the CFRP wrapped around the web sides at 2 inches from the bottom. These gages were used to measure the CFRP strain at the

level of the bottom prestressing strand to verify the intended 18 ksi stress range under the service live load conditions. The stress range was found using:

$$S.R. = \varepsilon_f E_f)_{7.5k} - \varepsilon_f E_f)_{0.5k} \qquad (5.3)$$

Using the data directly from these gages and assuming strain compatibility to hold at this cracked section the corresponding stress range in the strand, after 1 million cycles is in the range of 19.5-40.5 ksi for the gages that were placed over mid-span, Figure 5.15. At this point, a static loading was applied up to 13 kips to induce and open new cracks in the constant moment region. One crack opened up exactly at 1 ft. north of mid-span where a strain gage was already installed. This section was chosen to expose the upper strand and perform further instrumentations.

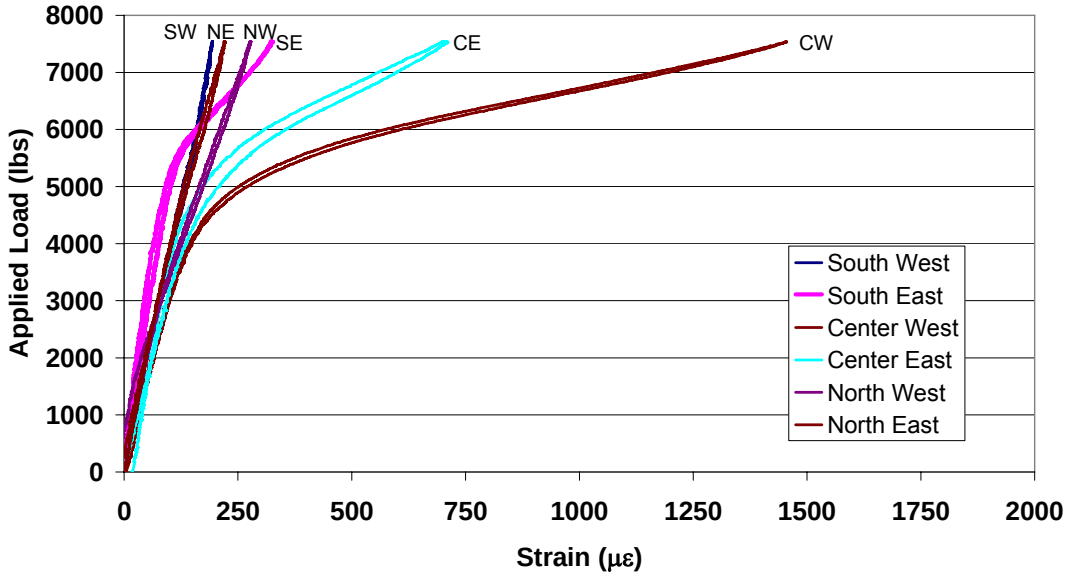

FIGURE 5.15. Load-strain values on CFRP at 2 inches from bottom at 700,000 cycles.

From these results, it is apparent that these strains may be higher than those developed in the prestressing strand at the same height. This is attributed to the better CFRP bond across the crack compared to that of the prestressing strand, which

requires a relatively longer slip distance to develop perfect bond strains, as shown in section 5.2.2. To prove this argument that the strand was indeed undergoing lower strains corresponding to the intended 18 ksi stress range, a small area of concrete in the constant moment region around the upper prestressing strand was removed in two locations and strain gages were applied directly on the strand, as described in section 3.6 and 3.7. This was done after completing 1,065,540 cycles of loading. The average prestressing stress range design was 18 ksi. Thus it is expected that the upper prestressing strand would experience a slightly lower stress range as it is closer to the neutral axis. The average experimental stress range, recorded by the strain gages on the exposed strand, is found to be around 15 ksi, Figure 5.16.

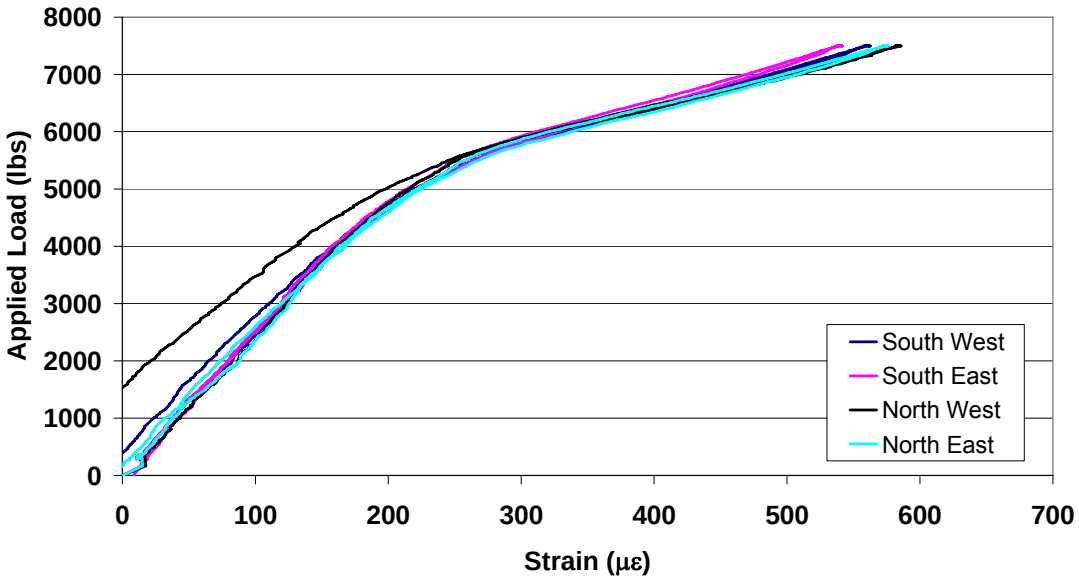

FIGURE 5.16. Load-strain values directly on exposed prestressing strand.

From the two preceding figures, it is evident that the strains in the CFRP and these in the prestressing strand cannot have the same values. One explanation for this is that the bond between the concrete and the CFRP is superior to that with the strand. Accordingly, CFRP develops a higher tensile force adjacent to the crack to compensate

for the partially developed strand force at the same section. Figure 5.17 has the strain data for both the CFRP at 2 inches up from the web bottom and the exposed prestressing strand at 4 inches up from the bottom. The difference in height however does not produce that large of a difference in strains.

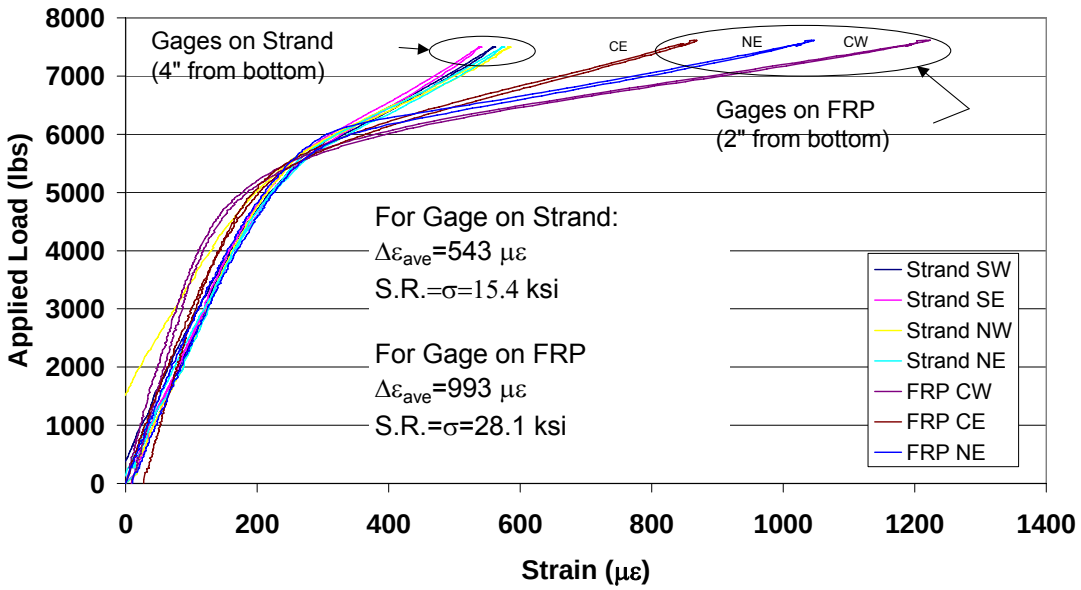

FIGURE 5.17. Load-strain readings for both prestressing strand and CFRP on web side.

Once the stress range in the strand was verified Beam 3 was then loaded statically to failure. Its ultimate load was 25.3 kips with a deflection of 3.3 inches including the contribution of the spreader beam, Figures 5.18 and 5.19. This failure point is clearly in agreement with that of Beam 2 indicating that the strength and ductility were not influenced by the fatigue loading.

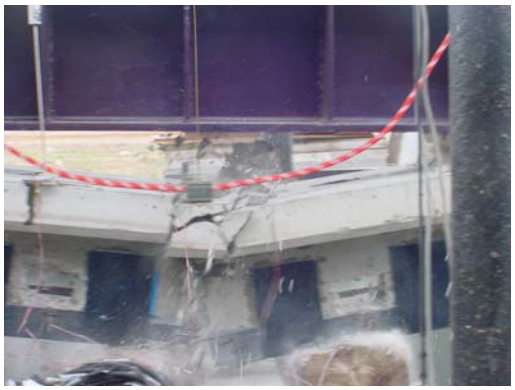

FIGURE 5.18. Failure of Beam 3 just after CFRP rupture.

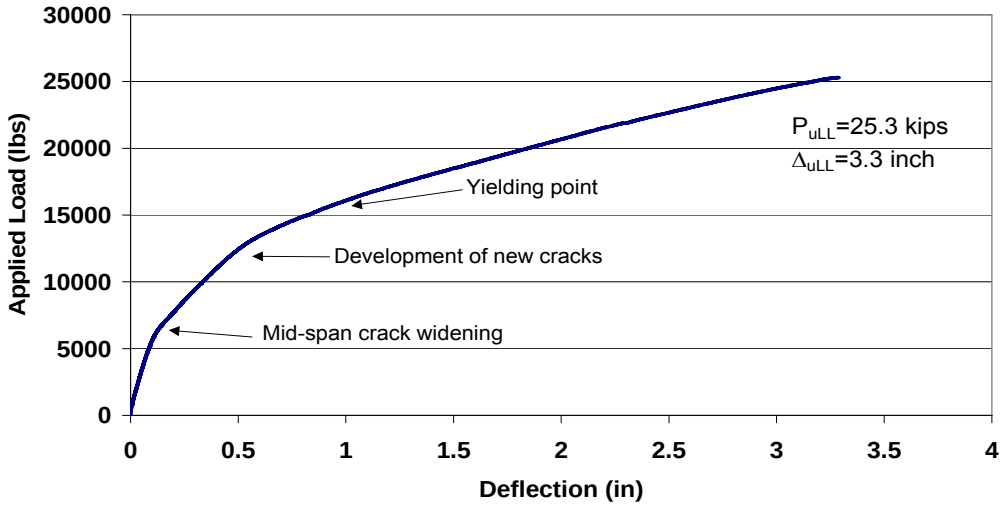

FIGURE 5.19. Load-deflection for Beam 3.

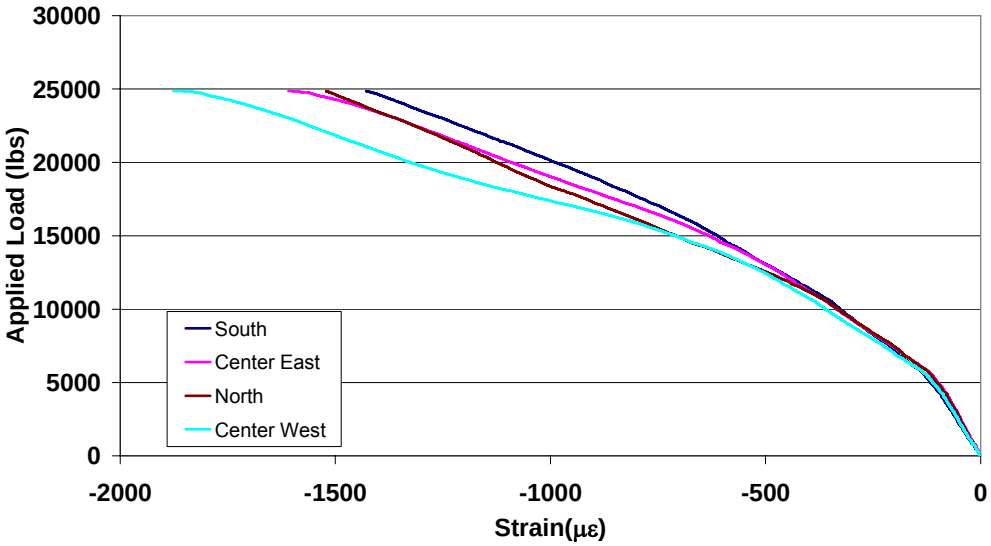

FIGURE 5.20. Load-strain for top concrete at mid-span of Beam 3.

The ultimate failure mode for Beam

3 was CFRP rupture. Figure 5.18 shows the failed beam just after collapsing and impacting the supporting blocks, which caused the shear cracks in the constant moment region. The strains in the concrete extreme fiber in compression at ultimate were around 1400-1800 microstrain, Figure 5.20. From this, it can be concluded that the concrete was far from reaching crushing. On the other hand, CFRP is seen to exceed 17,000 μ_ε in one location and to average about 14,000 μ_ε in the constant moment region, Figure 5.21.μ_ε

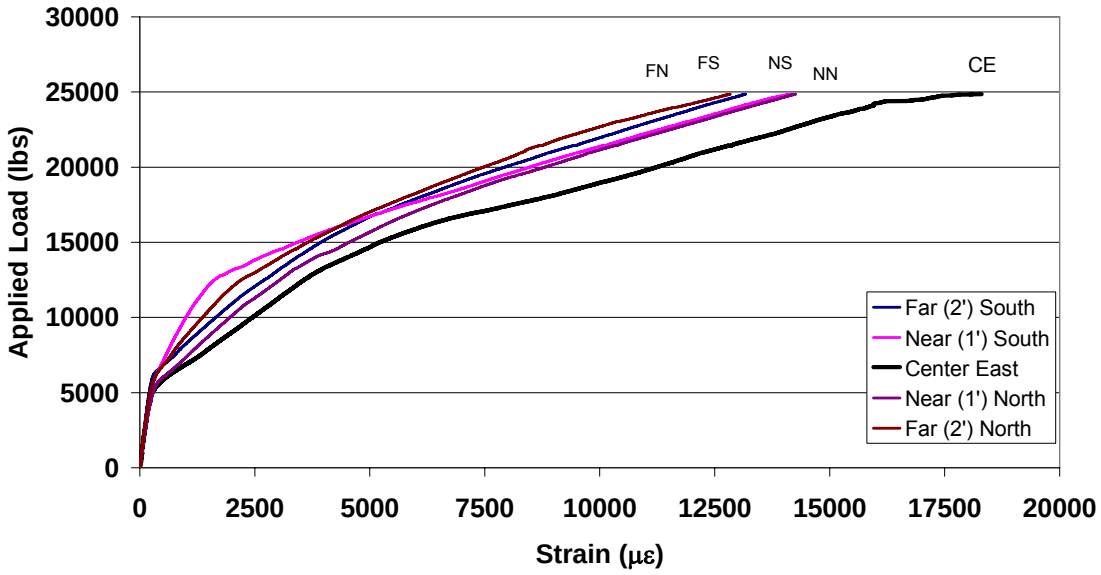

FIGURE 5.21. Load-strain for bottom web CFRP during the final static loading.

Figure 5.21 presents has the strain results for the gages at the bottom of the web mounted on the CFRP and recorded up to ultimate flexural strength during the final monotonic static loading. Strain data for the CFRP at 2 inches from the bottom of the web were also recorded during the final stat loading, Figure 5.22. The corresponding results of the exposed prestressing strand at 4 inches from bottom of the web are also presented, Figure 5.23. By comparing the average peak values from both graphs and

adjusting for the height difference it is concluded that strain compatibility does not hold between the CFRP and the prestressing strand at the same height of the cracked sections due to the different bond-slip characteristics of both materials with concrete.

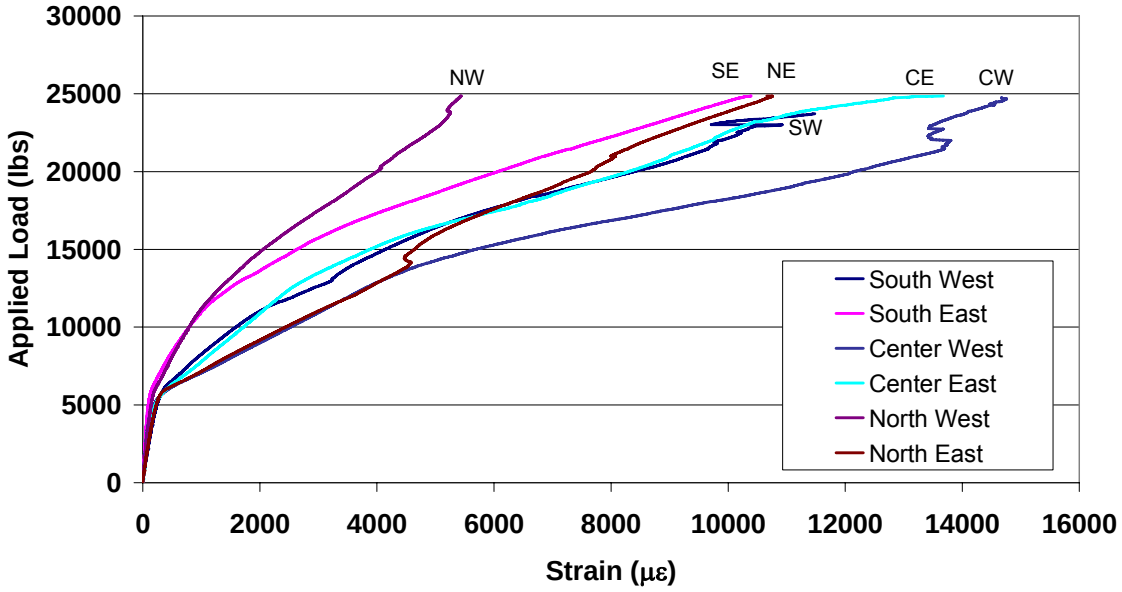

FIGURE 5.22. Load-strain response for CFRP at 2" from bottom during final static loading.

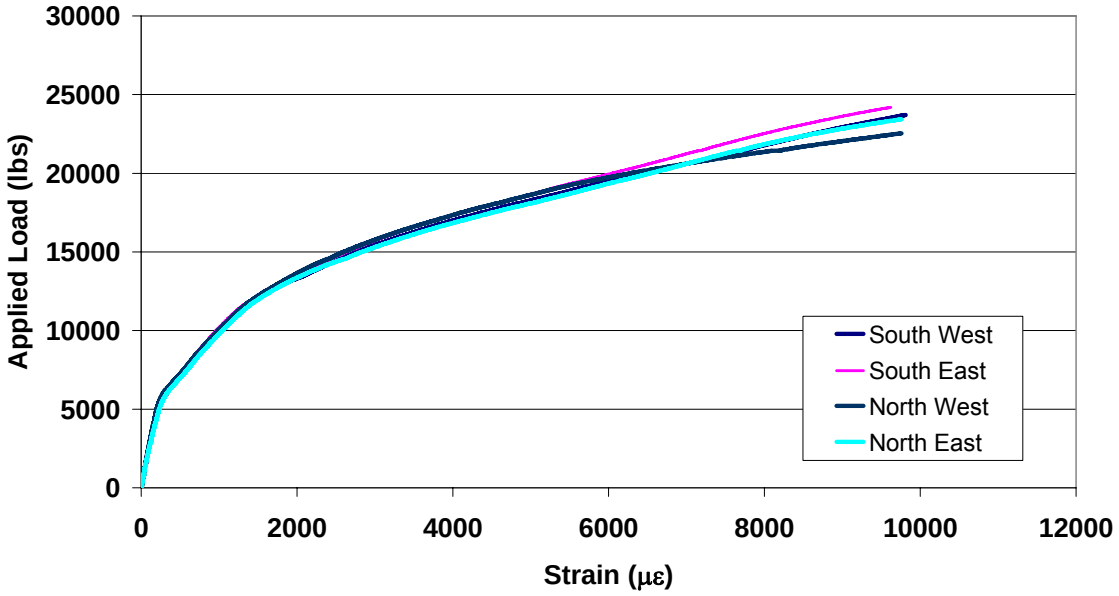

FIGURE 5.23. Load-strain response for exposed prestressing strand during the final static loading.

5.2.4 BEAM 4

Beam 4 was strengthened to have the 36 ksi stress range design. This beam was tested monotonically to failure to establish a benchmark for the ultimate strength of this design. It reached its ultimate capacity at 32.2 kips with a deflection of 4.0 inches, Figure 5.24. The maximum strain that the CFRP underwent at the bottom of the web in the constant moment region was slightly over 14,000 microstrain, Figure 5.25. The strains in the CFRP at 2 inches from the bottom of the web were also recorded during the loading, Figure 5.26. It can be seen from this figure that the CFRP also picks up higher strains upon first cracking or crack opening. The stress range that the CFRP is experiencing here is 73 ksi, which is noticeably higher than the 36 ksi that the strand was designed for at the level of upgraded service load (0.5 kips – 9.8 kips) range. The concrete compressive strains in the top flange at failure only reached 1,800 microstrain,

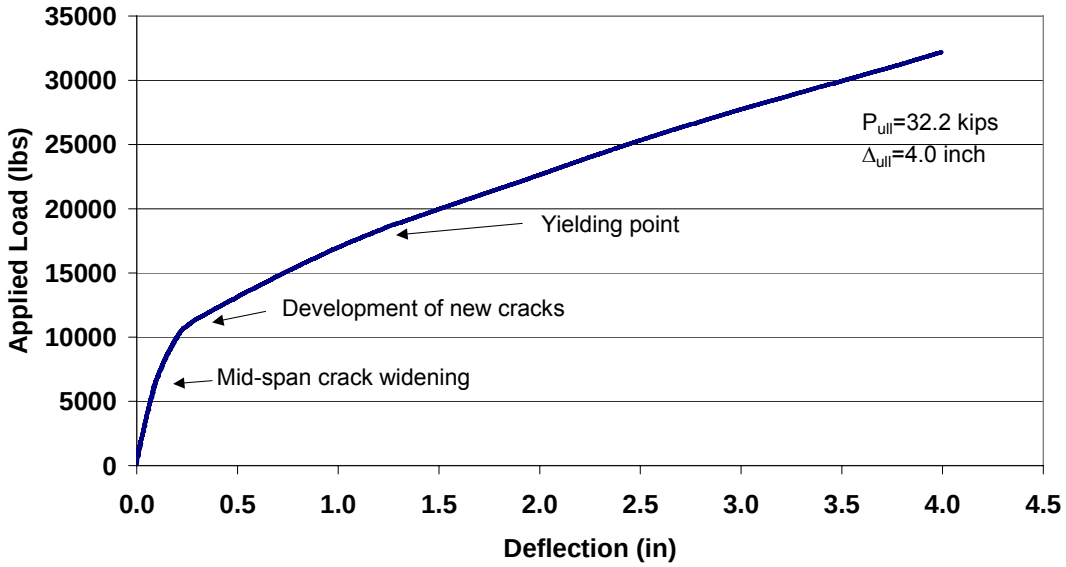

FIGURE 5.24. Load-deflection curve for Beam 4.

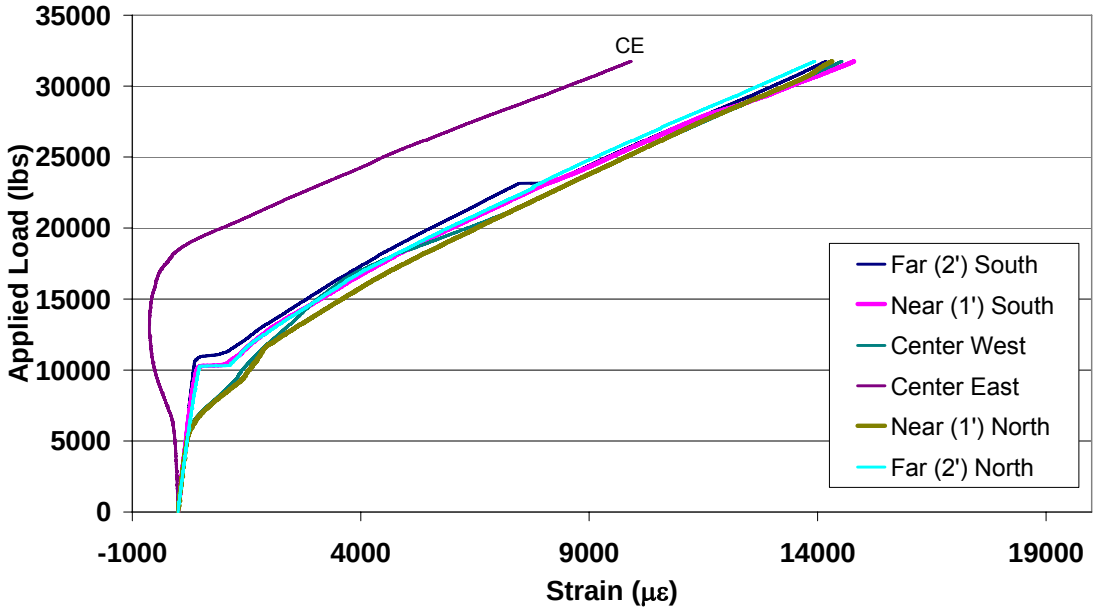

FIGURE 5.25. Load-strain curve for CFRP on bottom web of Beam 4.

Figure 5.27. This beam had an explosive sudden failure as the CFRP ripped concrete away from the beam at the time of attaining ultimate capacity, Figure 5.28.

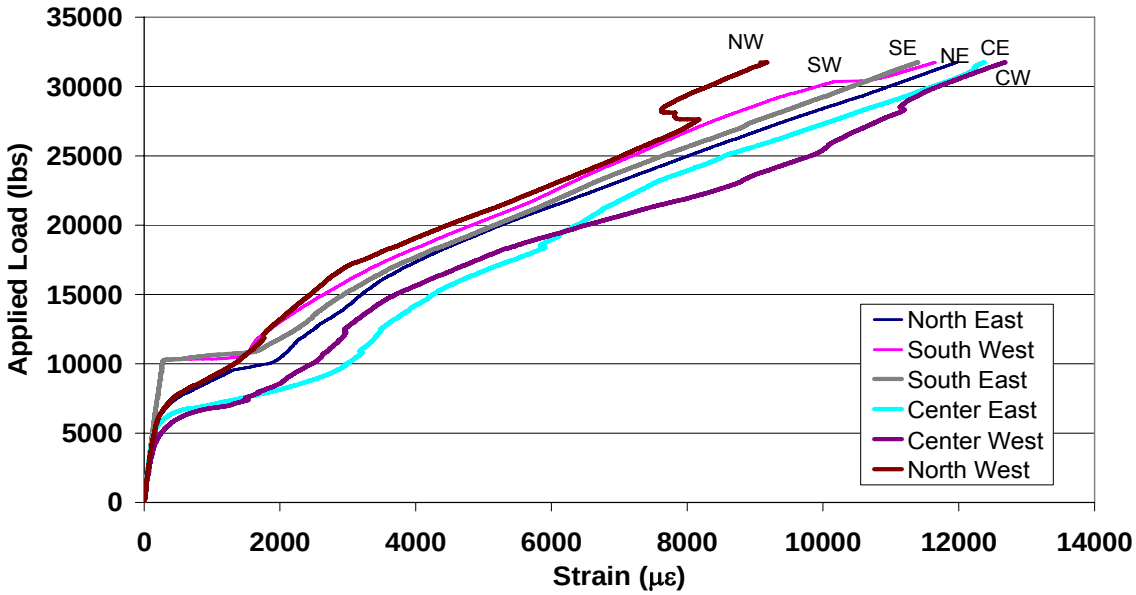

FIGURE 5.26. Load-strain curves for CFRP at 2" from bottom of web of Beam 4.

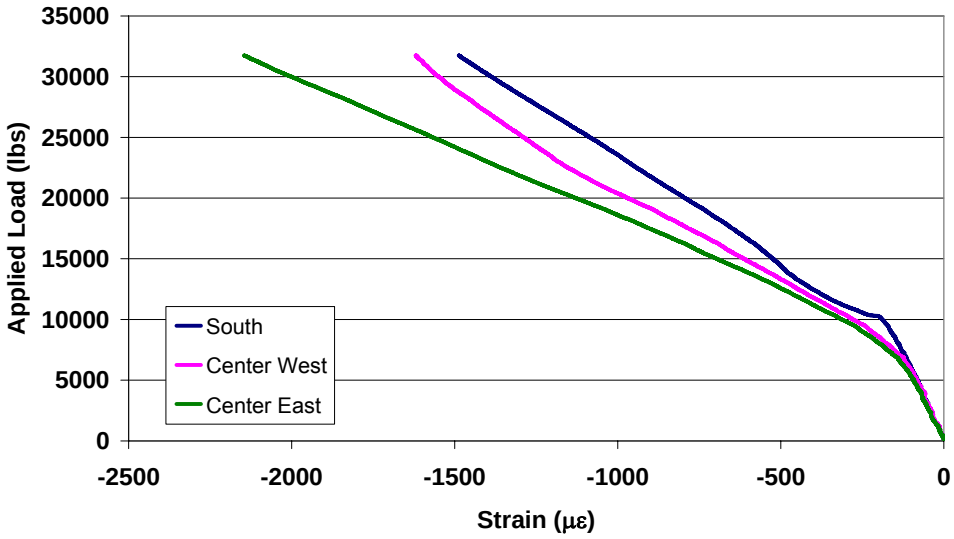

FIGURE 5.27. Load-strain response for concrete top flange of Beam 4.

(a)

(b)

(c)

FIGURE 5.28. Explosive failure of Beam 4 (a) Overall failure (b) Spalled concrete in failure region (c) Close up of CFRP rupture and peeling off.

5.2.5 BEAM 5

Beam 5 was also strengthened to have the 36 ksi stress range design. It was tested cyclically for 3 million times before it was statically loaded up to failure. There was some loss of stiffness observed throughout the cycling process and this can be attributed to new secondary flexural cracks opening up in the constant moment region associated with further loss of standard CFRP bond. It was interesting to observe, for the first time the cracks opening up behind the external stirrups causing matrix cracking in between the transverse fibers, as seen in Figure 5.29. This was not present in the previous tests but rather appeared due to the excessive fatigue loading of Beam 5.

Also the presence of matrix cracking can be seen in the longitudinal CFPR layers in the constant moment region in between the stirrups, Figure 5.30. This is caused by transverse tension strains in flexural CFRP due to bonding to concrete that prevents the flexural sheets from transverse contraction due to the primary longitudinal tension and Poisson ratio effects.

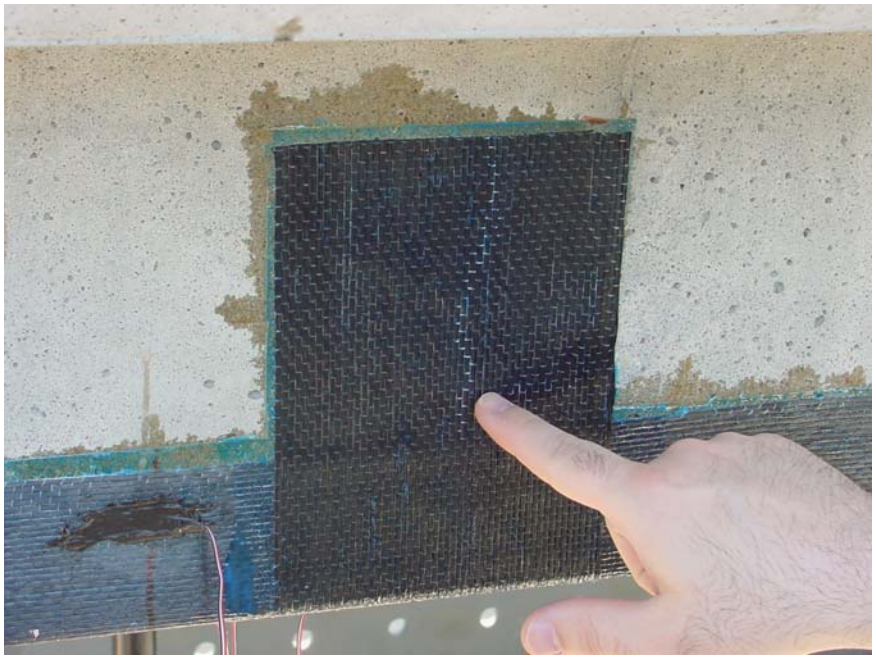

FIGURE 5.29. Existence of concrete flexural cracks in the constant moment region behind the external stirrups that developed during cycling.

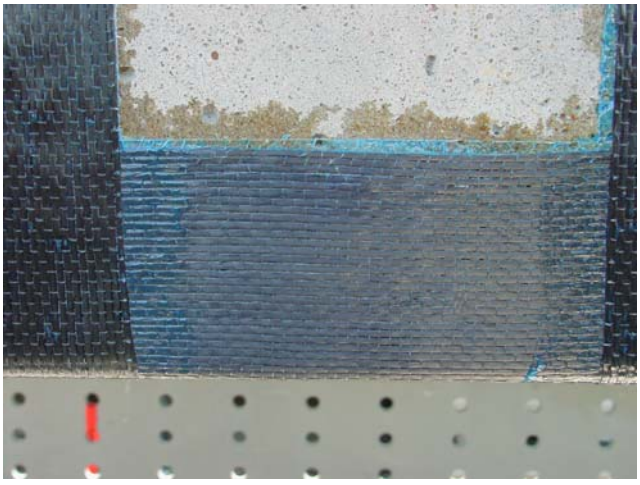

FIGURE 5.30. Matrix cracking in flexural CFRP in between stirrups.

As mentioned earlier, this beam was cycled over 3 million times before it was loaded monotonically to failure. The static readings show that there was some gradual loss of stiffness throughout the fatigue life of the beam, Figure 5.31.

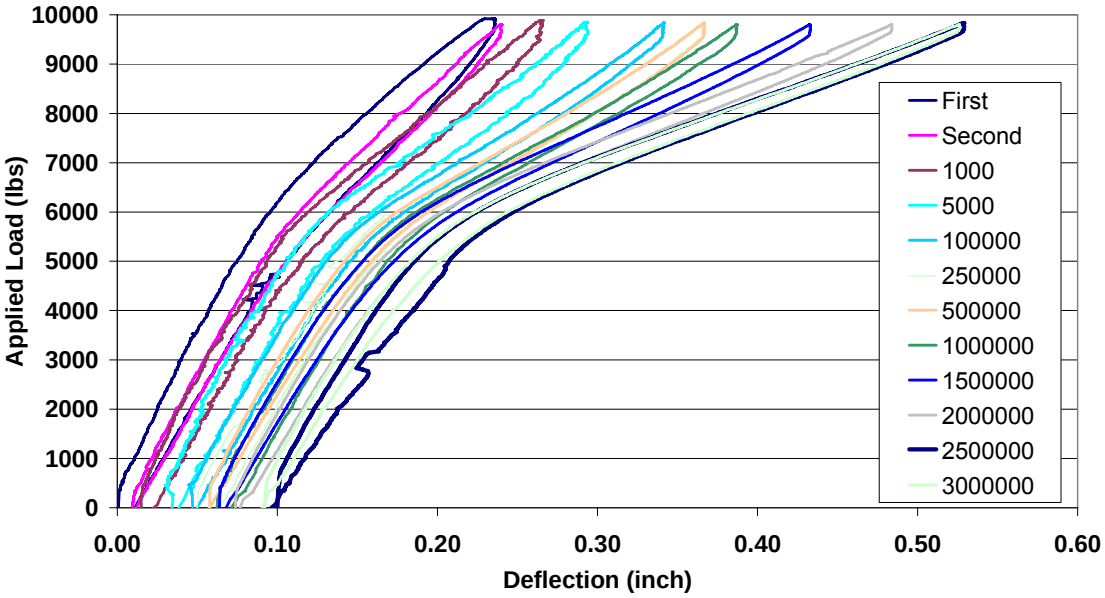

FIGURE 5.31. Load-deflection response for Beam 5 up to 3 million cycles.

The recorded strain values also changed throughout the cyclic life of the beam. The strains in the CFRP at the upper live load limit did not show any proportion to strain compatibility at all the critical sections during the first reading, Figure 5.32a and Figure 5.33a. It is clear that the CFRP strains at the level of the lower strand (2" from the bottom) were around 4 times those at the bottom of the web. This is attributed to the highly localized point-wise strain measurements in the absence of an underlying duct tape that helped smear the bond effects over a 2-inch wide region including the crack. On the other hand, CFRP strain results are seen to get more in line with strain compatibility after 2 million cycles, Figure 5.32b and Figure 5.33b. The CFRP strain at bottom of the web significantly increased while that at the level of the lower strains

substantially reduced due to bond slip on both sides of the crack faces that helped smear the localized effects. Also, the loading and unloading paths show closer matching as more and more cycles were applied to the beam. To demonstrate the above observations, the readings that were taken from the first static loading and these taken after 2 million cycles are plotted. Figure 5.32 shows the strain values for the bottom CFRP over the mid-span. The maximum strain reading from the first static loading gave a strain of around 800 microstrain while this value after 2 million cycles increases to just less than 2,000 microstrain.

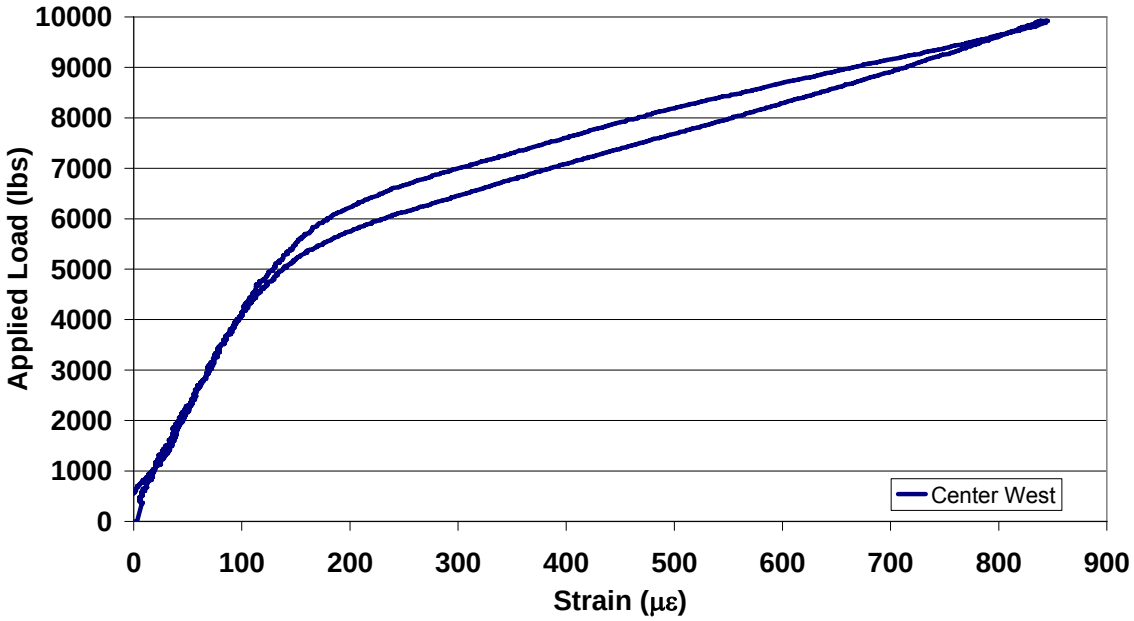

(a)

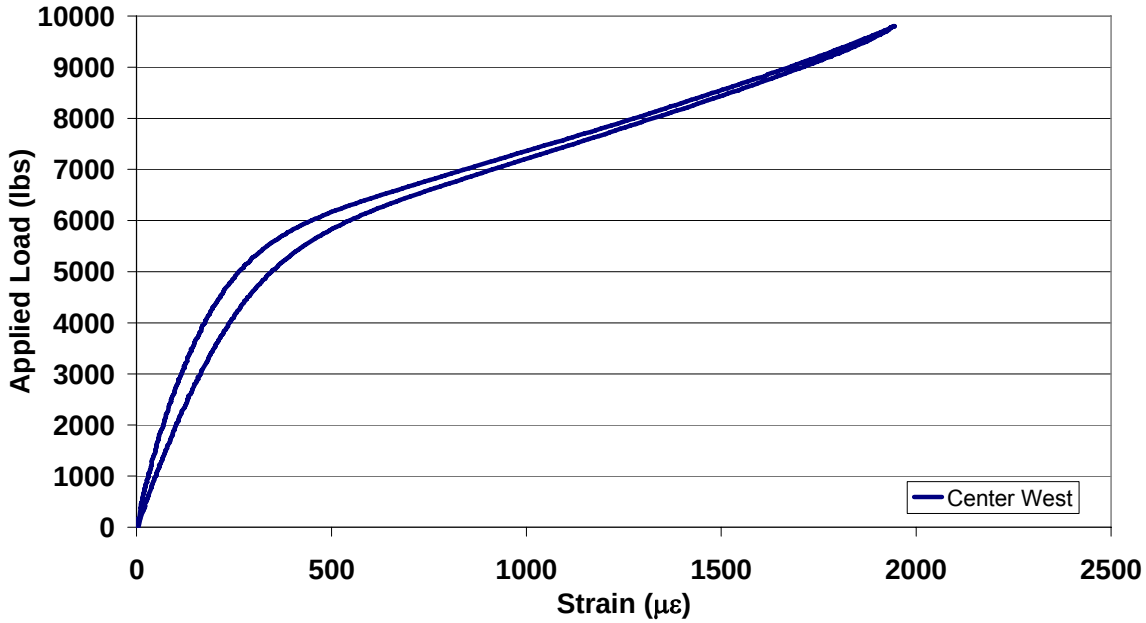

(b)

FIGURE 5.32. Load-strain curve for bottom CFRP at mid-span. (a) First cycle (b) After 2 million cycles.

The change in strains for the CFRP that is at 2 inches above the bottom web is a drop of a little over 1,300 microstrain as 2 million cycles are applied to the beam, Figure 5.33.

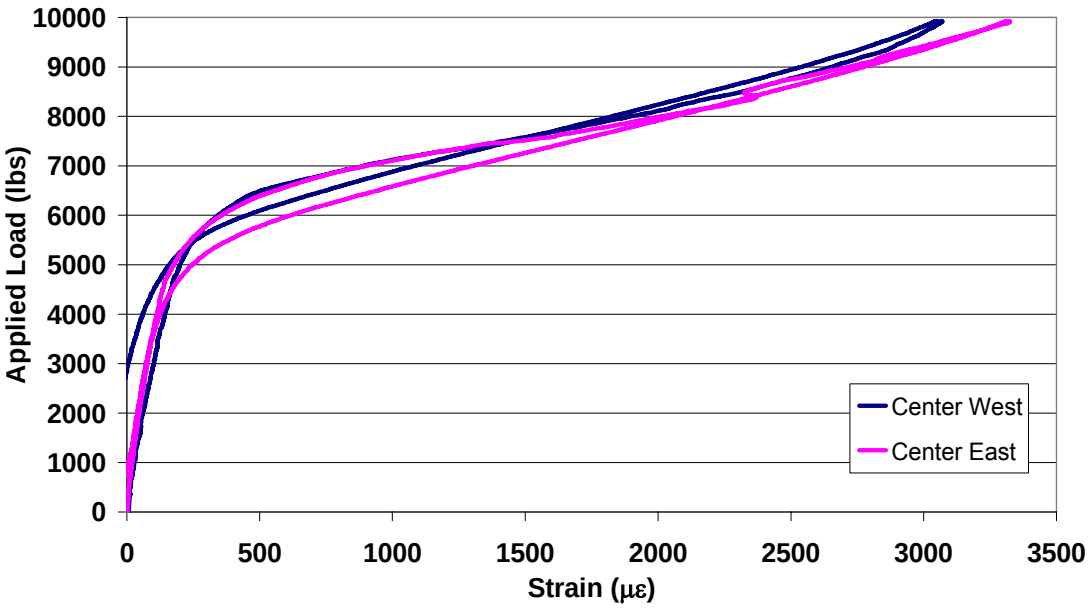

(a)

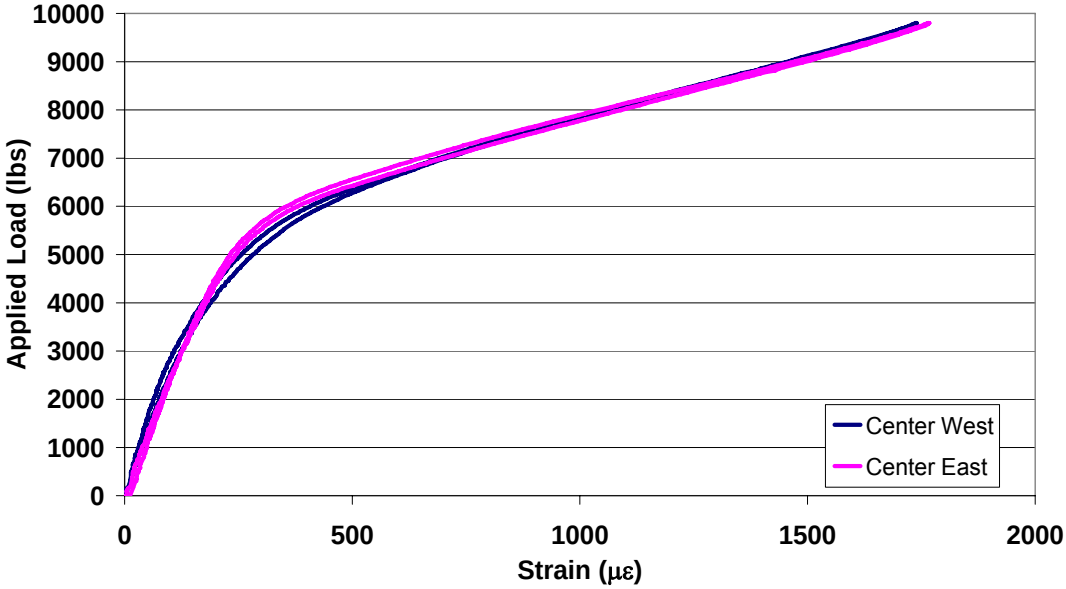

(b)

FIGURE 5.33. Load-strain curve for CFRP at 2" up (a) First reading (b) After 2 million cycles.

The strains in the top concrete flanges in compression also change as more cycles are applied. These slightly increase as the cycling continues, Figure 5.34.

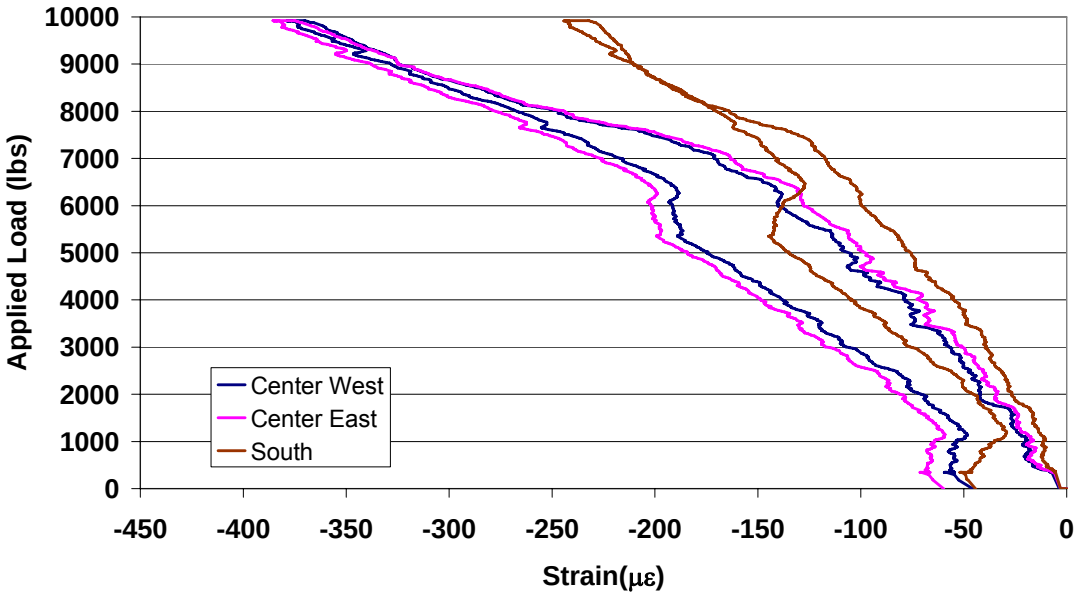

(a)

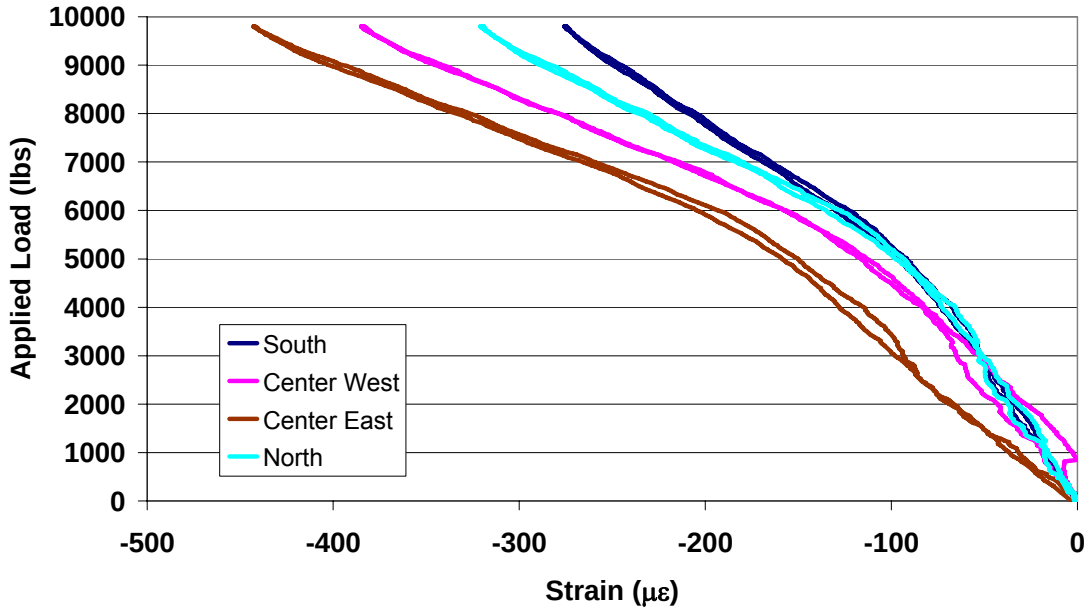

(b)

FIGURE 5.34. Load-strain curve for top concrete compression strains (a) First cycle (b) After 2 million cycles.

Once 3 million cycles were reached, cycling on Beam 5 was stopped and the specimen was loaded statically to failure. However, the beam failed prematurely with an ultimate load capacity of only 26.2 kips and a deflection of 2.6 inches, Figure 5.35.

This was obviously lower than the capacity of developed by Beam 4, having the same strengthening design, and lower than the load predicted by analysis is presented in the following sections. This is attributed to the reduction in the strength capacity of the CFRP sheets or prestressing strand due to the excessive cycling up to 3 million cycles. It is reasonable to expect that the fatigue life span of this specimen might not have exceeded 3 million cycles by a noticeable margin. The maximum strain that the CFRP underwent on the bottom web at mid-span was less than 12,000 microstrain, Figure 5.36. The sudden softening in the strain curve for the Center East gage suggests a locally increased CFRP strain due to extra tight closure of crack at that point, which reverts back to the typical response curve at a higher load due to bond slip causing redistributed or smeared strains.

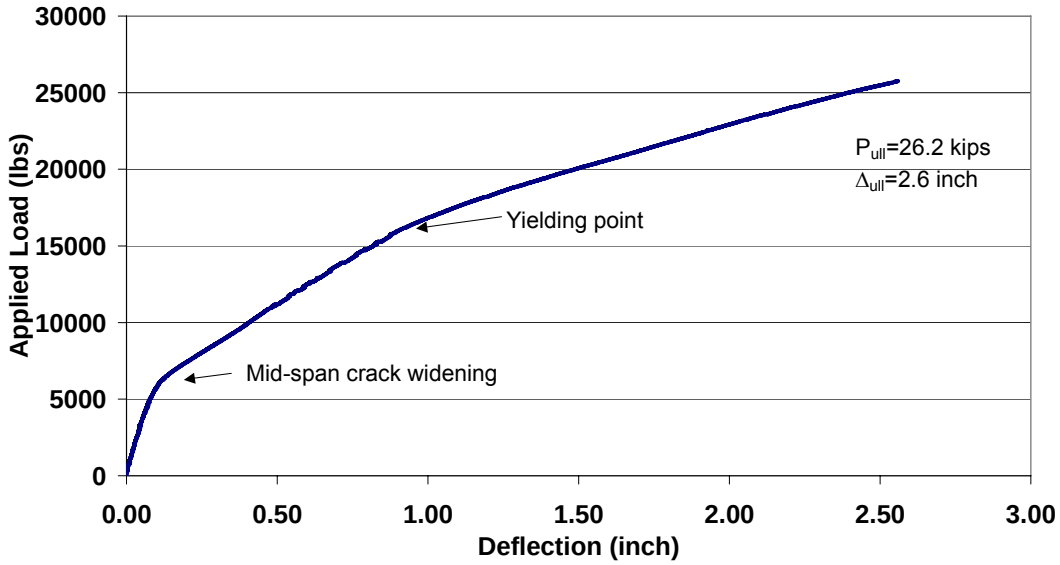

FIGURE 5.35. Load-deflection curve for Beam 5.

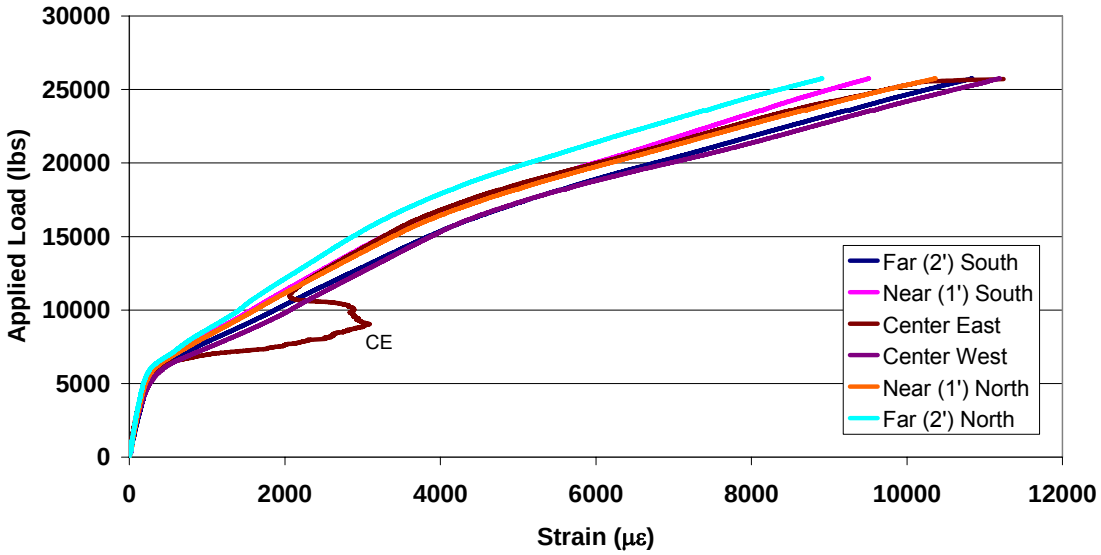

FIGURE 5.36. Load-strain response for bottom web CFRP.

As mentioned earlier, further cracks in the constant moment region started to initiate and propagate during the cycling process. These cracks, however, were held closed by the stirrups. Once a large enough load level was applied to the beam, the cracks propagated beyond the height of the stirrup, Figure 5.37. The values of compression strain that the top concrete flange was undergoing at failure were between 1,100 and 1,600 microstrain, Figure 5.38.

FIGURE 5.37. Flexural cracks held together by stirrups at failure

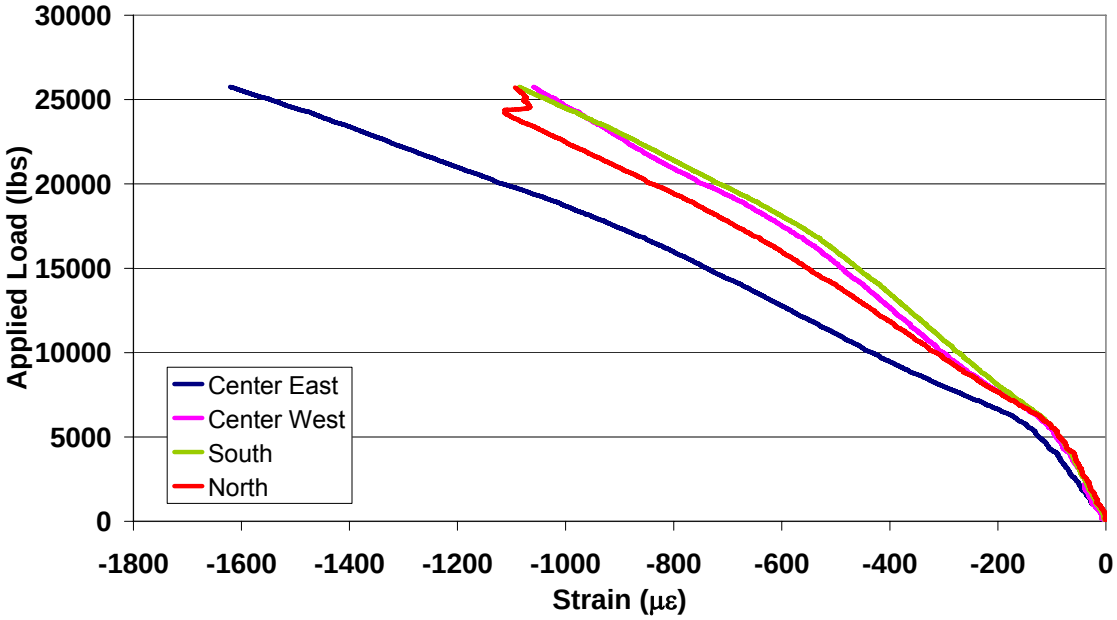

FIGURE 5.38. Load-strain curves for top concrete compression flange.

The strains that the side CFRP have undergone at 2 inches above the bottom of web at failure were in the range of 8000-10000 microstrain are shown in Figure 5.39. Figure 5.40 shows the deflected beam during loading.

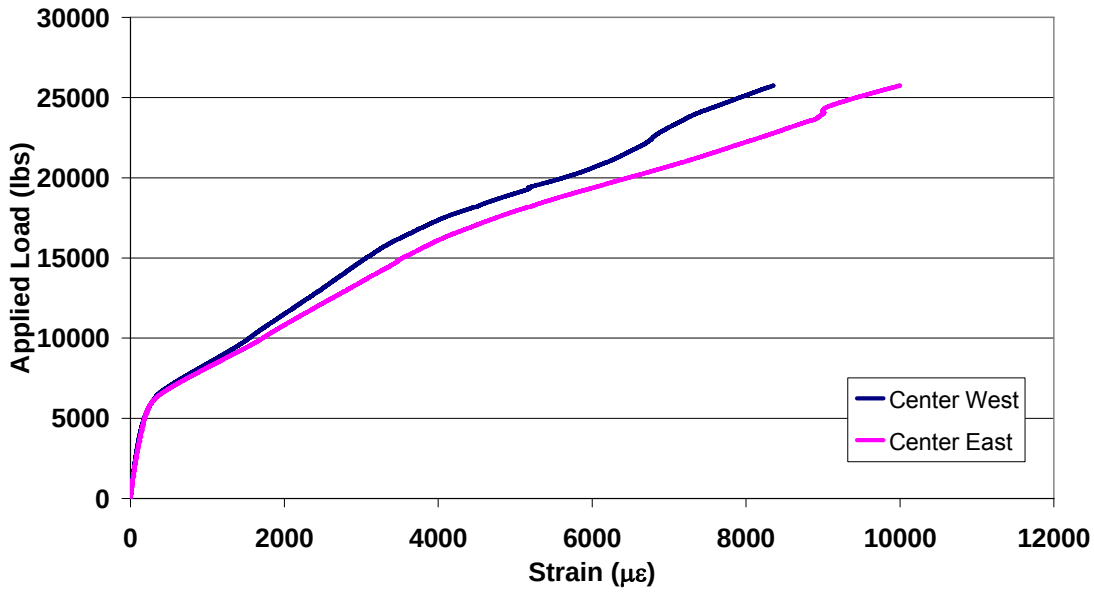

FIGURE 5.39. Load-strain curves for web side at 2" from bottom lower strand height.

FIGURE 5.40. Beam 5 during loading.

5.3 EXPERIENTAL BEAM COMPARISONS

Relevant comparisons between the beams will be shown here. Load-deflection graphs for similar beams will be compared here along with load-strain curves of different locations in the beams. Figure 5.41 presents the load-deflection response of Beams 1, 2, and 3. It is very interesting to see the strengthened beams improve in both strength and ductility. This is not typical to observe but it is attributed to the CFRP rupture failure mode that corresponds to significantly high strength and strains at failure. The actual strengthening index is 70% for Beam 2 and 68% for Beam 3. The actual ductility index $\left(\frac{\Delta_{u\,strengthened} - \Delta_{u\,control}}{\Delta_{u\,control}} \right)$ is 49% for Beam 2 and 42% for Beam 3. Beam 3 failed at a load level which is only 0.4 kips less than that of Beam 2 and a maximum deflection which is only 0.15 inches smaller than that of Beam 2. One of the major effects of applying 1 million cycles on Beam 3 was its softer cracking and post-cracking load-deflection response compared to Beam 2 after the crack opening point. This is attributed to the deterioration of strand bond stress in the service load range of Beam 3 due to the 1 million fatigue cycles applied. However, other than that difference, the responses of

both beams follow the same curve. This indicates excellent confidence in retaining the target strengthening level even after long term fatigue cycling.

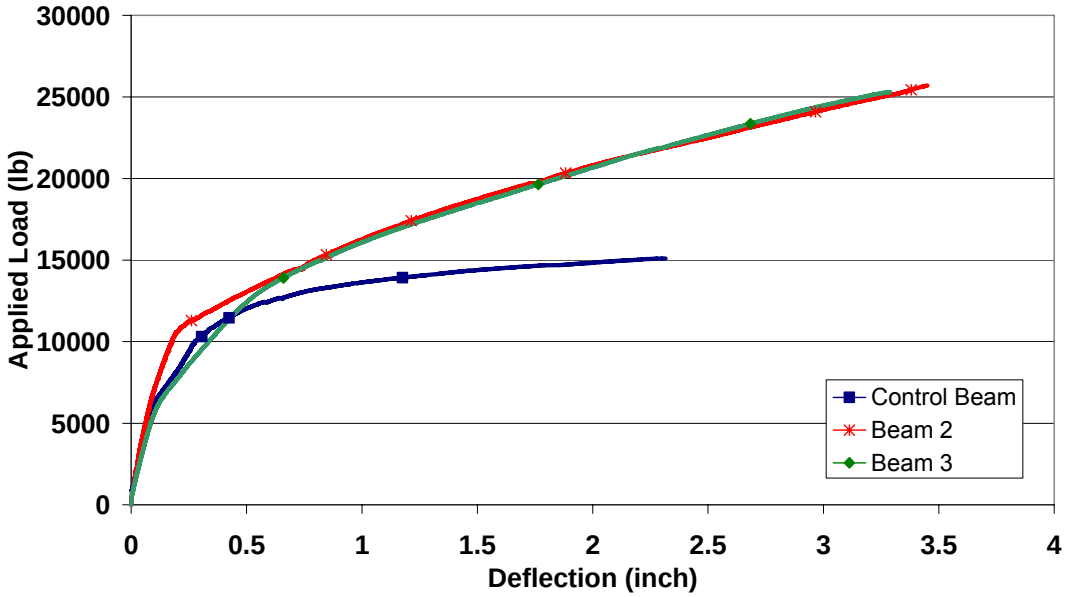

FIGURE 5.41. Load-deflection comparison for control beam, Beam 2 and 3.

Beams 4 and 5 had the same strengthening design but failed at much different load and deflection levels, Figure 5.42. The fact that Beam 5 had undergone 3 million cycles prior to failure was the major contributor to this significant loss in strength. As was seen in Beams 2 and 3, the beam that was fatigued was much softer after the crack opening load was reached. However, in both cases, the specimens subjected to fatigue regained the same stiffness after yielding and matched the response of their monotonically loaded twin beams. The actual strengthening index for Beam 4 is 113% while it is only 74% for Beam 5 due to its premature failure after the 3 million fatigue cycles. Similarly, the ductility index is 72% for Beam 4 and it is only 12% for Beam 5.

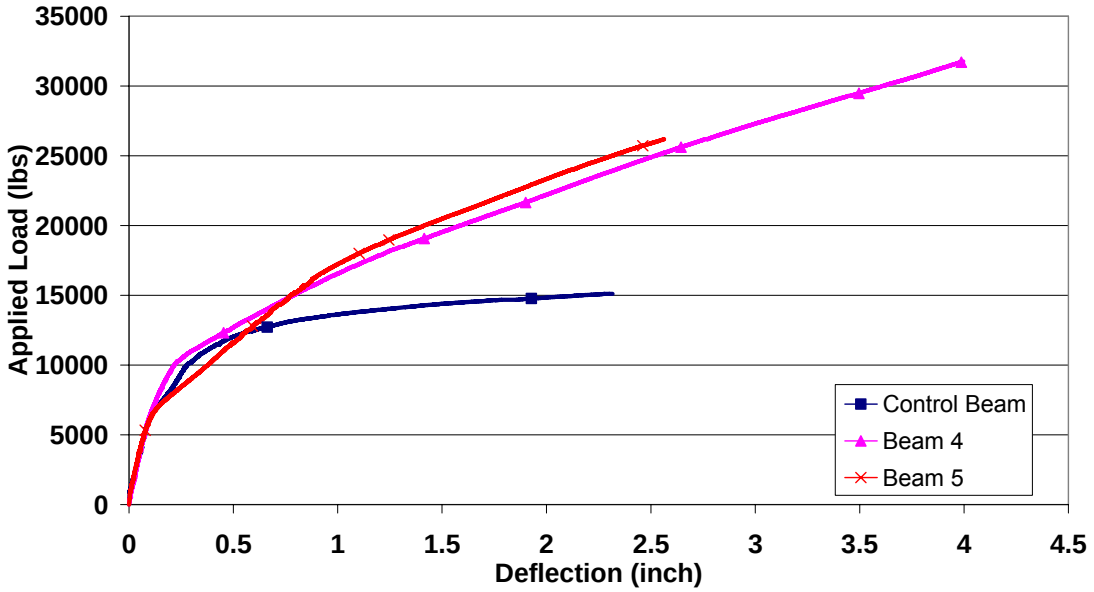

FIGURE 5.42. Load-deflection comparisons for Control Beam, Beam 4 and 5.

Comparing the monotonic response of all five of the beams, one sees that the three beams that were not cycled (Control Beam, Beam 2 and Beam 4) had relatively close values of deflection up to their yield points, Figure 5.43. Beams 3 and 5 were much softer up to that point but they both regained the same stiffness of their twin beam, Figure 5.43. The two beams with the 36 ksi stress range (Beams 4 and 5) showed slightly higher stiffness past the yielding point. This is expected due to the fact that it had more than twice the CFRP that Beams 2 and 3 had which in turn led to a stiffer response and higher ductility as well as strength.

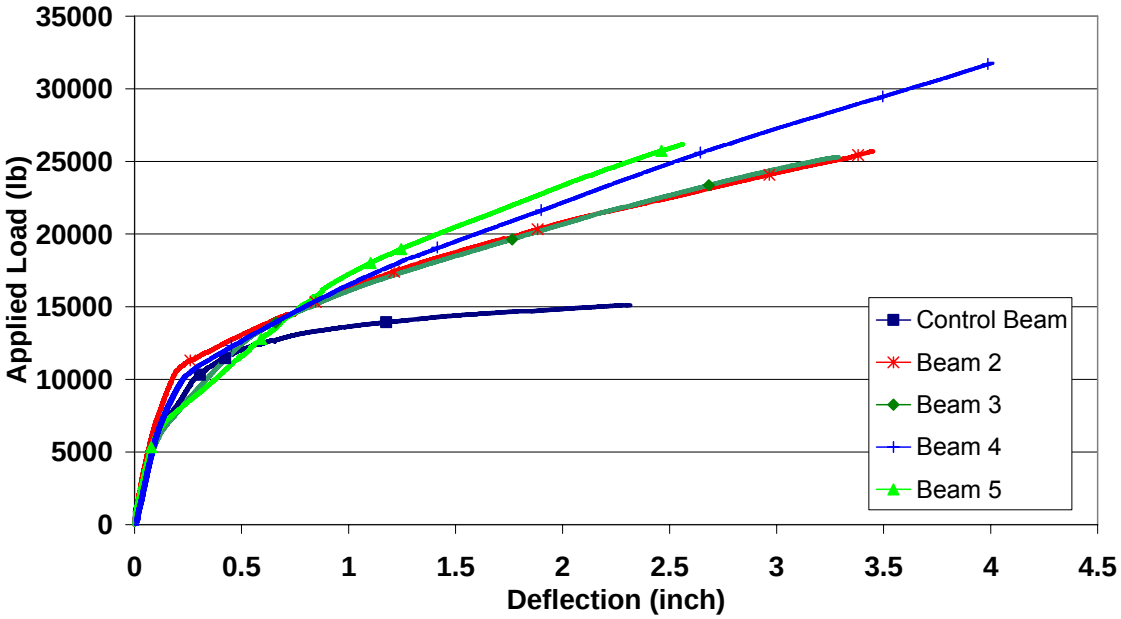

FIGURE 5.43. Load-deflection for all 5 beams.

The ultimate strains of the CFRP in Beams 2, 3, and 4 are much closer to the actual $\varepsilon_{fu}\,(14,000\,\mu\varepsilon)$ obtained from coupon testing (Reed 2002) than those in Beams 5, Figures 5.44 and 5.46. This is due to the fact that Beam 3 only had 1 million cycles applied to it while Beam 5 had 3 million cycles at double the stress range and those extra cycles are expected to have fatigued the CFRP bringing its maximum strain to around 11,000 μ_ε. The bottom strains for Beams 2 and 3, Figure 5.44, show that they were all relatively close except for the Center East gage in Beam 3 peeled off prematurely during the monotonic loading after 1 million cycles of fatigue. It is relevant to reconfirm here the important observations that the FRP is consistently picking up higher strains right after cracking due to their (compared to strain compatibility) superior bond across cracks, thus, relieving the strand strains in the service load range. The top concrete strains of Beams 2 and 3, Figure 5.45, were relatively the same except that the fatigued beam (Beam 3) shows similar softening response for strains up to the yielding

point as that evident in the load-deflection curve. However after yielding the strain begin to equal out.

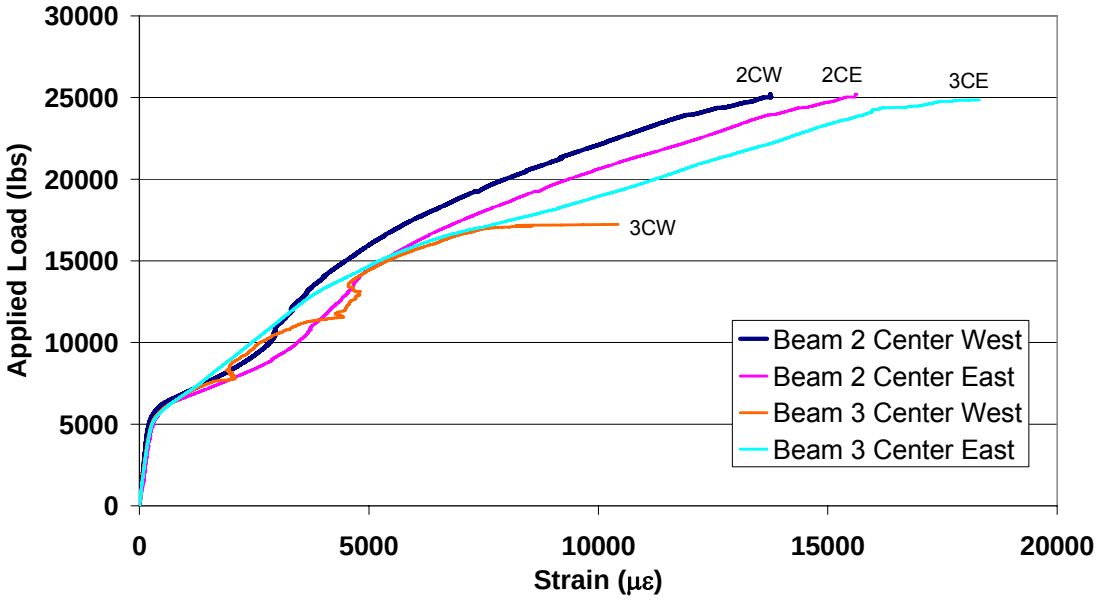

FIGURE 5.44. Bottom CFRP load-strain for Beams 2 and 3.

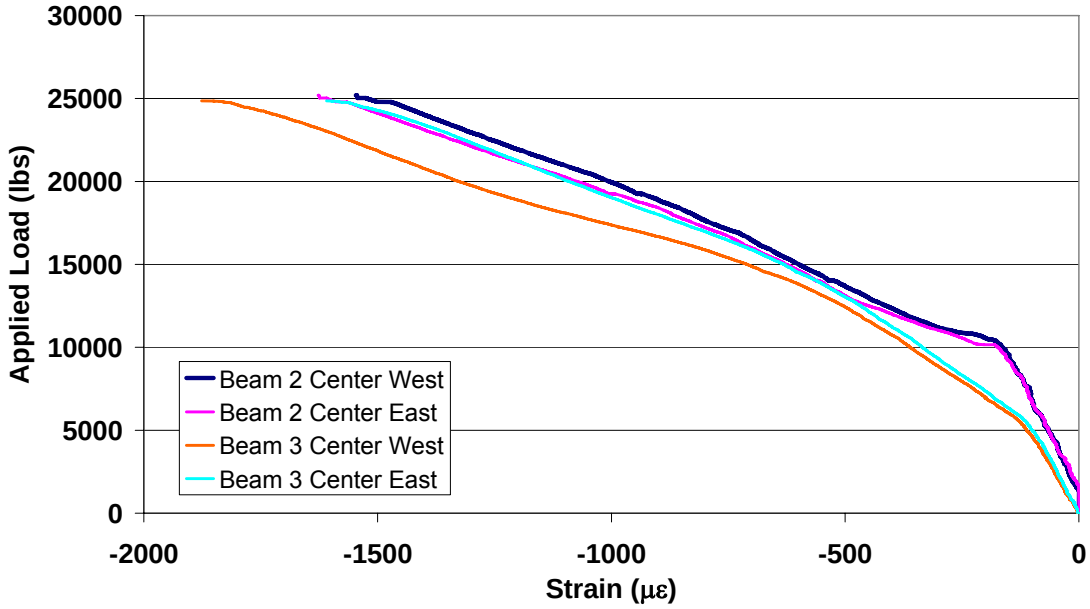

FIGURE 5.45. Top concrete load-strain curve for Beams 2 and 3.

The strains that the CFRP on the bottom web experienced was very close to the same values for both Beams 4 and 5, Figure 5.46. The Center East gage for Beam 4 started off reading compression but it eventually began picking up identical stiffness as the other gages. This could have resulted from a gage misalignment or that there was an air bubble trapped in the concrete depression under the CFRP at that location. The CFRP at 2" above the bottom of the web of Beam 4 is seen to be experiencing much higher strains after cracking than Beam 5, figure 5.47. This is a direct result of Beam 5 being subjected to extensive fatigue cycling that is expected to have contributed to degrading the CFRP bond across cracks causing the strains after crack opening to follow strain compatibility more closely.

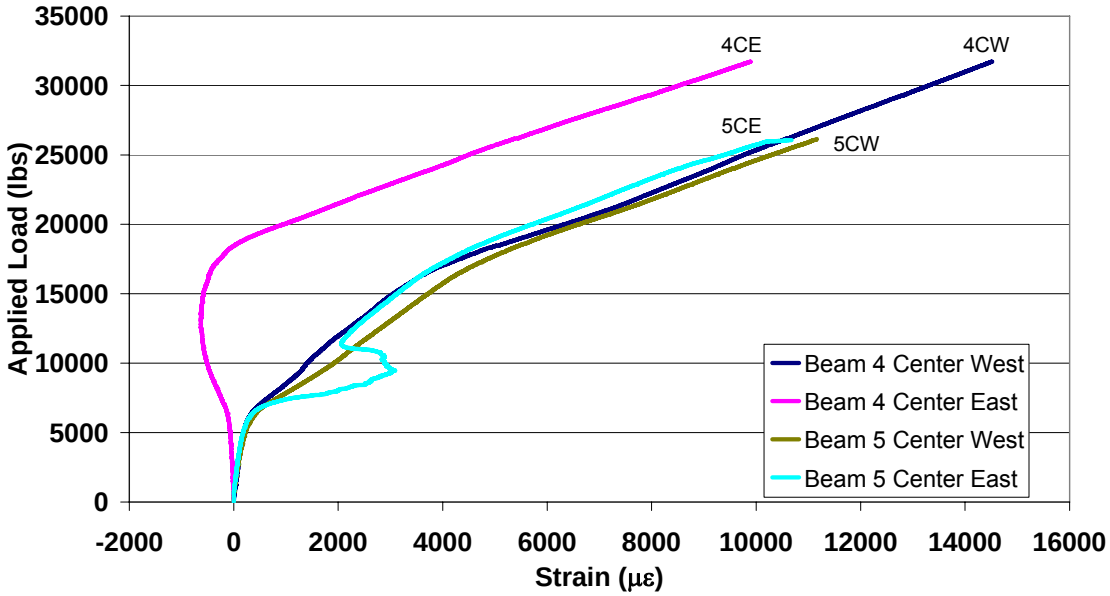

FIGURE 5.46. Bottom CFRP load-strain for Beams 4 and 5.

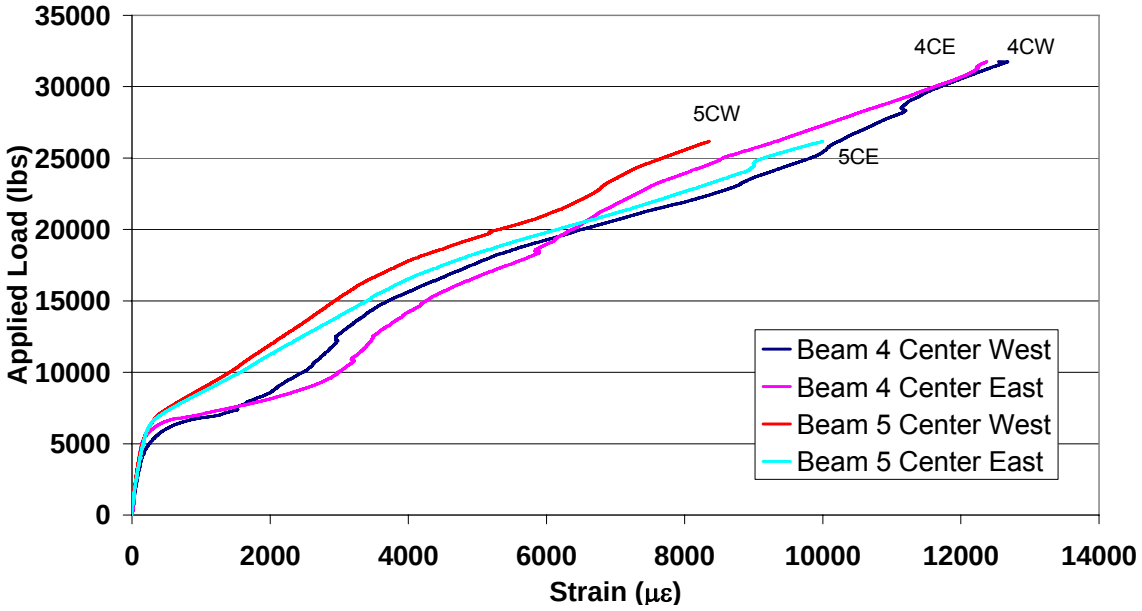

FIGURE 5.47. Side CFRP (2" from bottom) load-strain for Beams 4 and 5.

The load-strains response at the top concrete flange in compression for Beams 4 and 5 is presented in, Figure 5.48. On average, they all follow the same response and the different failure strains are due to the fact that Beam 5 fails well before Beam 4. It is also clear that the Center West gage in both beams consistently reads lower strains. This could be attributed to some minor flange twisting rotation.

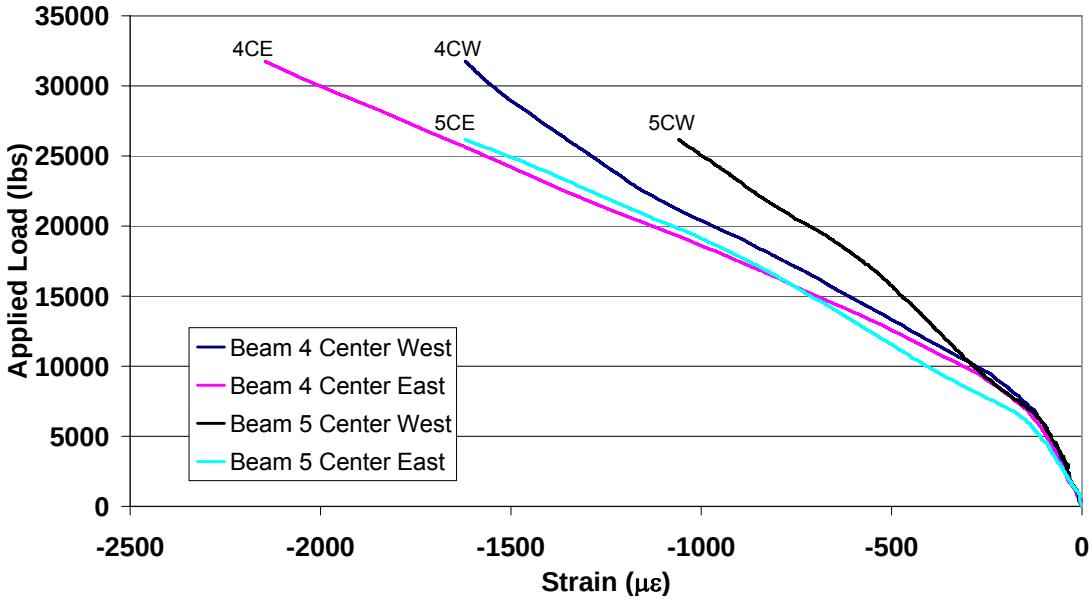

FIGURE 5.48. Top concrete load-strain for Beams 4 and 5.

5.4 ANALYTICAL COMPARISONS WITH EXPERIMENTAL RESULTS

The results of the non-linear analysis program are now compared against the actual experimental results. For the load-deflection graphs, two different types of analyses were performed. One of the analytical results pertains to all sections being fully pre-cracked and the f_r of the concrete was set to zero. This was not the true case during the experimental testing because there was only a single pre-crack at mid-span. The other analytical case started off with the beam initially un-cracked. This model had f_r of the concrete set to $3.3\sqrt{f_c'}$ and took into the account of tension stiffening effects between cracks. It can be seen that the load-deflection curves of the experimental results compare fairly well to those that the analysis, Figure 5.49-5.51.

It can be seen that the analysis load-deflection results for the control beam assuming the initially un-cracked beam yields noticeably good correlation with experiment, thus, providing a more representative means for predicting the behavior of the beam, Figure 5.49. The reason why the analysis has a much larger deflection at failure is that the experiments were run in force control and data points were recorded every second so the deflection at the ultimate failure point may not have been instantaneously recorded while the analysis is based on deformation control. Tension stiffening was found to be effective in this beam up to a tensile concrete strain of 50 ε_{cr}. Comparing the experimental response of Beams 2 and 3 with the analytical results, for the 18 ksi stress range design, the load-deflection curve is also seen to produce good correlation, Figure 5.50. The analysis for the initially un-cracked beam compare very well with Beam 2 up to the yielding point because it only had the one single pre-crack at mid-span. On the other hand, the comparison is still good with both beams after

yielding and the small difference could be attributed to the slightly stiffer strand response compared to that of the standard 270 ksi used in the analysis. Due to additional stiffening effect of CFRP, tension stiffening was found to be effective up to 70 ε_{cr}. Comparing the response of Beams 4 and 5 with the analytical results of the 36 ksi stress range design, the load-deflection curves also produced good correspondence, Figure 5.51. The analysis for the initially un-cracked beam showed excellent correspondence against the Beam 4 curve up to the yielding point and compared very well after that all the way to failure. On the other hand, Beam 5 compared well with the analytically pre-cracked beam results after the crack opening point. The fact that the initial stiffness of all the experimentally strengthened beams was matching the analytical initial stiffness once again shows that the bond between the CFRP and the concrete is excellent.

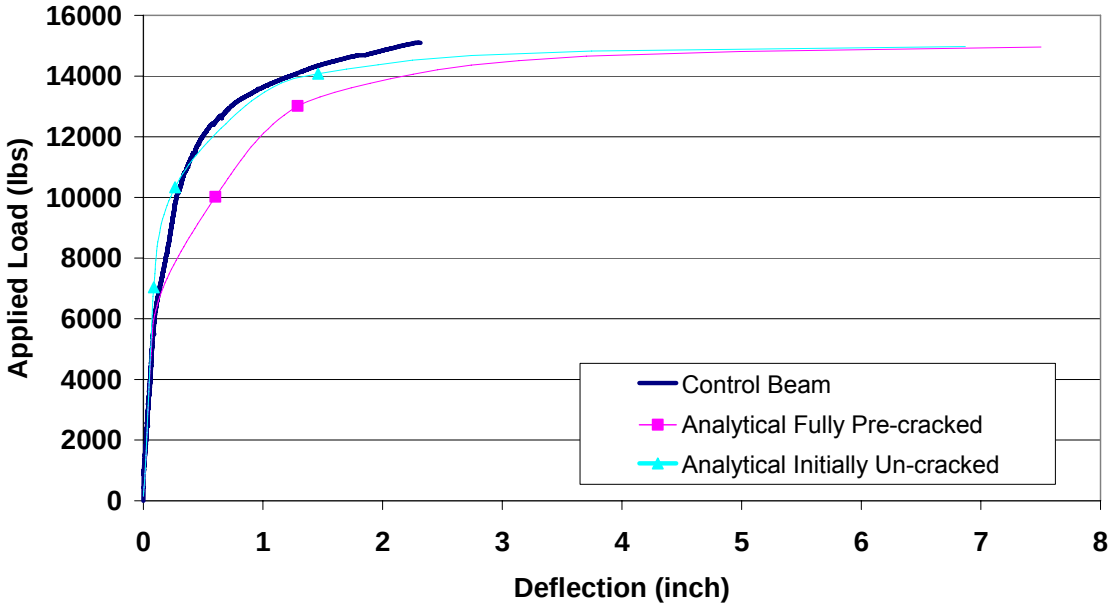

FIGURE 5.49. Analytical against experimental load deflection results of control beam.

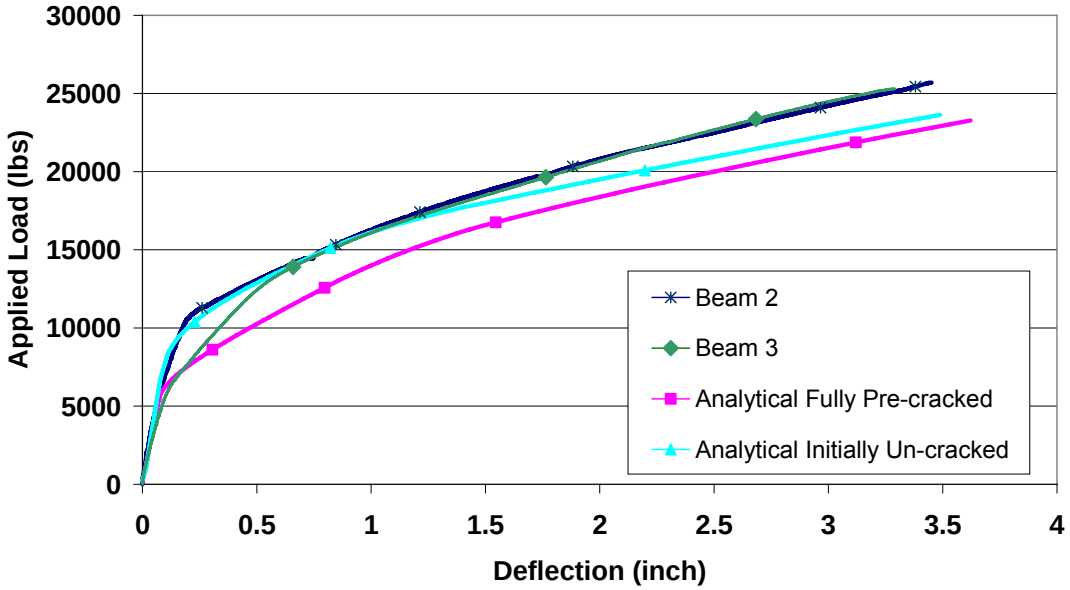

FIGURE 5.50. Analytical against experimental load-deflection results of Beams 2 and 3.

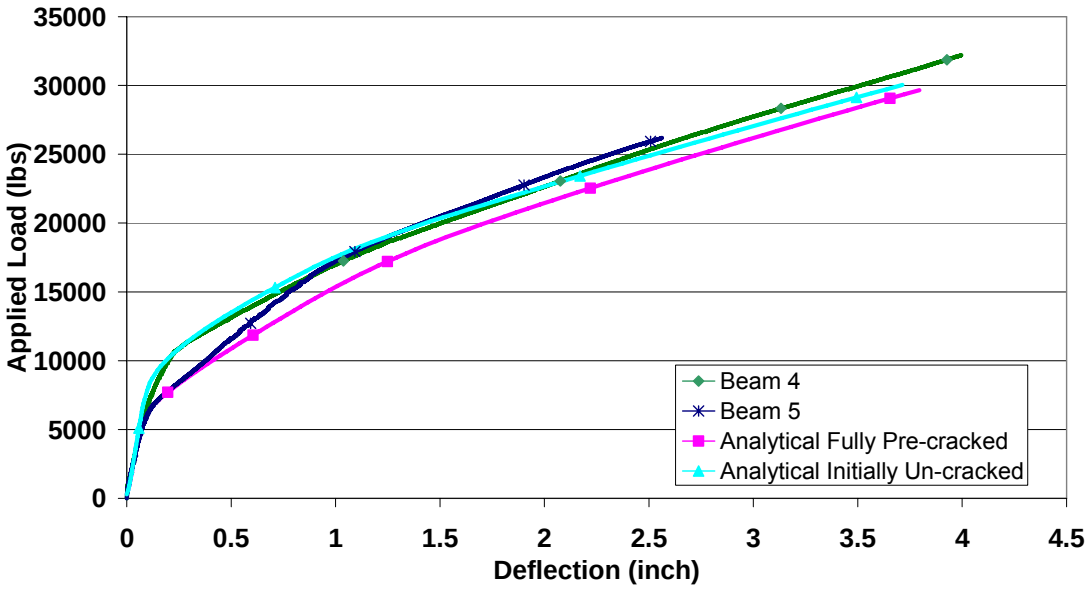

FIGURE 5.51. Analytical against experimental load-deflection results of Beams 4 and 5.

The service load deflections for the analytical fully pre-cracked beam are shown against those of the Control Beam, Beam 2, and after the first and final load cycle for Beam 3, Figure 5.52.

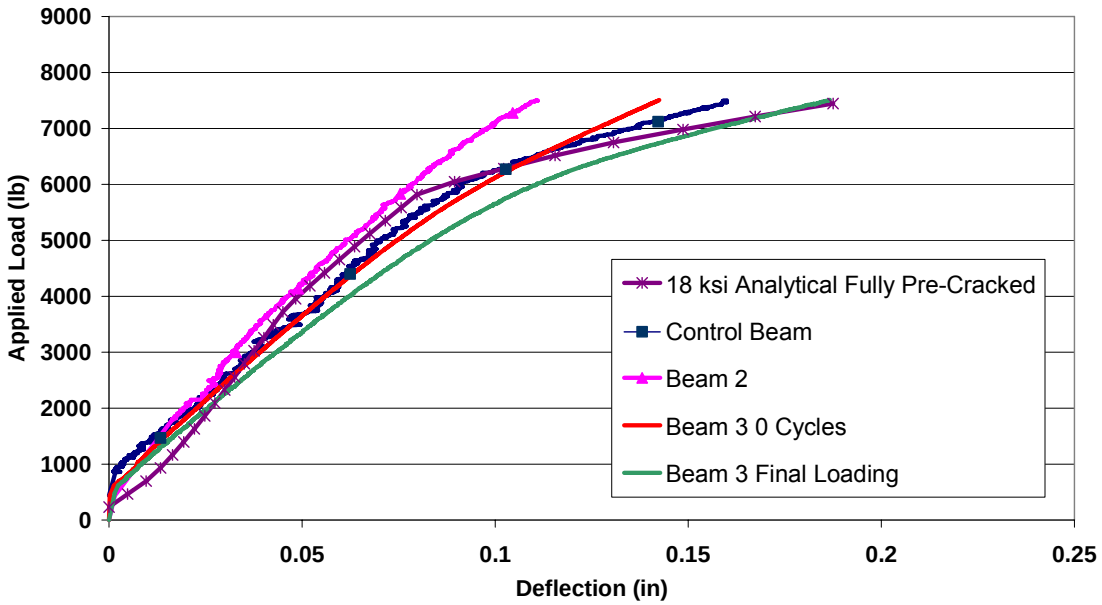

FIGURE 5.52. Service load-deflection response.

When comparing the experimental and analytical strains, a pre-cracked section analysis is implemented since the focus is to study the response at critical (pre-cracked) sections. Comparing the analytical top concrete compression strains against the corresponding actual strains for Beams 2 and 3 and Beams 4 and 5 netted very good correspondence, Figures 5.53 and 5.54 respectively. The analysis and experimental strains in the CFRP compared very well in the post yielding range, Figures 5.55 and 5.56. On the other hand, the CFRP had much higher strains in the experimental results within the live service load range than those strains from the analysis. A major reason for this is that the CFRP in the experimental beams are picking up a much greater strains across cracks than expected from strain compatibility. This is due to the excellent bond between the CFRP and the concrete across cracks. Other than this, the minor difference in the load-strain curves between the different gages and the analysis

is attributed to the localized nature of this response that change strain values according to their proximity to cracks.

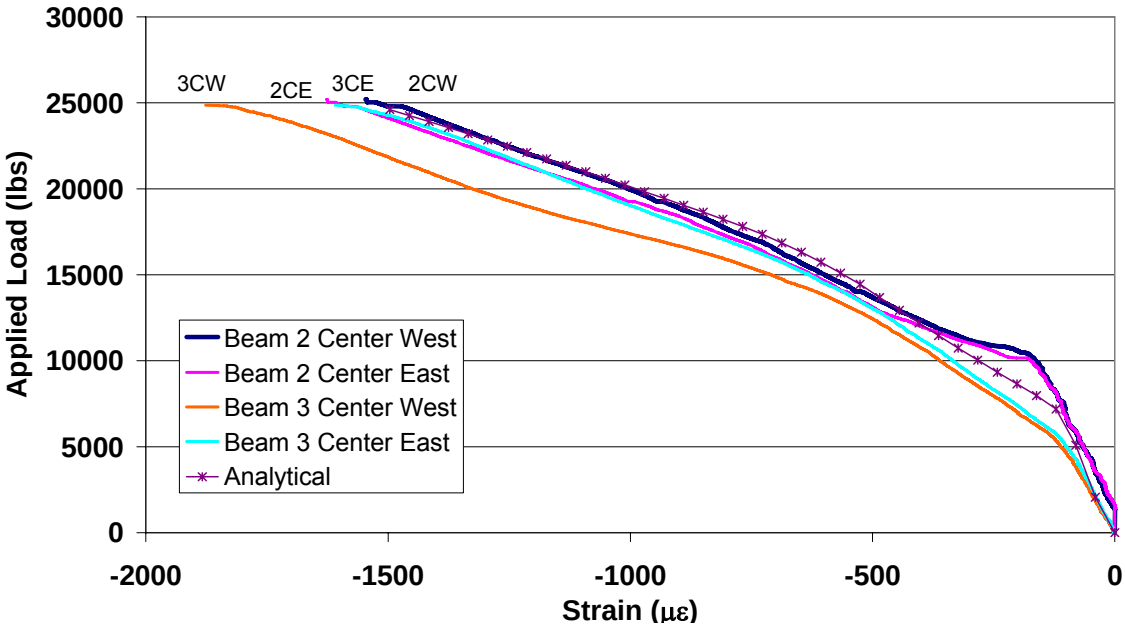

FIGURE 5.53. Analytical vs. experimental compression strains for Beams 2 and 3 (Top concrete).

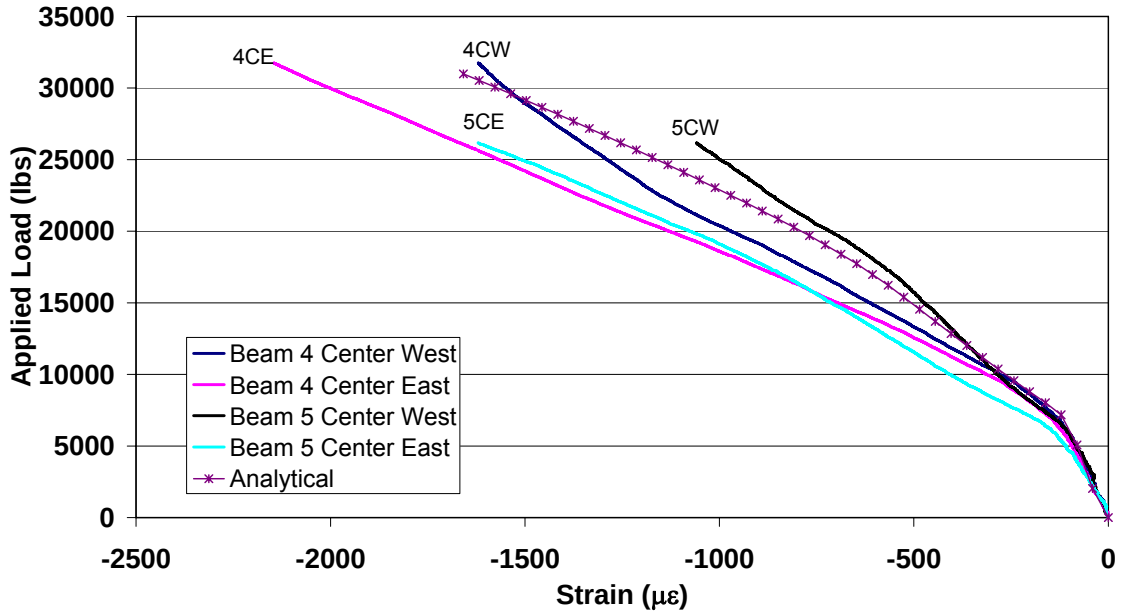

FIGURE 5.54. Analytical vs. experimental compression strains for Beam 4 and 5 (Top concrete).

The bottom CFRP strains for the experimental results showed noticeably higher strains than the analytical results after cracking for the 18 ksi stress range strengthened beams, Figure 5.55. These strains recover their strain compatibility values after the strand yielding range of the curve. The 36 ksi stress range strengthened beams show a much closer comparison, Figure 5.56. The one gage that did not follow the curve had very high post cracking strain attributed to possible direct bridging of the mid-span crack. However, it returned to the typical response as enough slippage took place.

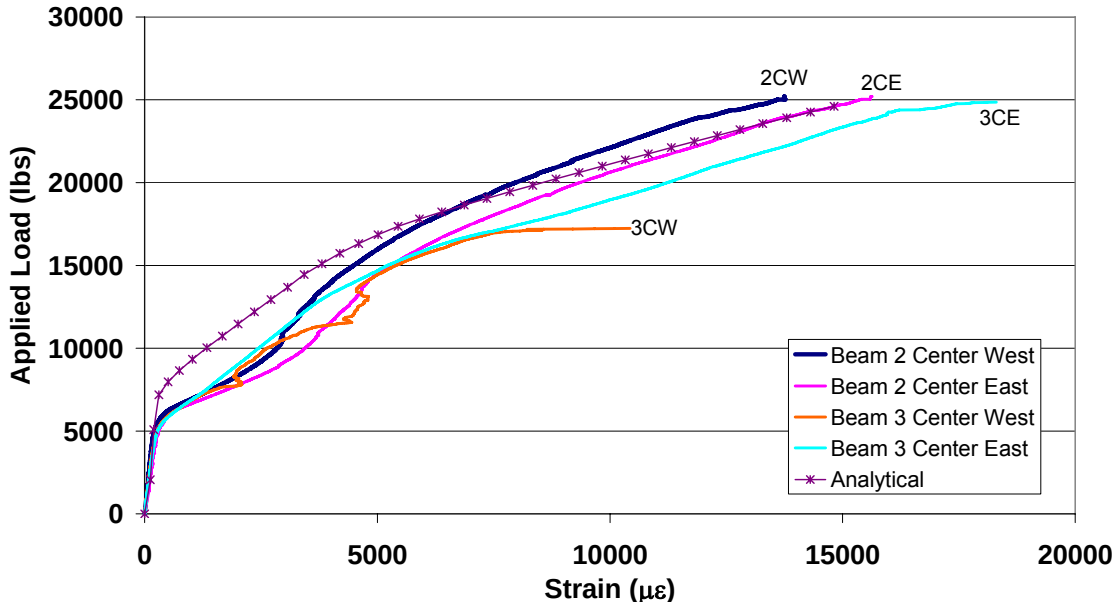

FIGURE 5.55. Bottom CFRP strains for 18 ksi stress range strengthened beams.

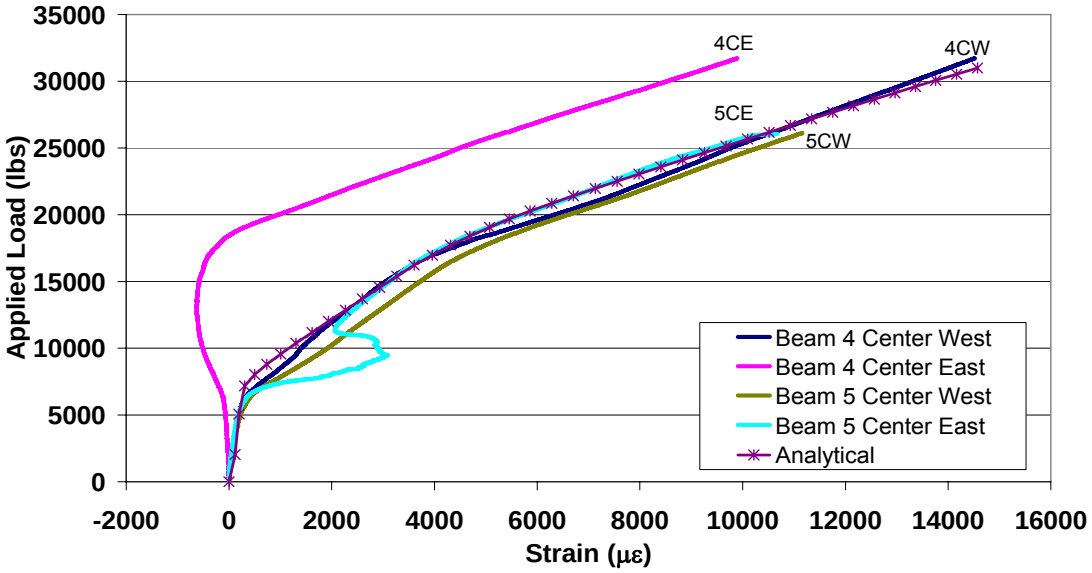

FIGURE 5.56. Bottom CFRP strains for 36 ksi stress range strengthened beams.

The side CFRP strains (at 2" up from the bottom of the web) for the experimental results resulted in much higher strains than the analytical results for the 18 ksi stress range strengthened beams as well, Figure 5.57. These strains began to get closer through the yielding zone of the curve. The comparisons for the 36 ksi stress range strengthened beams show similar behavior as that of the 18 ksi stress range strengthened beams, Figure 5.58.

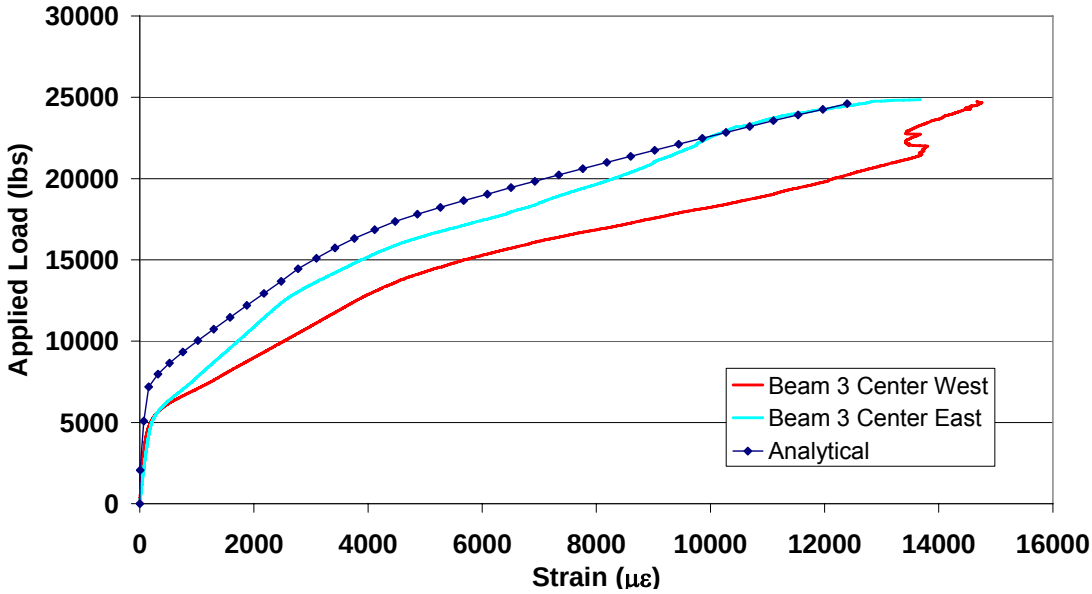

FIGURE 5.57. Side CFRP strains for 18 ksi stress range strengthened beams.

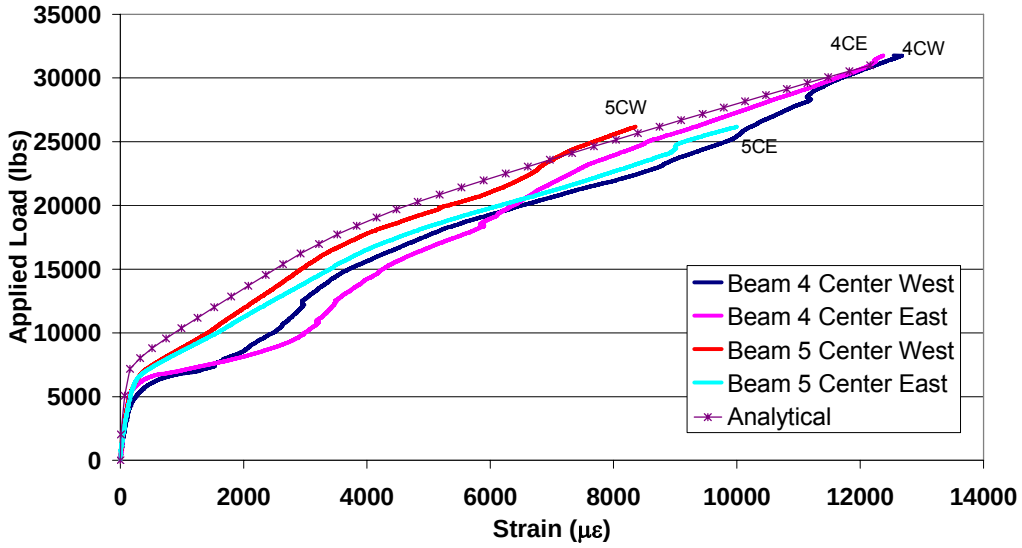

FIGURE 5.58. Side CFRP strains for 36 ksi stress range strengthened beams.

To verify the actual stress range that the strands have undergone under the 18 ksi based service load limits, the top strand in the constant moment region of Beam 3 is exposed, Figures 3.12 and 3.13. Gages were put on the top prestressing strand to fully investigate the stress range of that strand, Figure 3.14. Figure 5.59 shows that the experimental values at service load are slightly less than those from the analytical results. A slightly lower stress range in the top prestressing strand was expected because the CFRP was picking up more strain at this load level.

Comparing the CFRP strains of the bottom web in Beam 3 with the analytical results (from strain compatibility) for service load conditions show that the experimental measurement yields a noticeably greater strain in the CFRP, Figure 5.60. This is where it was first noticed that the CFRP was experiencing a much greater stress range than the prestressing strand was undergoing. Similar behavior was observed for those strains in the CFRP that are 2" up the side of the web on the same height as the bottom prestressing strand, Figure 5.61.

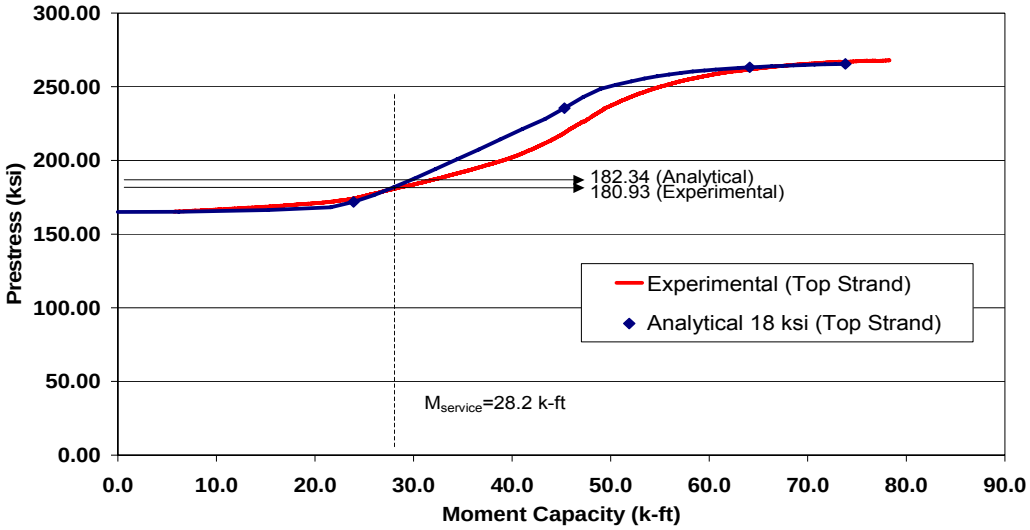

FIGURE 5.59. Experimental and analytical stress ranges of top strand for Beam 3.

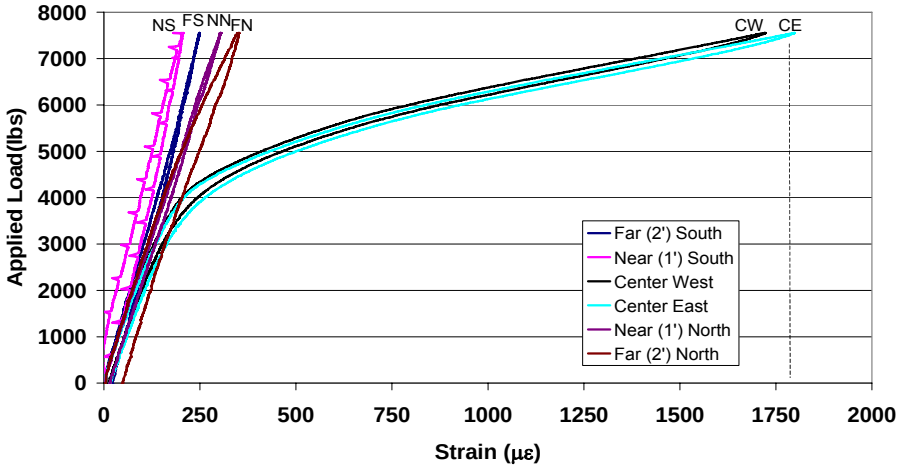

(a)

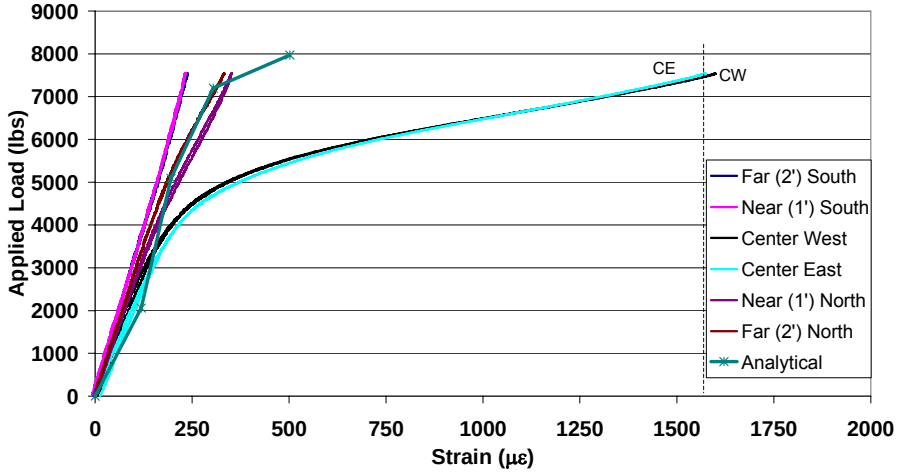

(b)

FIGURE 5.60. Bottom CFRP strains for Beam 3 under service load conditions (a) At 0 cycles (b) After 700,000 cycles.

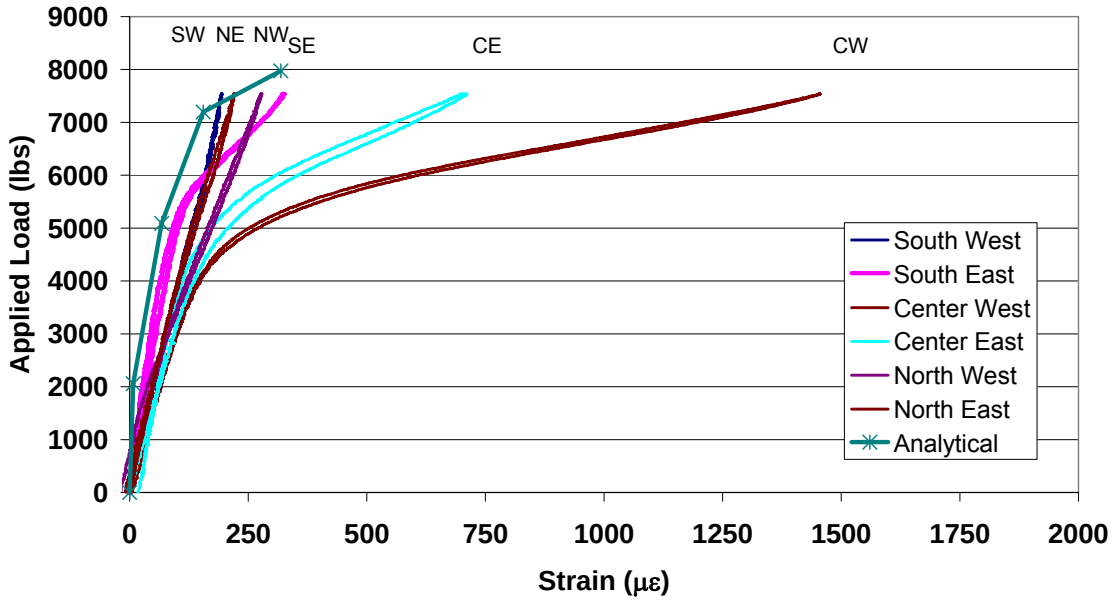

FIGURE 5.61. Side CFRP strains of Beam 3 under service load conditions after 700,000 cycles.

The top concrete strains for Beam 5 show a slightly higher strain response than that of the analytical results at 0 cycles, Figure 5.62a. The experimental values of these strains are seen to slightly increase after 2 million cycles, Figure 5.62b. This is attributed to some concrete creep that increases under repeated compression stresses. Figures 5.63 and 5.64 compare analytical and experimental results for bottom and side CFRP strains in Beam 5, respectively at 0 cycles and after 2 million cycles. The bottom CFRP strain compare better, however, the strain in the bottom CFRP is seen to increase under the same load level as the number of cycles is measured. The side CFRP is the opposite in that the CFRP strains are seen to decrease as the number of cycles increases which is the expected thing to happen due to the continuous degradation of CFRP bond across cracks.

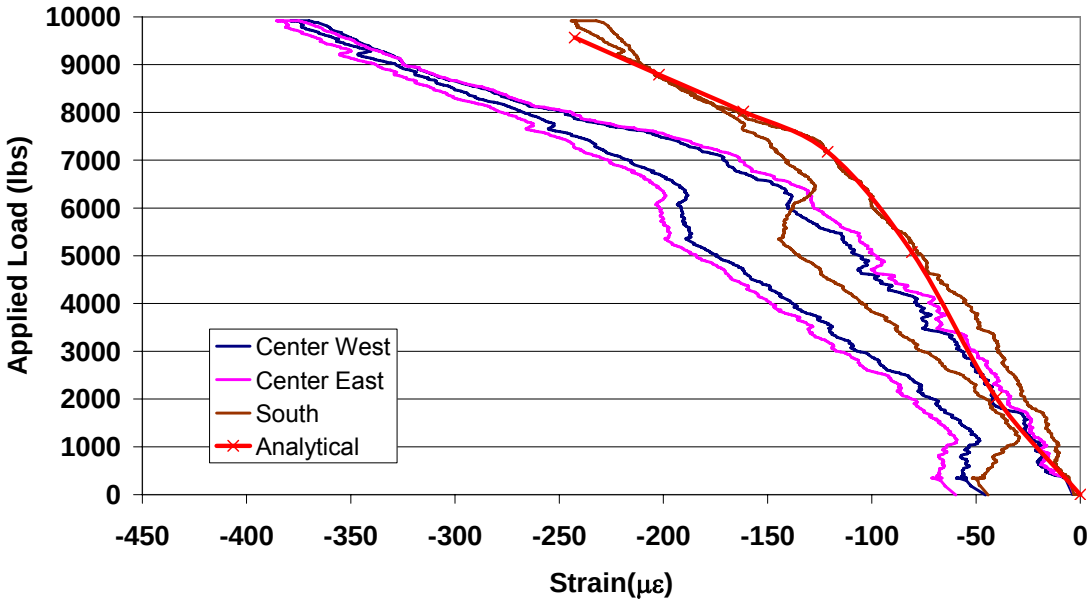

(a)

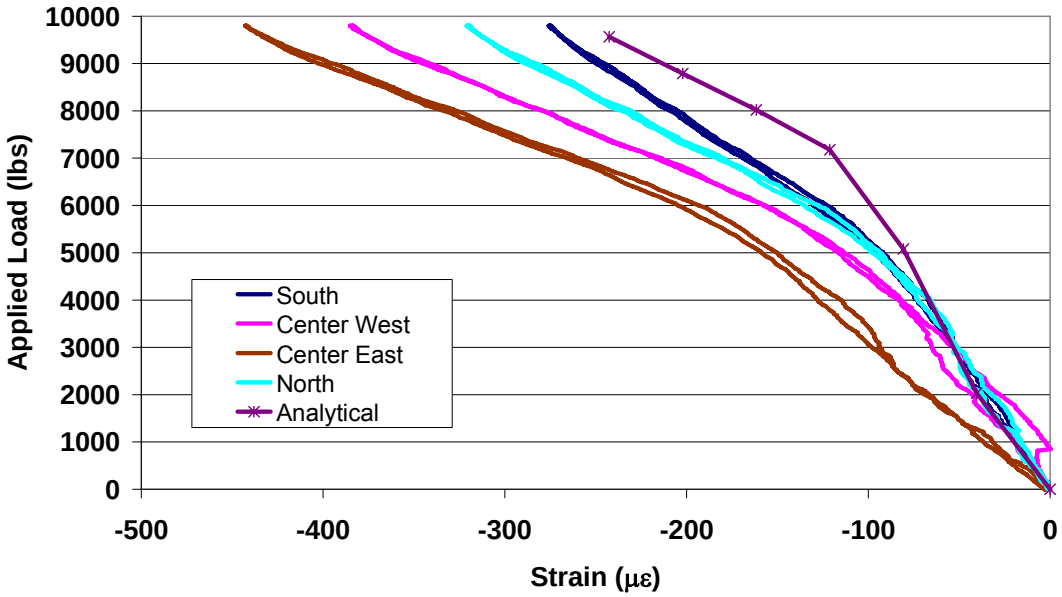

(b)

FIGURE 5.62. Top concrete strains at mid-span of Beam 5 (a) At 0 cycles (b) After 2 million cycles.

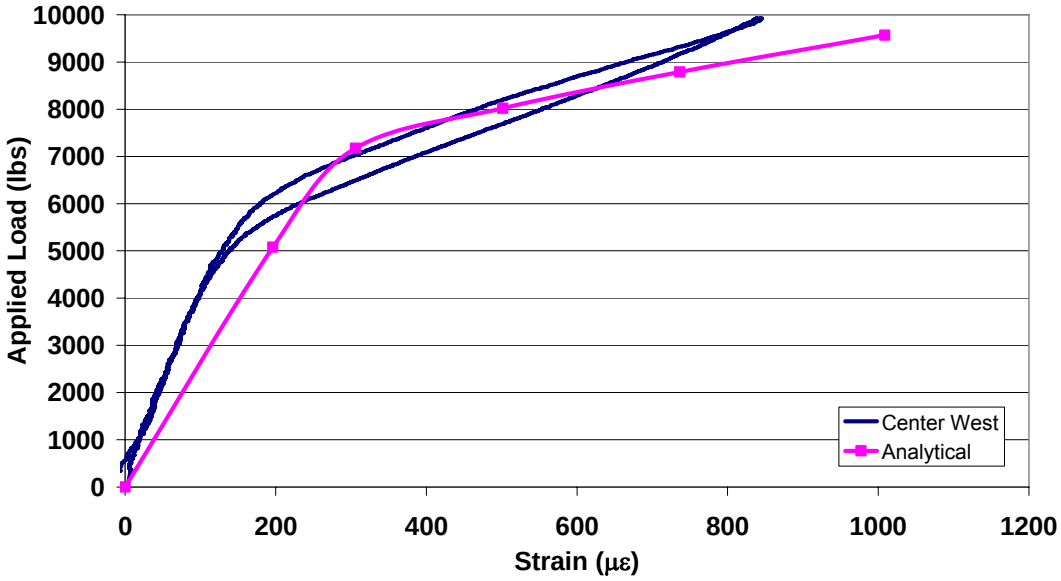

(a)

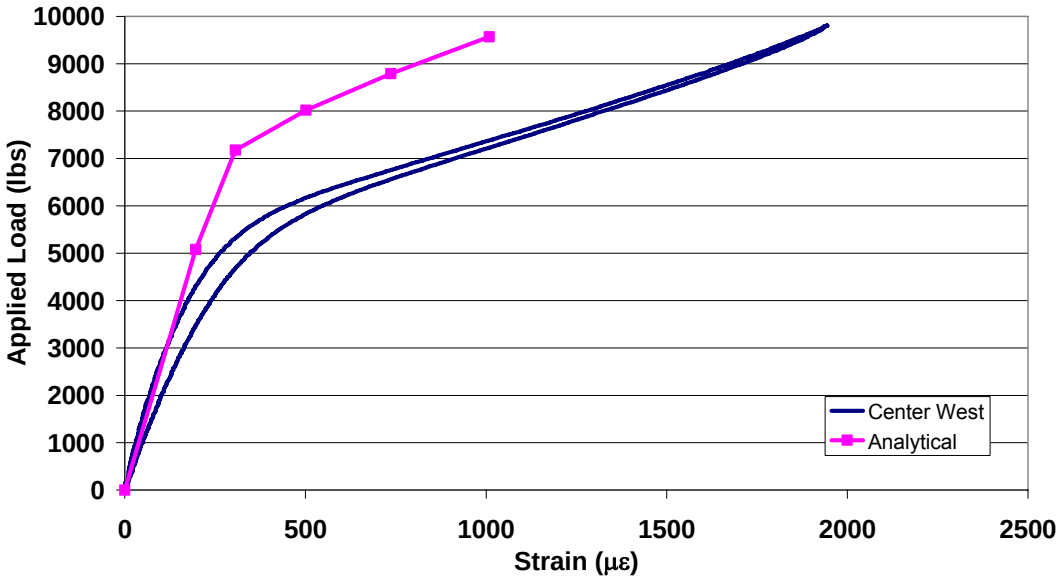

(b)

FIGURE 5.63. Bottom CFRP strains at mid-span in Beam 5 (a) At 0 cycles (b) After 2 million cycles.

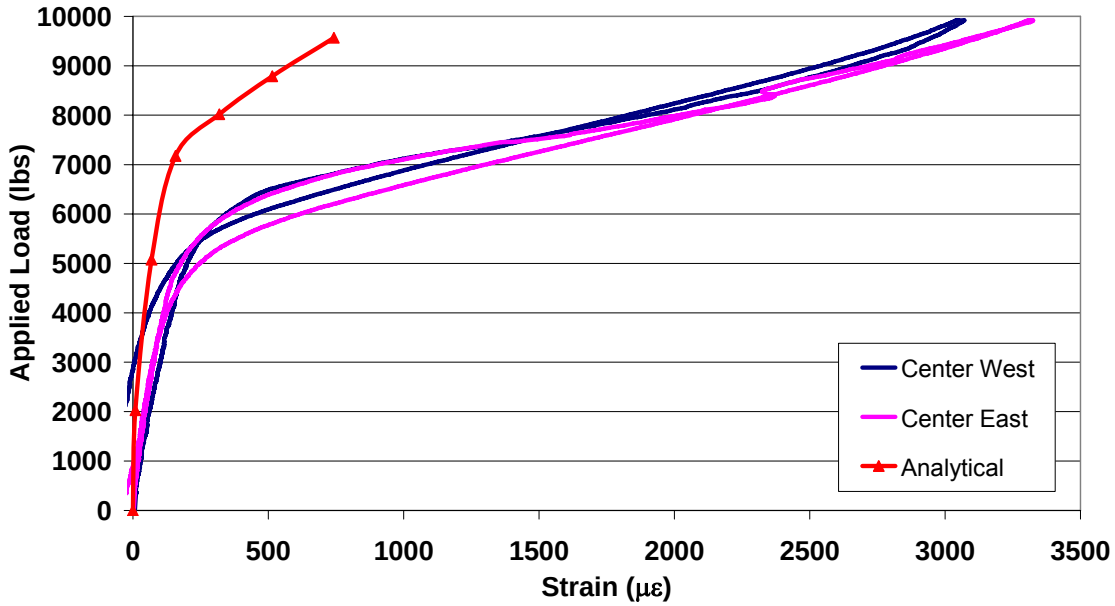

(a)

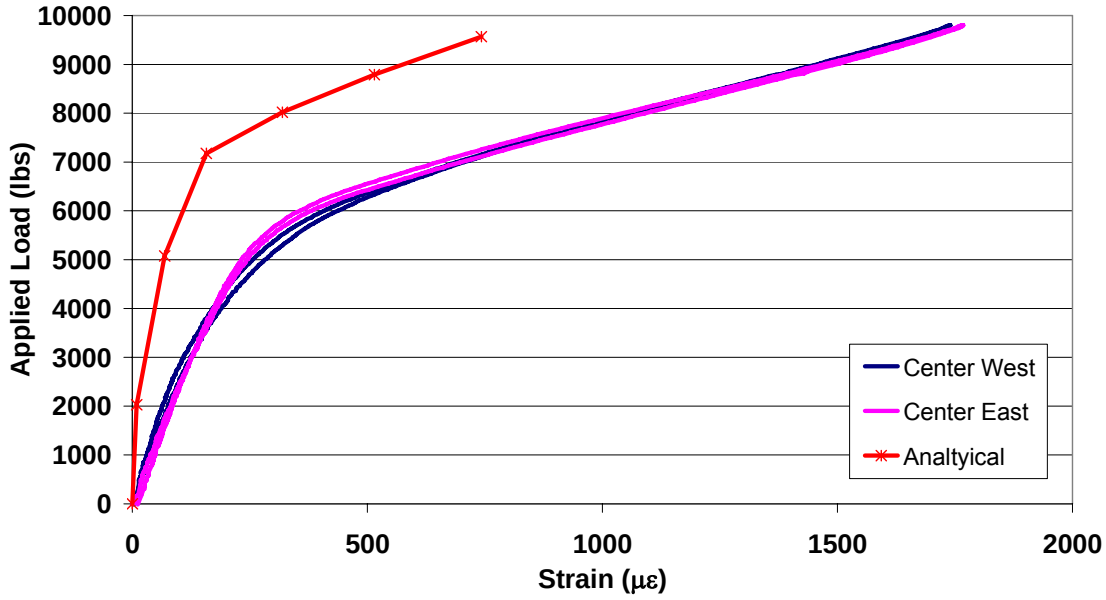

(b)

FIGURE 5.64. Side CFRP strains in Beam 5 (a) At 0 cycles (b) After 2 million cycles.

5.5 IN-ISOLATION STRAND FATIGUE TESTING

To independently verify the fatigue performance of the 3/8" straight prestressing strand, three specimens, 3.5 ft long each, were removed from lightly stressed areas near the supports of the girder specimen Beam 3 and tested alone. A special test setup was designed and built to ensure no stress concentration at the gripping points by passing 4" of the strand ends through an epoxy-filled thick metal cylinders. The cylinders that were used as tension grips have 1.125" outer diameter and 0.5" inner diameter and the strand extends 4" beyond each cylinder end leaving a gage length of 26" (total strand length is 42"), Fig. 5.65. The test fixture (strand and end grips) was subjected to cyclic tension in a testing apparatus as illustrated in Figures 5.66 and 5.67.

FIGURE 5.65. Embedding prestressing strand end through epoxy-filled thick metal cylinder grip.

Three different levels of strand stress range were examined, Table 5.2. The lower level of strand stress was kept the same as that in mid-span strands of the beams

tested in flexural fatigue. It is evident from the first test that cycling under 72 ksi stress range caused 3 external strand wires to break at 72,101 cycles hindering the ability to reload. The second test showed that 36 ksi stress range caused 3 external strand wires to break progressively at 2,505,505 for the first wire, 2,817,500 for the second wire and 3,179,669 for the third wire. This specimen could not be reloaded after the breakage of the third wire. This result matches very well the result obtained from Beam 5 that was able to successfully sustain 3 million cycles of fatigue. Furthermore, Beam 5 showed a reduced ultimate capacity under static monotonic loading after fatigue perhaps due to the breakage of a strand wire or two during the application of the 3 million cycles.

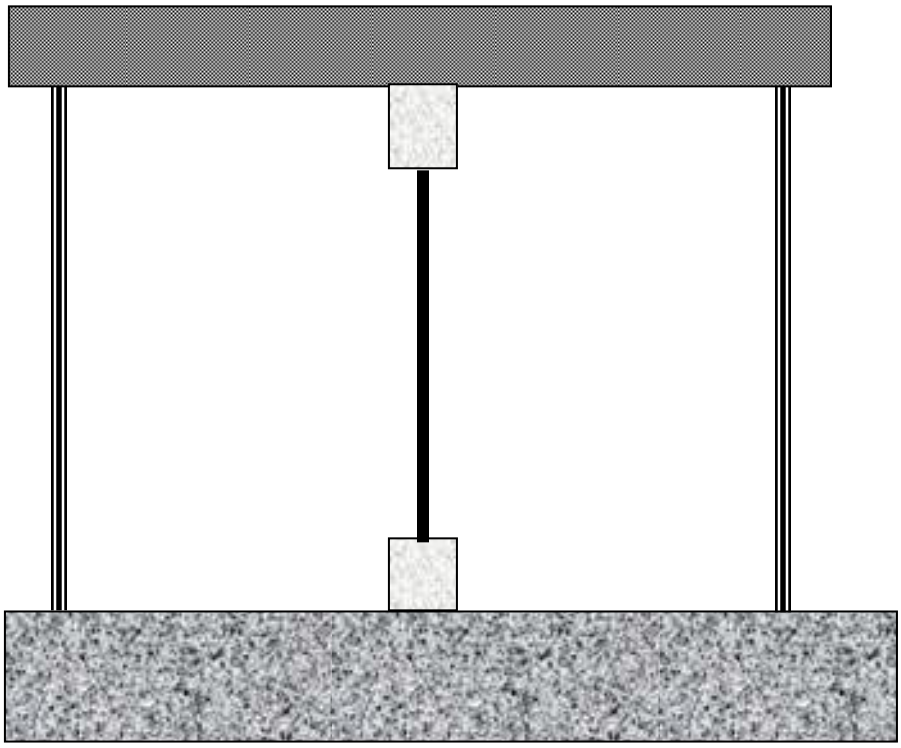

FIGURE 5.66. Schematic of test setup used for the fatigue of prestressing strand.

From the third test, it was seen that the 18 ksi stress range never caused any fatigue fracture even after 10 million cycles and this test was accordingly stopped. With

this result, it may be concluded that Beam 3, cycled under 18 ksi stress range, had easily sustained the 1 million cycles of fatigue and the degradation of stiffness beyond that point may be attributed to new flexural cracks opening in the constant moment region. AASHTO LRFD (1998) section 5.5.3.3 allows a straight prestressing strand to have up to 18 ksi stress range to avoid breakage under fatigue. This AASHTO section is indirectly verified by the present test results. On the other hand, the present tests indicate that State Departments of Transportation may double the strand stress range to 36 ksi when strengthening bridge girders to extend their lives for 10-20 more years if the number of equivalent fatigue cycles they will get subjected to is not in excess of 3 million.

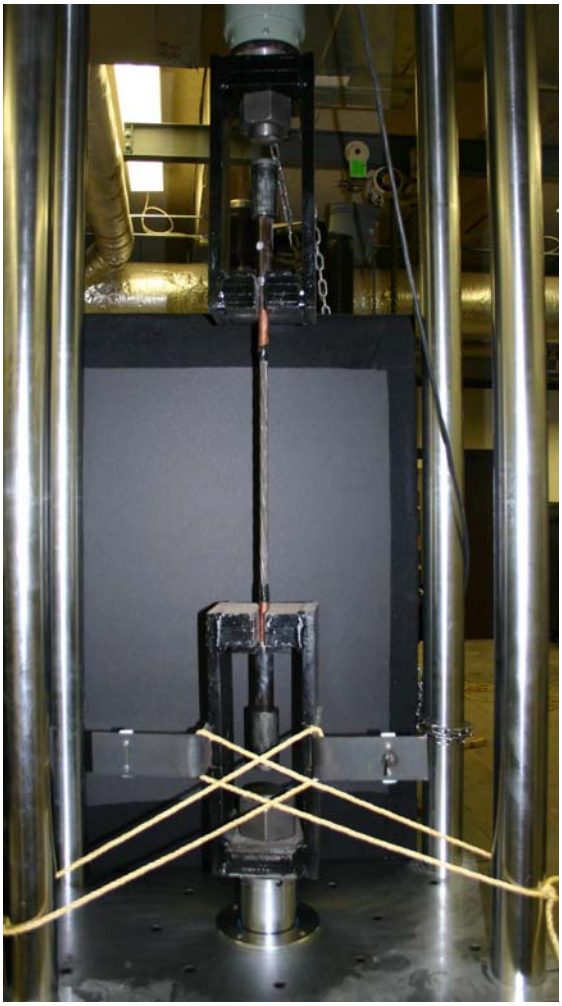

FIGURE 5.67. Photo of test setup used for the fatigue of prestressing strand.

Strand stress range	Stress limits	Load limits	Cycles to failure
18 ksi	165.3-183.3 ksi	14.05-15.58 kips	No fracture (>10 million)
36 ksi	165.3-201.3 ksi	14.05-17.11 kips	1st fracture at 2,505,505 2nd fracture at 2,817,500 3rd fracture at 3,179,669
72 ksi	165.3-237.3 ksi	14.05-20.17 kips	3 fractures at 72,101

TABLE 5.2. Results of strand fatigue testing.

CHAPTER 6

CONCLUSIONS AND RECOMENDATIONS

6.1 CONCLUSIONS

This part forms the second phase of a research project conducted for KDOT. In the first phase, 30-year-old PC T-girders decommissioned from an actual bridge were strengthened and tested in static loading and fatigue. These girders showed success in strengthening up to a 50% increase in ultimate capacity over the original control beam design. However, they showed a limited success in fatigue performance. This was attributed to a combination of interacting factors including stress concentration at push down or hold down device to harp strands, strand corrosion due to excessive pre-cracking, and a high strand stress range (37 ksi) for the strengthened girders. The latter should be limited to 10 ksi for harped strands and 18 ksi for straight strands as per the AASHTO LRFD 1998.

This follow-up study builds on the findings of phase I and isolates the variables to explore their effects. Accordingly, it focuses on studying the influence of stress range. Therefore, a series of five new precast, prestressed single-T girders with straight strands was constructed and tested. The girders are designed to have the same prestressing ratio as those of phase I. The research addressed two target average prestressing strand stress ranges. The first one related to the limit imposed by the AASHTO requirements and the second one tied to the stress range obtained in phase I (36 ksi). The beams were pre-cracked at a mid-span crack former to ensure high stress ranges at the cracked section.

This work has developed an iterative design procedure relating the serviceability stress range level targeted to the strengthening index furnished. The 18 ksi stress range beam design showed excellent fatigue performance after sustaining more than one million cycles (Beam 3). This beam also achieved the full ultimate strength and ductility of an identical specimen monotonically loaded to failure without cycling (Beam 2). This indicates that the fatigue life of Beam 3 under 18 ksi stress range may not have been exhausted by 1 million cycles of loading. This conclusion was further reinforced by strand tensile fatigue, in isolation, yielding 9 million cycles at the same stress range without breakage. The 36 ksi stress range beam design also showed a surprisingly outstanding fatigue performance. Beam 5 was cycled 3 million times at this higher stress range without showing signs of noticeable stiffness degradation. The beam, however, failed prematurely in static loading indicating that the ultimate strength of its CFRP or strand must have been significantly reduced by the 3 million load cycles. The results in Table 5.2 suggest that the strand is expected to have the reduced strength due to fracture of a couple of wires. The global stiffness response of Beam 5 matched that of Beam 4, monotonically tested to ultimate, indicating a fatigue impact on strength not stiffness degradation, which was the opposite in phase I. It is important to draw the following additional conclusions:

1. The excellent fatigue performance of the present CFRP strengthening designs for both stress range levels minimizes the influence of this factor in reducing fatigue life in phase I. That leaves the effects of stress concentration in harped strands and corrosion as the two factors to examine next.

2. It is proven to be possible to design for and achieve high strengthening levels (70% and 113%) while still controlling stress range fatigue requirements.

3. An interesting new phenomenon is observed and proven applicable through comparisons among various experimental results along with analysis findings. Due to its superior bonding to concrete across cracks, CFRP is seen to develop higher strains at critical sections than those recovered from strain compatibility. This is shown to reduce the strand stress range at such critical sections proving to be a beneficial bi-product of strengthening.

6.2 RECOMENDATIONS

The following are recommendations for future research extensions to part II:

1. Testing the prestressing strand from these beams and CFRP coupons in tensile fatigue to assess their performance under 36 ksi stress range.

2. Cycling same beams under higher stress range (54 ksi and 72 ksi) to identify the limiting effects of this factor on fatigue life.

3. Examining the effect of harped strand combined with a lower level of stress range (lower than that experienced in phase I) of 18 ksi for limited strengthening levels.

4. Combining significant strengthening levels, harped strand, and lower stress range of 18 ksi through stress relief by over reinforcing.

REFERENCES

AASHTO LRFD (1998). *AASHTO LRFD Bridge Design Specifications* (Second Edition). American Association of State Highway Transportation Officials, Washington D.C.

ACI Committee 318 (1999), *Building Code Requirements for Structural Concrete (ACI 318-99) and Commentary (ACI 318R-99)*. American Concrete Institute, Farmington Mills, MI.

El-Tawil, S.; Okeil, A. M., (2002). "LRFD flexural provisions for prestressed concrete bridge girders strengthened with carbon fiber-reinforced polymer laminates," ACI Structural Journal, Vol. 99, No. 2, pp. 181-190.

El-Tawil, Sherif, Ogunc, C., Okeil, A., and Shahawy, M. (2001). "Static and Fatigue Analyses of RC Beams Strengthened with CFRP Laminates," Journal of Composites for Construction, November, Vol 99. pp. 258-267.

Hassan, T.; Rizkalla, S., (2002). "Flexural strengthening of prestressed bridge slabs with FRP systems," PCI Journal, Vol. 47, No. 1, pp. 76-93.

M-Brace (1998). *M-Brace Composite Strengthening System-Engineering Design Guidelines* (Second Edition) Master Builders Technologies, Cleveland, OH.

Precast/Prestress Concrete Institute (1999). *PCI Design Handbook*, 5th Edition, Chicago, Illinois.

Reed, C., (2002), "Strengthening of 30 Year Old Prestressed Concrete Bridge Girders with Carbon Fiber Reinforced Polymers," Thesis submitted in partial fulfillment of Master's of Science, Kansas State University, USA, 95 pp.

Shahawy, M.; Beitelman, T. (1999). "Static and Fatigue Performance of RC beams Strengthened with CFRP Laminates," Journal of Structural Engineering, June, pp. 613-621.

NOTATIONS

A_f = the FRP flexure sheet area,

A_p= area of one prestressing strand,

b = the width of the section,

b_f = the width of the composite plate,

c = the neutral axis depth of the section,

d = the effective depth of the section to steel reinforcement,

d_f = the total depth to the centriod of the FRP plate,

e= eccentricity of prestressing force to the section centroid,

E_s = the modulus of elasticity of the reinforcing steel,

E_f = the FRP plate modulus,

E_c = the modulus of elasticity of the concrete,

f'_c = the compressive strength of the concrete,

f'_t =the tensile strength of the concrete,

f_s = is the stress in the tension steel,

f_f = the stress in the FRP plate,

f_r= modulus of rupture of concrete,

H = height of the section,

I_{gt}= un-cracked transformed moment of interia,

L = beam span,

M_{cr} = the moment at first cracking,

M_n = nominal ultimate moment of the section,

M_u = analytical ultimate moment of the section,

M_{SB}= maximum moment due to the spreader beam weight,

M_D= maximum moment due to the dead weight of the beam,

M_{LL}= maximum beam moment due to the applied live and spreader weight,

M_L= maximum beam moment due to the applied live load,

$M_{service}$= maximum beam moment due to dead load, spreader beam weight and live load,

M_{co}= moment at which crack begins to open,

P_e= prestressing force,

$P_{failure}$= load at which beam fails die to FRP separation,

P_{ull}=load at PC beam failure including the spreader beam weight,

y_t= distance of neutral axis to bottom fiber,

Δ_{ull}=ultimate live load deflection of PC beam with spreader beam deflection included,

ε_y = the yielding strain of the steel,

ε_{fu} = the design ultimate strain in the FRP plate,

ε_{cf} = the compressive strain of the extreme concrete fiber,

ε_y = the yielding strain of the reinforcing steel,

ε_o = the initial strain during the stage of strengthening,

ε'_c = the strain corresponding to f'_c,

APPENDIX A

CALCULATION OF PRESTRSSING STRAND LOSSES (Based on PCI Method)

$P_{jacking}$ per strand = 16,600 lb

$$f_i = f_{pj} = \frac{P_{jacking}}{A_p} = \frac{16,600\,lb}{0.08583\,in^2} = 193.41\,ksi \qquad \text{(A.1)}$$

$$f_{pu} = 270\,ksi$$

Immediate Losses:

1- Anchorage slip (AS)

$$AS = \Delta f = \frac{\Delta l}{l} E_p = \frac{0.25^{"}}{200^{'} * 12^{"}} 28,300 = 2.95\,ksi \qquad \text{(A.2)}$$

2- Elastic shortening (ES)

$$ES = K_{es} E_p \frac{f_{cir}}{E_{ci}} \qquad \text{(A.3)}$$

$$f_{cir} = K_{cir}\left(\frac{P_i}{A_{g_t}} + \frac{P_i e}{I_{g_t}} e\right) - \frac{M_{DL} e}{I_{g_t}} \qquad \text{(A.4)}$$

$$f_{cir} == 0.9\left(\frac{2*16.6}{125.34} + \frac{2*16.6*6.17^2}{1881.15}\right) - \frac{4.3*12*6.17}{1881.15} = 0.674\,ksi$$

$$ES = 1.0*28300\frac{0.674}{57\sqrt{3500}} = 5.66\,ksi$$

3- Creep (CR)

$$CR = K_{cr}\frac{E_p}{E_c}\left(f_{cir} - f_{cds}\right) \qquad \text{(A.5)}$$

$$K_{cr} = 2.0 \qquad f_{cds} = 0.0$$

$$CR = 2.0\frac{28300}{4784}.674 = 7.97\,ksi$$

4- Shrinkage (SH)

$$SH = 8.2*10^{-6} K_{sh} E_p \left(1 - 0.06\frac{V}{S}\right)(100 - RH) \qquad \text{(A.6)}$$

$$K_{sh} = 1.0 \qquad \frac{V}{S} = 2.02 \qquad RH = 65$$

$$SH = 7.14\,ksi$$

5- Relaxation (RE)

$$RE = \left[K_{re} - J\left(SH + CR + ES\right)\right]C \qquad \text{(A.7)}$$

$$K_{re} = 5.0 \qquad J = 0.04$$

$$C = \frac{f_{pi}}{f_{pu}} = \frac{193.6}{270} = 0.717\,ksi$$

$$RE = \left[5.0 - 0.04\left(7.14 + 7.97 + 5.66\right)\right]0.717 = 2.99\,ksi$$

Final Calculations

$$f_i = 193.6\,ksi$$

$$f_{pi} = f_i - ES - RE - AS = 182\,ksi \qquad \text{(A.8)}$$

$$f_{se} = f_{pe} = f_{pi} - SH - CR = 166.9\,ksi \qquad \text{(A.9)}$$

APPENDIX B

SHEAR CAPACITY OF INTERNAL STEEL STIRRUPS

Using ACI equations (Chapter 11) for shear capacity for prestressed concrete beams

$$s = \frac{\phi A_v f_y d}{V_u - \phi V_c} \tag{B.1}$$

$$4 = \frac{.85 * 0.12 * 11 * 80}{V_u - \phi V_c}$$

$$V_u - \phi V_c = 22.44$$

$$f_{pc} = \frac{P_e}{A_c} = \frac{28500}{125} = 228\ psi$$

$$w_{self} = 0.125\ k/\ ft$$

$$b_w = 4'' \qquad d = 11''$$

$$f_c' = 7{,}043\ psi \qquad L = 16'$$

$$e = 6.18'' \qquad c = 9.22''$$

$$r^2 = 14.8 \qquad I = 1849\ in^4$$

$$M_o = 0.875\ kip - ft \qquad V_p = 0$$

$$V_d = .875\ kips$$

$$V_u = \frac{L}{2}\left[1.4 w_{self} + 1.7 w_{live}\right] = 1.4 + 13.6 w_{live}\ \ kips \tag{B.2}$$

$$f_{pe} = -\frac{P_e}{A_c}\left(1 + \frac{ec}{r^2}\right) = -1089\ psi$$

$$f_d = \frac{M_o c}{I_c} = 52.4\ psi$$

$$M_{cr} = \left(\frac{I}{y_t}\right)\left(6\sqrt{f_c'} + f_{pe} - f_d\right) = 25.7\ kip - ft \tag{B.3}$$

$$V_i = w_{live}\left(\frac{L}{2} - 1\right) = 7w_{live}$$

$$M_{max} = \frac{w_{live}}{2}(L - 1) = 3.5w_{live}$$

$$V_{ci} = 0.6\sqrt{f_c'}\,b_w d + V_d + \frac{V_i M_{cr}}{M_{max}} = 54.5\,kips \tag{B.4}$$

$$V_{cw} = \left(3.5\sqrt{f_c'} + 0.3f_{pc}\right)b_w d + V_p = 15.9\,kips \tag{B.5}$$

$$V_c = min(V_{ci}, V_{cw}) = 15.9\,kips$$

$$22.4 = 1.4 + 13.6w_{live} - 0.85 * 15.9 \tag{B.6}$$

$$w_{live} = 2.53\,k/ft\ Max\ applied\ live\ load$$

Maximum moment bare beam can with stand is 81.0 k-ft.

For Beams 2 and 3, there were enough internal shear stirrups to prevent a shear failure. However, for Beams 4 and 5 the actual loading was slightly higher than this value. But the addition of the external CFRP stirrups are more than enough to help prevent a shear failure as well.

APPENDIX C

PLANT REPORTS

JOB NUMBER(S) IN THIS CAST :

RUN BY :

CURRENT DATE :

MODULUS OF ELASTICITY = 2.83E+07 PSI
ASSUMED CHUCK SLIPPAGE = .375 IN.
JACKING COEFFICIENT = .7 DECIMAL
ULTIMATE STRENGTH OF STRAND = 270 KSI
AREA OF PRESTRESSING STRAND = .08583 SQ. IN.
INITIAL JACKING FORCE = 3000 LBS.
STRESSING LENGTH = 200.5 FT.
NUMBER OF HEADERS IN CAST = 0

ALL STRANDS IN THIS CAST ARE STRAIGHT.
ELONGATION FOR STRAIGHT STRANDS = 13.10 IN.

TOLERANCE (PLUS OF MINUS) = 0.65 IN.

FINAL JACKING FORCE = 16,600 LBS.

NOTE: THE ELONGATIONS SHOWN ARE AFTER CHUCK SLIPPAGE

CAST DATE-3-17-02 JOB NUMBER-9-02

K No.	REPAIRS REQUIRED (PRE-POUR)	COMPLETED
88①		
88②		
	B 88 D4WW R Put in At 5" dim instead	
-44①	of 7" dim	
-44②		
-44③	B 44 D4WW R Put in At 6½" instead	
-44④	of 5" dim	
-44⑤		
-44⑥		
-44⑦		

K No.	REPAIRS REQUIRED (POST-POUR)	FOLLOW-UP	PRESHIP
88①			
38②	No Repairs		
44①			
44②			
	3day cyls 5809, 5730 broke 3-22		
44①	7 day cyls 6605, 6963 broke 3-26		
	14 day cyls 7281 7003 broke 4-2		
44④	28 day cyls 4456 Bad cap 7043 broke 4-16		
44⑤			
44⑥			
44⑦			

PLOT STRANDS ON GRID

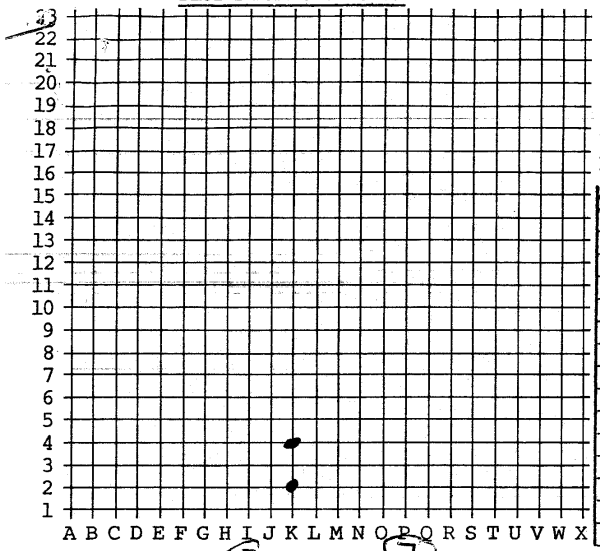

TENSIONING REPORT SIZE 5/8 BRAND ASW

ID NO'S

INITIAL ☐ 1000 ☒ 3000 JACK Hert

DEPRESSION ___ IN. ___ FORCE #1 S☐ D☐

DEPRESSION ___ IN. ___ FORCE #2 S☐ D☐

DEPRESSION ___ IN. ___ FORCE #3 S☐ D☐

GRID	COMP. ELONG	COMP. GAGE	ACT. ELONG	ACT. GAGE
K2	13 1/8 ± 5/8	16,600	13 3/8	16
K4	13 1/8 ± 5/8	16,600	13 1/4	

QUALITY CONTROL POUR REPOR

PROJECTS Kansas state

JOB NO'S 9-02 FORM SBT

DATE CAST 3-19-02 CAST N

LEADMAN C. B-TB INSPECTOR'S

FIRE LABELS: YES ☐ NO ☒ TYPE N

CONCRETE: TYPE 650 YARDS

TIME POURED: START 1:15

TEMPERATURES: AMBIENT 1) 47; FORM 1) 58; CONCRETE 1) 73

TESTS: SLUMP 1) 6; AIR 1) ___; UNIT WT. 1) ___; LOAD 1) 1

CURING: DURATION OF HEAT ___; PENETROMETER TEST: TIME ___; TIME ___; TIME ___; TIME ___

CYLINDER BREAKS: TIME 6 3/8 PSI 3[illegible]; TIME 5:40 PSI 3[illegible]; TIME ___ PSI ___

CAMBER: INITIAL COMP. ___

COMMENTS See sht 2 For Add.

PREPOUR / POST-POUR CHECK LIST

MARK NO.	B48		B44									
STR. PATTERN												
DESIGN LENGTH	16.6		16.6									
SET-UP LENGTH	—		—									
CAST LENGTH	—		—									
DESIGN WIDTH	1-6		1-6									
SET-UP WIDTH	—		—									
CAST WIDTH	—		—									
SET-UP SQ.	—		—									
CAST SQ.	—		—									
SET-UP END DET.	—		—									
CAST END DETAIL	—		—									
REINFORCING	—		—									
WELD BARS	N/A		N/A									
PLATES	N/A		N/A									
BLOCK-OUTS	N/A		N/A									
CHAMFER	—		—									
DOVETAIL	N/A		N/A									
INSERTS	N/A		N/A									
SLEEVES	N/A		N/A									
HAUNCHES	N/A		N/A									
PICK-UPS	—		—									

The following pictures show the pre-cast prestressing plant while reinforcing, pre-casting and transporting the beams

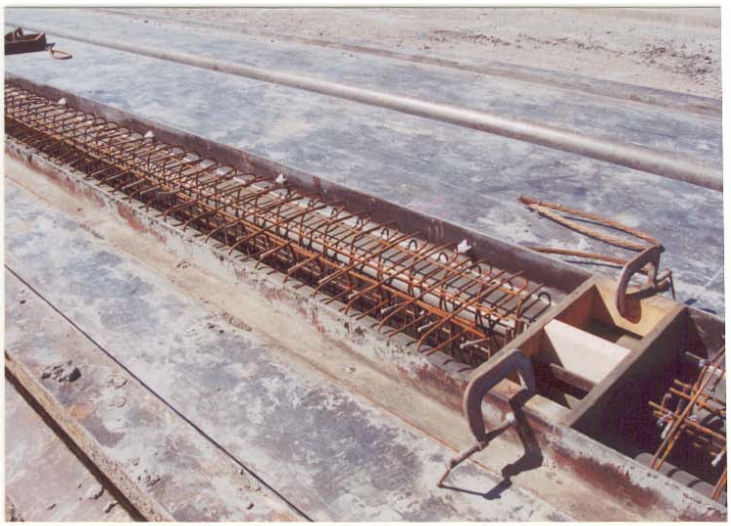


CAUTION


13
PYD 537

K-TRAN

KANSAS TRANSPORTATION RESEARCH
AND
NEW - DEVELOPMENTS PROGRAM

A COOPERATIVE TRANSPORTATION RESEARCH PROGRAM BETWEEN:

KANSAS DEPARTMENT OF TRANSPORTATION

THE UNIVERSITY OF KANSAS

KANSAS STATE UNIVERSITY